OZONE GENERATION USING ELECTRICAL DISCHARGES:

A comparative study between Pulsed Streamer Discharge and Atmospheric Pressure Glow Discharge

By

Zolkafle Buntat

A doctoral thesis submitted in partial fulfilment of the requirements for the award of
Doctor of Philosophy of Loughborough University

February 2005

Dedicated to my mother, wife and all my sons and daughters

ABSTRACT

This thesis deals with an investigation into atmospheric pressure glow discharge and pulsed streamer discharge techniques of ozone generation, in an attempt to compare their performances in the generation of a high concentration and high yield of ozone. It is motivated by the desire to exploit further the ability and potential possessed by both techniques for ozone generation and to provide support to the increased demand for ozone in many areas of application.

Chapter 1 of the thesis provides a brief history into the application of ozone. In Chapter 2, a basic understanding of the gas discharge is given for both thermal and non-thermal plasmas, and the theory of non-thermal plasma is presented. The different types of electric discharges commonly used for ozone generation are explained. A review of the effect of both the physical configuration and the electrical parameters on the ozone yield and concentration is presented in Chapter 3, with the three main parameters that limit the efficiency of the production being highlighted.

The second part of the thesis describes a thorough experimental investigation. In Chapter 4, a study is made of the stability of the atmospheric pressure glow discharge (APGD) which is found to be more stable when perforated electrodes are used rather than a fine steel wire mesh. Following this, a comparative study between APGD and pulsed streamer discharge (PSD) is presented in Chapter 5. A detailed investigation into both APGD and PSD in air is described. The effects of varying the input voltage, gap distance, chamber length, air flow rate and gas residence time are all used to evaluate the performance of both techniques. The PSD is found to generate a higher concentration but with a lower ozone yield. On the other hand, the APGD generates a lower concentration but with a higher yield.

Chapter 6 presents the effect of a cross magnetic field on an AC corona and the PSD techniques and its influence on ozone generation. Results show no apparent effect of the magnetic field in either technique. Chapter 7 describes the use of dimensional analysis in investigating the effect of the electrical and the discharge configuration parameters on ozone production in oxygen by means of a PSD. Ozone destruction factors are taken into account in the model, and predicted results are shown to be in good agreement with experimental findings.

ACKNOWLEDGEMENTS

First of all, I would like to thank God for everything, including the ability to learn, the pleasure of sharing it and the wisdom of appreciating it.

I would also like to thank my first supervisor, Dr. J.E.Harry and my second supervisor Prof. I.R.Smith for their support, encouragement and enthusiastic discussions. I have been very fortunate to have the opportunity to work with them, and I can never thank both of them adequately for their help on both academic and non-academic matters.

Thank are also due to Mr. J.G.Kettleborough, my Director of Research, for making many valuable suggestions and to those technicians who provided invaluable help, from the early stages of my research until its completion.

I want to thank my mother and family for the love and support they have provided throughout the three years of my research, without which I would not have reached my current goals and aspirations.

A special vote of thanks is due to all of my friends, fellow research students and staff in the Department of Electronic and Electrical Engineering at Loughborough. All my experiences and interactions with these people have shaped my work and helped make my graduate experience worthwhile and unforgettable.

Finally, I would like to thank the Public Services Department of Malaysia for sponsoring my research, and my home institution, University Technology Malaysia, for granting me leave to carry out this research.

GLOSSARY

APGD	Atmospheric pressure glow discharge
PSD	Pulsed streamer discharge
UV	Ultraviolet
ppmv	Volume per part per million
DC	Direct current
AC	Alternating current
LTP	Low temperature plasma
PSA	Pressure-swing absorption
LOX	Liquid oxygen
RSG	Rotating spark gap
HV	High voltage
RPM	Rotations per minute
pps	pulses per second
FWHM	Full-width half maximum
CRO	Cathode ray oscilloscope
STP	Standard temperature and pressure
PVC	Polyvinyl chloride
BOC	British Oxygen Company

NOMENCLATURE

B	Magnetic flux density (T)
Cd	Dielectric capacitance (F)
Cg	Gap capacitance (F)
x, d_d	Dielectric thickness (mm)
d,d_g	Gap spacing or gap distance (mm)
ε_r	Dielectric constant or relative permittivity of dielectric (F/m)
ε_o	Dielectric constant or absolute permittivity of input gas (F/m)
E	Electric field intensity (V/m)
E_d	Electric field intensity at dielectric (V/m)
E_g	Electric field intensity at the gas gap (V/m)
E_i	Electric field intensity at the gas gap at corona inception value (V/m)
V_a	Applied voltage (V)
p	Gas pressure (bar)
T	Absolute temperature (K)
α_p	Specific ozone molar absorption coefficient (cm^{-1} atm^{-1})
α	Townsend's first ionization coefficient (m^{-1})
γ	Townsend's second ionization coefficient (m^{-1})
E/p, E/n	Reduced electric field
n	Number density of background gas
α_{eff}	Townsend's first ionization coefficient in mixtures of noble gas (m^{-1})
∂	Attachment coefficient
γ_i	Emission coefficient of ions
γ_m	Emission coefficient of metastables

γ_p	Emission coefficient of photons
$\sigma 1$	Space charge effect coefficient
Vb	Breakdown voltage (V)
σ	Surface discharge density (C/m^2)
η	Ozone yield (g/kWh)
$C(O_3)$	Ozone concentration (ppmv)
P	Dissipated/discharge power (Watt)
f_r	Gas flow rate (l/min)
f	Frequency/pulse repetitive frequency (Hz/pps)
V_{min}	Minimum external voltage at which ignition occurs (V).
V_p	Peak input voltage (V)
r(p,d)	Radius of micro-discharge (μm).
R_t	Residence time (s)
k_f	Reaction rate coefficient of ozone formation
k_d	Reaction rate coefficient of ozone destruction.
ΔT_g	Average increase of temperature (^oC)
T_g	Gas temperature (^oC)
T_w	Wall temperature (^oC)
#	Number of meshes per inch.
Er	Input energy to the reactor per pulse (J/pulse)
τ	Pulse duration (s)
I/ Io	Transmittance of the ozone sample (%)
L	Path-length (m)
k1 – k8	Indices of variables
$\pi 1$- $\pi 4$	Dimensionless variable
Dc	Dimensional constant

List of Figures

List of Tables **Page**

CONTENTS

CHAPTER 1

INTRODUCTION

1.1 Research background

Ozone is now attracting much attention worldwide as an environmental friendly oxidant for a wide range of applications, including deodourization, decolourization, disinfection, various bleaching processes, gas treatment and chemical synthesis. In each of these, it requires less energy than does the alternative chlorination process [1]. The consequent surge in demand has brought about the requirement for its generation at the rate of grams per kilowatt hour (g/kWh), at the same time as producing concentrations of many volume per parts per million (ppmv). To fulfil these demands, extensive research has been undertaken recently on a number of different experimental configurations and discharge techniques.

Ozone is usually generated by means of an electric discharge, when a high-energy electric field exists between two electrodes separated by a dielectric and a discharge gap and with a gas containing oxygen or air flowing between them. The high electric field in the resulting low current discharge causes an electron flow across the discharge gap, and by providing sufficient energy to dissociate the oxygen molecules leads to the formation of ozone. However, ozone cannot be stored and must be generated at the point of its use [2,3,4].

The major shortcoming in the production of ozone by conventional method is related to the low efficiency of the process, which makes ozone expensive. At present, commercial techniques have an energy yield of 60 – 120 g/kWh from dry air and 200 – 274 g/kWh from pure oxygen gas [2-7]. Since the theoretical limit of

energy yield is about 1220 g/kWh in oxygen and about 400 g/kWh in pure air, almost 90% of the energy is lost as heat [3,4,6,8]. In addition to the obvious waste of useful electrical energy, the heat needs to be removed from the reactor, because the decomposition of ozone into oxygen atoms and molecules is very sensitive to temperature. The cooling systems for such equipment will therefore always be expensive, and it is recognized that their large size is imposed by the low efficiency of the process.

For many years, the dielectric barrier discharge has been commonly used both to generate ozone and for other chemical processes [3,5,8-11]. The use of a dielectric material on one or both sides of the electrodes is necessary, as it serves to distribute evenly the micro-discharges that appear over the entire electrode area and thereby to limit the charge and energy that are fed into any individual micro-discharge [3,5,8,11]. Other techniques used for ozone generation include corona discharge [12,13], surface discharge [14-16], pulsed streamer discharge [2,7,17-21] and atmospheric pressure glow discharge [22-29].

This thesis focuses on the production of ozone using atmospheric pressure glow discharge (APGD) and pulsed streamer discharge (PSD). A study of the relevant literature has confirmed that both techniques have the potential to generate ozone more efficiently and effectively than the dielectric barrier discharge. For this reason, an efficiency study of each type of discharge technique for ozone generation has been undertaken in the same discharge configuration. Furthermore, a comparative study between atmospheric pressure glow discharge and pulse streamer discharge techniques has been conducted, in order to identify the most effective method for ozone generation.

A study was also made to determine the effect of a cross magnetic field on ozone generation. The results were compared with those for the same configuration but without application of the magnetic field. Results from experimental work and an outline of future work are also presented.

1.2 Early history of ozone technology

Ozone was discovered in 1839 by C.F. Schonbein during his studies into the electrolytic decomposition of water, although It took more than two decades of scientific dispute before the constitution of this new substance was clearly identified as a three atomic molecule containing only oxygen. J.L. Soret named it ozone in 1865. About the same time, in 1857, Werner von Siemens found that ozone could also be generated in gas discharges. He designed an ozone generator that has since evolved into the present day, cylindrical dielectric type used in most of the commercially available equipments, and which has sometimes been called the " Siemens Type" generator [30].

In the Siemens Type apparatus, ozone is produced by allowing oxygen to pass between two electrodes separated by a dielectric barrier, usually glass. A high voltage applied to the electrode arrangement produces an alternating ion flow, resulting in the conversion of oxygen into a mixture of oxygen and ozone. The output of such generators normally ranges from 2% to 15% ozone in oxygen, depending on the reactor design, with the purity of the oxygen fed in determining the concentration of ozone that is achieved. Air gives only half as much ozone as does pure oxygen, for the same electrical energy input. In large-scale units about 90% of the oxygen input is lost, unless the unused oxygen is recycled. In the recycling process, impurities might mix with the oxygen and this has proved to have a detrimental effect on the ozone yield. Many different methods of ozone generation have been implemented throughout the years, especially for inorganic chemistry purposes. For large industrial applications only an electrical discharge generation process is considered, and the present investigation concentrates therefore on such methods.

The earliest experiments on the use of ozone as a germicide were conducted in 1886 by de Meritens in France [30]. In 1893, the first drinking water treatment plant utilizing ozone for disinfection was constructed and operated in Oudshoom,

in the Netherlands. Plants were also constructed at Paderborn in 1902 and at Wiesbaden in 1903. In 1907 the City of Nice, France began operation of a new water treatment plant incorporating ozone, to deliver 22,500 cubic metres/day to the inhabitants of the city [30]. This Bon Voyage plant operated continuously until 1970, when it and two others plants in Nice, built subsequent to 1910, were replaced by the new and modern Super Rin-dez plant. The use of ozone in the United States can be traced back to the 1940s. Today, ozone is used in several thousand drinking water plants throughout the world, with more than half of these located in Europe [30]. The 25 largest installations consume, on average, more than 1 MW for ozone generator alone, indicative of the fact that its generation has become a major plasma chemical process.

In the first large ozone installation for water treatment (Nice 1907), the generators alone required 25-28 kWh/kg and the total energy consumption was about 140 kWh/kg [30].

1.3 Ozone properties and its chemistry

Ozone is usually colourless gas and appears in dark blue in liquid state whose chemical symbol is O_3. It has a characteristic pungent odour that can be detected by the nose at low levels (0.02 ppm) to provide warning of toxic exposure. It dissolves in many solvents and the resulting concentrated solution becomes blue at low temperatures [31].

Ozone (O_3) is formed when three atoms of oxygen are bound together, instead of the normal two. The extra atom makes ozone the most powerful oxidizer and sanitizer readily available, and it is increasingly being used in place of other bactericides in a diverse number of applications in particular sterilization, deodourization and bleaching. Its high germicidal activity rate against both

cryptosporidium and coliform bacteria [2,17] is reported to be 100 to 1000 times greater than that of chlorine or chlorine dioxide,.

Ozone is however highly unstable, readily reverting, particularly in the presence of organic compounds, to the benign form oxygen. This instability, though in one sense inconvenient, is essentially why the gas is environmentally preferable in chemical processes. Ozone cannot be stored and must be generated at its point of use [2-4], and in normal air it lasts for only about one hour. In normal pool water it lasts just long enough to purify the water (less than 1 s). A major disadvantage of using ozone is related to its generation process, which is very inefficient and makes ozone expensive, when compared with other less environmental friendly compounds such as chlorine, which is a cheap by-product of many chemical processes.

An ozone concentration as low as 0.1 mg/l is capable of inactivating 99.9% of a bacterial suspension within 1 min [32]. Great care must be exercised near the boiling point at ~112°C, since liquid ozone decomposes explosively when subjected to various shocks and impurities: One reason why it is normally never stocked but is produced on site.

In recent years, ozone has become a significantly popular subject for the attention of the media, and it is one of the components of photochemical pollution on which much attention is focused in periods of heavy air pollution. Although far from being a major pollutant, the ozone level is, in many respects, an indicator of the air quality [32].

Ozone occurs naturally in the atmosphere, where it has great biological and meteorological significance [33]. At higher altitudes the concentration changes in a cyclic manner during a 24-hr period, as well as seasonally throughout the year. It is principally concentrated, up to 27% by weight, between altitudes of 15 and 25

km (ozone layer), where it is formed by solar UV radiation in the range between 240 nm and 300 nm via the reactions.

$$O_2 + UV \rightarrow 2O$$
$$O + O_2 \rightarrow O_3. \qquad (1.1)$$

Ozone adsorbs UV radiation from 200 nm to 360 nm, which leads to a partial reversal of these reaction and thus to the establishment of a steady state concentration. The net result of all these processes is adsorption and the conversion to heat of considerable solar UV radiation that would otherwise strike the earth's surface.

1.4 Mechanism of ozone generation

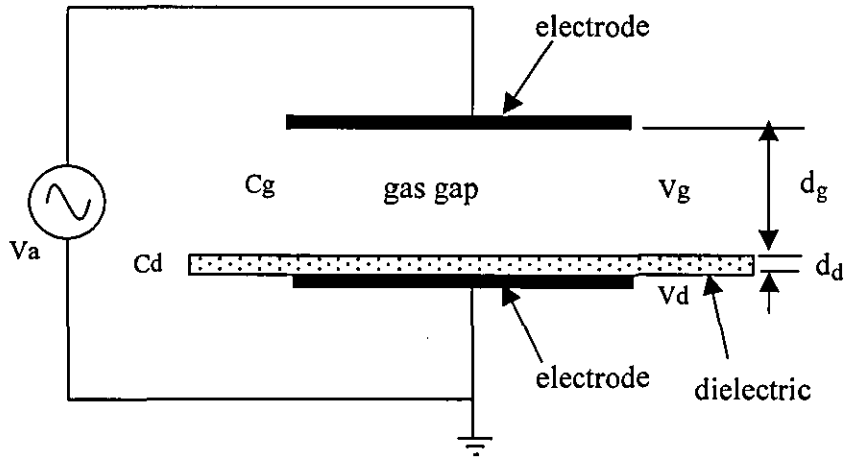

Figure 1.1 : Electrical measuring system

An alternating voltage is applied between the two electrode of figure 1.1, which have a separation of d_g, and a dielectric layer of thickness d_d is attached to one of the electrodes. The voltage division between the gap and the dielectric is determined by the relative capacitance of the air gap C_g to that of the dielectric layer C_d as [34,35]:

$$\frac{V_g}{V_d} = \frac{C_d}{C_g} = \varepsilon_r \frac{d_g}{d_d} \tag{1.2}$$

where ε_r is the relative permittivity of the dielectric layer. While V_g and V_d are the voltages across the gap and the dielectric. It follows from equation (1.2) that the corresponding values of the non perturbed electric fields E_g and E_d are

$$E_g = \frac{V_a \varepsilon_r}{d_d + \varepsilon_r d_g} \qquad E_d = \frac{V_a}{d_d + \varepsilon_r d_g} \tag{1.3}$$

As the applied voltage (V_a) is increased, E_g and E_d naturally both also increase. Nothing else happens however until the electric field in the gas gap attains the discharge inception value E_i required to produce ionization by electron collision. When ionization takes place, two phenomena arise. Firstly, ozone is created as a result of the electrochemical reaction and secondly charges resulting from the discharge process are deposited on the surface of the dielectric adjacent to the air gap. The polarity of the charge is that of the electrode on the opposite side of the air gap and consequently this charge accumulation has the effect of reducing the electric field in the gap, until the discharge ceases (at just below the inception value). When a discharge ceases, no further charge is of course generated and no further charge can be deposited [35].

The process is therefore self regulating. Even if the applied voltage is increased the field in the air gap and the voltage across it are maintained at E_i and V_i respectively, since any further discharge produces an increase in the accumulated charge on the dielectric and a consequent reduction of the gap field to E_i until the discharge is quenched. Obviously increasing the applied voltage increases the stress on the dielectric, which represents a practical limit to the maximum voltage capability of any device. When a sinusoidal voltage is applied the discharge will cease before the peak value of the applied voltage, due to surface charge accumulation, and it will be re-established during the following half cycle at a time (even before the voltage zero) when the gas gap field again achieves the inception value (but now in the reverse direction). If, on the other hand, the applied voltage is decreased, the voltage across the dielectric layer is clamped at the previously achieved value, since the charge on the dielectric surface is, to all intents and purposes, rigidly bound. This occurs at the peak value of the applied voltage and is equal to the difference between that peak voltage and the inception voltage. The instant at which the discharge commences again is dependent upon the value of the applied voltage and the dimensions of the particular generator [34,35].

1.5 Ozone formation in oxygen

A typical micro-discharge in oxygen, at about atmospheric pressure, lasts for only a few nanoseconds and transports a charge of less than 1 nC. The current pulse in each micro-discharge channel is of very short duration, less than 5 ns [3,36]. Therefore the current in the micro-discharge channel during its active phase is mainly an electron current, although the most abundant charge carriers are positive ions such as O_2^+ and the negative ions O^-, O_2^- and O_3^-. This is due to the fact that the mobility of electrons is more than a factor of 100 higher than that of ions [5].

Ozone formation is a two-step process [5,37] that starts with the dissociation of molecular oxygen by the electrons responsible for the current flow in a micro-discharge. According to Eliasson et al [3], ozone is produced through two different mechanisms in pure oxygen:

$$e + O_2 \rightarrow e + O_2(A\,^3\textstyle\sum_u^+) \qquad \text{at 6 eV}$$
$$\rightarrow e + O(^3P) + O(^3P)$$
$$\rightarrow O_2 + O(^3P) \rightarrow O_3. \qquad (1.4)$$

$$e + O_2 \rightarrow e + O_2(B^3\textstyle\sum_u^+) \qquad \text{at 8.4 eV}$$
$$\rightarrow e + O(^3P) + O(^1D)$$
$$\rightarrow O_2 + O(^3P) \rightarrow O_3. \qquad (1.5)$$

where

$O_2(A\,^3\sum_u^+ , B^3\sum_u^+)$ = two excited states of oxygen molecule.

$O(^3P , ^1D)$ = two excited states of atomic oxygen.

It is believed that ozone is generated initially at a slow rate by reaction (1.4), and subsequently at a greater rate by both reactions (1.4) and (1.5), which explains the well known enhancement in the rate at which it is produced.

Following dissociation, oxygen atoms can form ozone by the following three-body reaction

$$O + O_2 + M \rightarrow O_3 + M \qquad (1.6)$$

where M is a third body collision partner which can be any molecule such as oxygen or nitrogen and is essential for the reaction to take place.

Figure 1.2 shows a simulation [5] of ozone formation due to one micro discharge. While the charge carriers disappear, typically in less than 10 ns, ozone formation takes a few microseconds. The main results can be summarized as [5]:

1) Dissociation of O_2 by electron impact is the main reaction path leading to ozone formation.
2) Ionic reactions contribute little to ozone formation;
3) There is an optimum micro-discharge strength;
4) Large ozone formations have to be built up by a large number of micro-discharges.

The most common figure of merit in ozone generation is the efficiency, expressed in grams of ozone per unit of energy (usually kWh). The maximum theoretical efficiency for ozone generation in oxygen through a dielectric barrier discharge is about 1220 g/kWh [5,8].

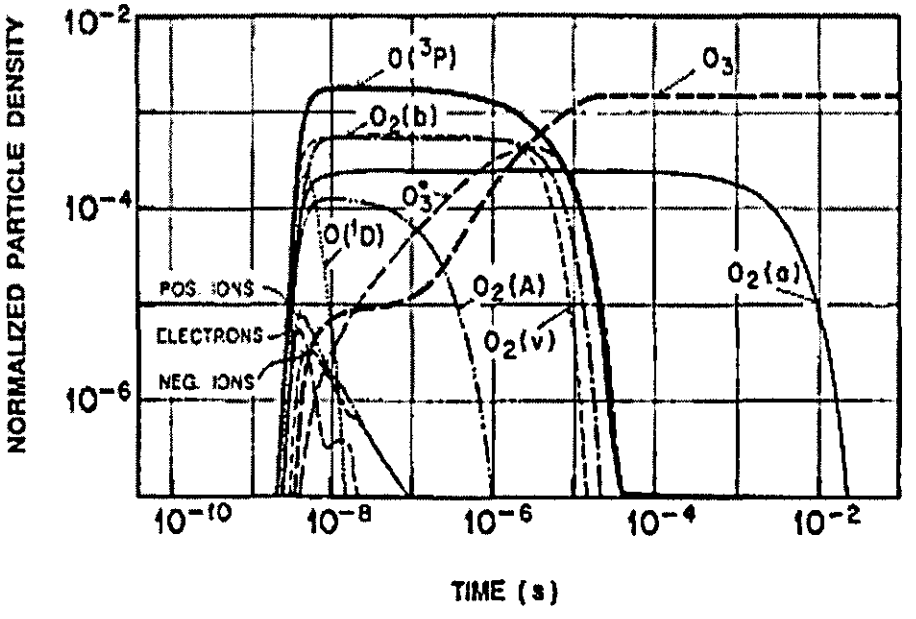

Fig. 1.2 : Numerical simulation of ozone formation due to one microdischarge in pure oxygen (homogeneous model, p=1 bar, T=300 K) [5]

The most important parameter affecting the efficiency is the atomic concentration that determines how many oxygen atoms really form ozone molecules. The ideal situation, in which every atom of oxygen reacts with molecular oxygen to form ozone, is obtained only if the relative atomic concentration $[O]/[O_2]$ is less than 10^{-4} [10]. At 1% atomic concentration the efficiency is already halved. If the micro-discharge becomes too strong, the concentration of oxygen atoms reaches a level at which undesired side reactions gain importance [5]. Thus

$$O + O + M \rightarrow O_2 + M \quad (1.7)$$

$$O + O_3 \rightarrow 2O_2 \quad (1.8)$$

$$e + O_3 \rightarrow O + O_2 + e \quad (1.9)$$

and especially

$$O + O_3 \rightarrow 2O_2 \quad (1.10)$$

Dissociation is very fast (in ns) and is completed during the current pulse. Ozone formation, on the other hand, is completed after only about 10 μs. The presence of O_3 reduces the final ozone level and increases the time constant of its generation. With increasing background ozone concentration inside the reactor, a number of additional reactions involving O_3 become important. The result is that the efficiency of individual micro-discharges decrease with rising background concentration.

Once the saturation concentration is reached, each additional micro-discharge destroys as much ozone as it creates, resulting in net zero production. The following ozone destruction reactions are recalled [5]:

$$O + O_3 \rightarrow 2O_2 \quad (1.11)$$

$$O(^1D) + O_3 \rightarrow O_2 + 2O \quad (1.12)$$

$$O_2(\upsilon) + O_3 \rightarrow O_2 + O_3 \quad (1.13)$$

$$e + O_3 \rightarrow e + O_2 + O \quad (1.14)$$

Particularly important is reaction (1.14), that describes ozone decomposition due to electron impact. The decomposition rate can easily be supposed to depend on the electric field strength, because the threshold energy for dissociating ozone lies around several eV, where an increased or decreased in the electric field strength has significant influence on the distribution of electron energy [38]. The detail reaction of ozone formation and decomposition in oxygen is shown in appendix 1a.

1.6 Ozone formation in air

Ozone generation in air follows the same pattern as does ozone generation in oxygen. Although the use of air has the advantage that it, unlike oxygen, is readily available, the concentration of ozone produced is lower than that obtained using oxygen. The maximum theoretical efficiency for ozone generation in air through a dielectric barrier discharge is about 400 g/kWh [5,8]. In addition, the presence of moisture and particulate matter in air will cause nitric acid to form, interfering with the discharge formation and reaction kinetics, and creating the potential for corrosion that can adversely affect the performance of the generator and increase the need for maintenance.

Figure 1.3 shows simulation results for ozone formation in air. One obvious difference to ozone formation in pure oxygen is the change in the time scale and the appearance of the additional species: NO, N_2O, NO_2, NO_3 and N_2O_5, all of which can be detected by spectroscopic techniques and by dynamic mass spectrometry. The main features of ozone formation in air can be summarized as [5]:

1) Under normal operating conditions of an ozonizer, only the oxides N_2O and N_2O_5 can be detected in addition to ozone. Their concentrations are two orders of magnitude lower than the ozone concentrations;

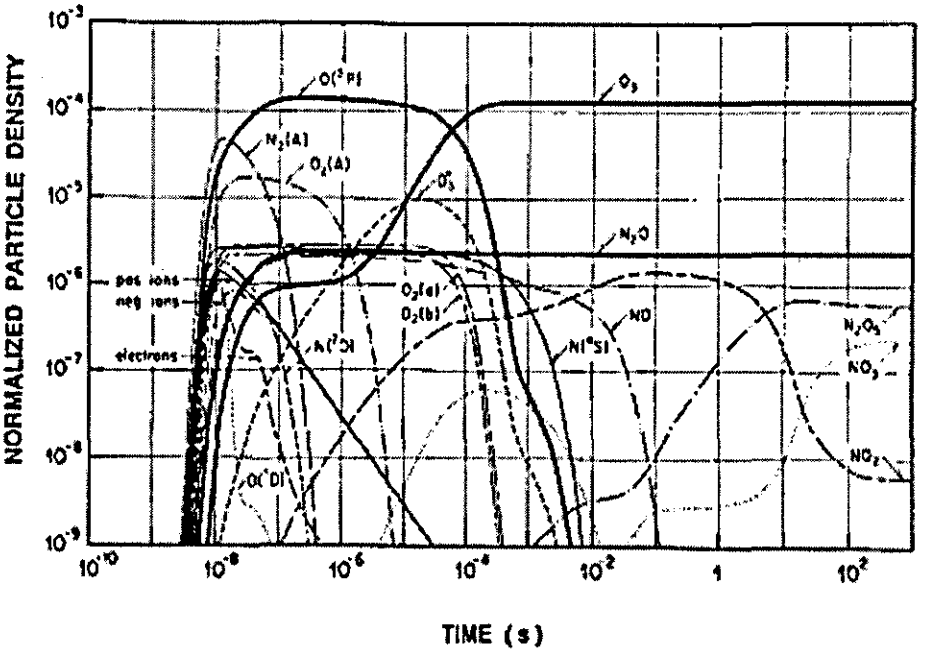

Fig. 1.3: Chemical species generated by a microdischarge in "air" (80% N_2 + 20% O_2, p= 1 bar, T= 300 K, homogeneous model) [5].

2) At very high specific energies the ozone production breaks down and only nitrogen oxides are produced (discharge poisoning, ozoneless mode). In this mode the lower oxides NO and NO_2 are found, in addition to N_2O;

3) Ozone production in air (concentration and efficiency) is higher than would be expected from the oxygen content in air.

Because ozone is such a powerful oxidizer, it will also oxidize nitrogen (N_2) in air to nitric oxide (NO_2). Moisture reacts with nitric oxide to produce nitrous (HNO_2) and nitric (HNO_3) acids, that are highly corrosive to the electrodes, piping, and

other equipment of the ozonation system. Under the normal operating conditions of commercial generators, nitrogen oxides reach only about 1% of the ozone concentration [39], although at large specific energies they can inhibit ozone formation completely and destroy all previously generated ozone. This is called "discharge poisoning" [40]. The following reactions involving the destruction of ozone have been reported to occur in air feed system [21,41]

$$N + O_3 \rightarrow NO + O_2 \quad (1.15)$$

$$NO_2 + O \rightarrow NO + O_2, \quad (1.16)$$

$$NO + O_3 \rightarrow NO_2 + O_2 \quad (1.17)$$

$$NO_2 + O_3 \rightarrow NO_3 + O_2 \quad (1.18)$$

$$N_2 + O_3 \rightarrow N_2 + O_2 + O \quad (1.19)$$

For efficient ozone production the air has to be dried to a dew point below $-60^{\circ}C$. Moisture measurement is desired in ozonizers because, at higher dew point temperatures, the generation is adversely affected. The efficiency of the ozonizer is reduced; that is, less ozone is produced from the same electrical discharge. For example, raising the dew point from -60°C to -50°C can mean as much as a 15% decrease in the production efficiency [3]. A detail reaction of ozone formation and destruction in air is shown in Appendix 1b.

1.7 Conventional ozone generation

1.7.1 Ultra violet (UV) light method

This method is similar to the formation mechanism of ozone in the stratosphere (20-30 km); that is, oxygen atoms, formed by the photo-dissociation of oxygen by short wavelength UV radiation (<240 nm), reacting with oxygen molecules. At low conversions, the limiting quantum yield is ~ 2.0 [42]. The steady state ozone concentration (~ 3.5 mol % max) depends on temperature, pressure, and whether oxygen or air is employed; the time-to-steady-state depends on the light intensity. Efficiencies as high as 9% can be obtained, at low ozone concentration, by using narrow-band UV radiation produced by a xenon excimer laser operating at 172 nm [42].

In practice, ozone concentrations obtained by commercial UV devices are low. This is because the low intensity, low pressure mercury lamps employed produce not only the 185 nm radiation responsible for the ozone formation, but also the 254 nm radiation that destroys ozone, resulting in a quantum yield of ~ 0.5 compared to the theoretical yield of 2.0. Furthermore, the low efficiency (1%) of these lamps results in a low yield of 2 g / kWh [42].

The typical output of a commercial 40 watt UV lamp using air is 12.5 g/kwh of ozone and a maximum concentration of 0.25 wt% [42]. The low concentrations of ozone available from UV generators preclude their use for water treatment because the transfer efficiencies of ozone from air into water is low and large volumes of carrier gas must be handled. More than 44 kWh are required to generate one kg from dry air by UV radiation under high gas flow rates and low concentrations [42].

1.7.2 Radioactive ray irradiation method

Ozone can be produced using radioactive ray irradiation methods. It however does not popular because it is difficult to handle the radioactive ray and the controlling of the radiation source [43].

1.7.3 Electrolysis method

Ozone can also be formed by electrolysis of an electrolytic liquid (Sulphuric acid or hydrochloric water solution). The method can produce high concentration ozone and it does not form a nitrogenous oxide. However, the consumption of electric power is high when compared with the electrical discharge method.

1.7.4 Electrical discharge method

Most common methods of producing ozone use electrical discharges. The widely employed technique produced much higher concentrations than does the UV method, and is more practical and efficient for the large scale production. A detailed discussion in this method is presented in Chapter 2.

1.8 Typical application of ozone

1.8.1 Drinking water treatment

When ozone is used, as a gas, for drinking water treatment, it is done primarily because of its high oxidation strength, which allows it to be effective in the reduction or elimination of color, taste and odour. These may all be fundamental

problems associated with a specific water supply. More importantly, ozone will effectively destroy bacteria and inactivate viruses more rapidly than any other disinfectant chemical. It is also used to oxidize heavy metals; iron and manganese can be reduced to very low, safe levels in water supplies through ozone oxidation. This same process is used to liberate organically bound heavy metals, which are otherwise not easily removed.

Ozone, properly applied at the start of a water treatment process, will not lead to the formation of halogenated compounds such as trihalomethanes (THMs) which are formed when chlorine is added to raw water containing humic materials (organic compounds found in the soil). Once a THM is formed, it is difficult, if not impossible to oxidize, even with ozone. Thus ozone can be used as an oxidant, where it is applied at the latter stages of water treatment. Whatever gas is not consumed during the treatment of drinking water is collected and converted back to oxygen through ozone off-gas destructors, before release to the atmosphere [30,43].

Ozone is very effective against bacteria because even concentrations as low as 0.01 ppmv are toxic to bacteria. Whereas disinfection of bacteria by chlorine involves the diffusion of HOCl through the cell membrane, disinfection by ozone occurs with the lysing (i.e. rupture) of the cell wall. The disinfection rate depends on the type of organism and is affected by ozone concentration, temperature, pH, turbidity, clumping of organisms, oxidisable substances, and the type of contactor used. The presence of oxidisable substances in ordinary water can retard disinfection until the initial ozone demand is satisfied, at which point disinfection is observed. It has been observed [6] that 0.1 mg/l of active chlorine requires 4 hours to kill 6×10^4 E- *coli* cells in water, whereas 0. 1 mg/l of ozone requires only 5 s. When the temperature was raised from 22°C to 37°C, the ozone inactivation time decreased from 5 s to 0.5 s [43].

1.8.2 Wastewater treatment

The treatment of wastewater with ozone, again primarily for disinfection or at least a high level of bacterial reduction, was a key focus of its use in the United States during the late 1970s and early 1980s. More than twenty plants were installed, in various locations with various design consideration, The key reason for the use of ozone was however disinfection, and this approach is again being considered in light of the desire to avoid chlorination [30,43].

Drinking water applications normally require only around 0.5 mg/l of ozone to sufficiently inactivate the microorganisms present, as the presence of large quantities of microorganisms is generally low. For the disinfection of water which contains large quantities of microorganisms, and may also contain a large proportion of solid mass, such as primary or secondary treated wastewater, considerably larger doses of ozone are required. After ozone has been used to disinfect secondary municipal effluent, it is difficult to distinguish it visually from potable water. [30,42] Ozone disinfected water is saturated with oxygen and safe for the receiving stream, whereas chlorinated water is toxic to trout and other forms of aquatic life. In addition, ozone is a more effective disinfectant than chlorine since it lowers the colour, the chemical oxygen demand, and the turbidity. Ozone also removes suspended solids by an induced flotation process, which is initiated by precipitating a naturally occurring ferrous ion such as ferric hydroxide, which functions as a coagulant [30,42]. Applied ozone concentrations of 1.5 mg/l were sufficient to achieve sterilization of the water after 10 minutes, when applied to an initial cell population of 2.5×10^4 cells/ml. Raising the dosage rate to 1.9 mg/l allowed sterilization of the same initial cell population to be achieved in 1 min. However, for these applications, solid particulates have to be removed prior to ozonation.

1.8.3 Odour control and air treatment

The application of ozone or ozone in combination with other chemicals for the treatment of malodorous air has a long history of success. Typically, in wastewater treatment plants, foul air can be collected and treated with ozone to reduce the odour. Ozone is usually applied in combination with wet scrubbing equipment, and when used at 2 - 10 ppmv, it oxidises odour-forming compounds in the gas or aqueous phase. Odour properties are usually associated with functional groups of high electron density, e.g. sulphides, amines, and olefins. Some industrial odours oxidised by ozone include those from dairy processing plants, compositing operations, fish processing, paper mills and food processing [43].

1.8.4 Pulp and paper wastewater treatment

As a general negative reaction to the dispersion of waste effluents containing chlorinated disinfection by-products increases, consideration of the use of ozone in many phases of the pulping process grows. It should be pointed out that the pulp and paper industry has been examining the use of ozone for many years. Ozone can be applied as a final polishing treatment to the waste effluent from the plant. It is also applicable in the bleaching process and, similar to wastewater plant foul air deodorization, it can be applied to the odour which emanates from the process [30,43].

1.8.5 Fish hatcheries

Using ozone instead of chlorine has some significant advantages here. Firstly, the ozone carrier gas will increase the dissolved oxygen level in the fish tanks.

Secondly, the fish will not be exposed to by-products of chlorination, with all the ramifications that are entailed. Dosage rates for fish hatcheries are typically in the same order of magnitude as for low level water treatment [43].

1.8.6 Process water

Ozone is employed to a limited extent in the treatment of process water, such as cooling tower water, where it functions primarily as a biocide. It has no direct effect on corrosion or scaling, since these are dependent on water chemistry and water quality. Ozone also has potential applications where quantities of microorganisms are present, such as in the brewing industry, where large amounts of yeast are likely to be present in process water. The use of ozone in these applications would allow inactivation of the microbial population enabling either the water to be recycled or its safe disposal [30,43].

1.8.7 Ultrapure water

The use of ozone in the printed and integrated circuit board industry for the production of ultrapure water is a well documented application. It is also applied to the deionized water that is used to wash substrates during the production of printed circuit boards [44].

1.8.8 Other uses of ozone

Ozone is also used extensively in the bottled water industry, where it is required that a residual ozone concentration should be included with the water in the bottle. The residual disinfects the inside of the bottle where contact is made with the water; some ozone, however, escapes into the gas phase where it also

disinfects the inside of the cap and container, which is not in contact with the water.

In pharmaceutical applications the sterility of deionised water is maintained by using a residual ozone concentration maintained at >0.3 ppmv in the water recirculation loop. Prior to the water being used, it is subjected to UV radiation for <1 s to allow any residual ozone to be removed [43].

Ozone is also used in the electronics industry to remove trace organic materials from electronic components by immersion in deionised water containing a residual ozone concentration of around 0.5 - 2 ppmv [43].

CHAPTER 2

ELECTRIC DISCHARGES USED FOR OZONE PRODUCTION

2.1 Introduction to Gas Discharges

Electric gas discharge is a phenomenon that is observed when an electric current passes through a gaseous medium. When two electrodes, either the anode and cathode of a gas discharge tube or in any other configuration, are supplied with a high voltage, an electric field is created between them. In the presence of this field, a free electron will accelerate away from the cathode and toward the anode. When such an electron collides with a gas molecule in its path, it may transfer some of its energy to the molecule, raising this to an excited (high-energy) state. A discharge is initiated in the gas, with an electric current flowing through it, resulting from collisions between molecules in the gas and electrons of the current [44]. The establishment of a discharge which is self-maintaining (i.e independent of external sources of primary electrons or photons), is largely controlled by the rate at which the collision process in the discharge occurs, and by the transport properties of the electrons and ions. Any electric field enhancement will cause an increased rate of ionization due to an increased rate of collisions, which in turn will produce an increased velocity of discharge propagation [45,46].

Electrical discharges are the basis for plasma in industry. Industrial plasmas can be divided into two categories;

(i) Equilibrium plasma, also known as thermal plasma, with almost equal temperatures of electrons and ions.

(ii) Non-equilibrium plasma, known also as non-thermal plasma, in which the electrons are hotter than the ions but the gas temperature remains or much lower than the atmospheric pressure and ambient temperature.

Whereas corona discharge, streamer discharge and glow discharge are non-equilibrium plasmas, the arc discharge can be in either state. In an equilibrium or thermal plasma, electrical energy heats the gas to very high temperatures (which can be in excess of 20,000 K) [47], and most thermal plasma applications are therefore in areas such as arc welding and plasma torches. In a non-equilibrium or non-thermal plasma, the energy is used to excite and dissociate molecules and atoms to form highly reactive species. Non-thermal plasma applications are thus based on the utilization of active species, either to enhance chemical reactions or to utilize the intense radiation from such sources. The study described in this thesis focuses on non-thermal plasma for ozone generation.

2.2 Gas breakdown at moderate and high pressures

Breakdown can be defined as the transformation of a non-conductive medium into a conductive one, when a sufficiently strong electric field is applied. The relation between creation and removal of charge carriers under specific conditions determines the breakdown threshold [46] and the time to its onset. The time lag of the breakdown is given by the sum of the retardation time and the formative time. Retardation time depends on the probability of having primary electrons between the electrodes that are able to begin multiplication. It also depends on the discharge geometry, e.g. in very narrow gaps it can be up to 100 times longer than in wide gaps at the same pressure, with typical values being of the order of 10^{-5} - 10^{-3} s. Formative time is the effective time to buildup the current and it usually varies between 10^{-8} s and 10^{-4} s, depending on the processes responsible for electron multiplication [46].

In the Townsend theory of breakdown, charge carriers are produced by volume processes, described by the ionization coefficient α and by surface processes characterized by the secondary emission coefficient γ. For initiating a self-sustaining discharge, one primary electron lost at the anode has to be replaced by at least one secondary electron created in the gas or at the cathode. For a homogeneous electric field the condition for a self-maintaining discharge is [48,49]:

$$\gamma.[\exp(\alpha d)-1] = 1 \text{ or } \alpha d = \ln(\gamma^{-1} + 1) \qquad (2.1)$$

where d is the distance between the electrodes. While α and γ are the 1st and 2nd Townsend coefficients respectively.

The coefficient α gives the electron multiplication in the gas, i.e. the average number of ionizations induced by an electron per unit length in the direction of the electric field. It is a function of the reduced electric field, E/p or E/n (E is the electric field, p the gas pressure inside the discharge volume and n the number density of the background gas). From Townsend's semi-empirical relation [48]:

$$\alpha = Ap \exp(-Bp/E) \qquad (2.2)$$

where the constant A and B are specific to a given gas.

In discharges operated in mixtures of noble gases or electronegative gases, like oxygen or the halogens, the coefficient α has to be replaced with α_{eff}, given by:

$$\alpha_{eff} = \alpha - a \qquad (2.3)$$

where a is the electron attachment coefficient , which is also E/p dependent.

The coefficient γ describes the processes that take place at the gas-cathode interface and it represents the ratio of secondary electrons released per incident particle on the cathode surface. It depends on the material of the cathode, the gas and on the reduced electric field. The effective secondary electron emission coefficient includes the effect of ions γ_i, fast neutrals, especially metastable atoms γ_m and photons γ_p, and it can be written [45]:

$$\gamma = \gamma_i + \gamma_m + \gamma_p \tag{2.4}$$

At low pressures, secondary electron production is caused mostly by ions impinging on the cathode surface, while at high pressures the metastable atoms and photons also play an important role [48].

In addition, the space charge can also enhance electron multiplication, by distorting the local electric field. Space charge effects are described by a coefficient σ, but its influence can be neglected in the early stage of the breakdown.

Taking into account the dependence of both α and γ on the reduced electric field, combining (2.1) and (2.2) and (if the electrodes are plane-parallel) writing $E = V_b/d$, enables the breakdown voltage V_b (ignition potential) to be obtained as [48] (see appendix 2 for detail):

$$V_b = \frac{Bpd}{\ln(Apd) - \ln\left(\ln\left(1+\gamma^{-1}\right)\right)} \tag{2.5}$$

The dependence of the breakdown voltage on the product pd is shown by the so-called Paschen curves of Figure. 2.1 .

On the right-hand side of the curve, it can be observed that the breakdown voltage increases as the pd increases, since, for relatively large pd (i.e elevated pressures and large gaps), the probability that an electron produces ionization is very high, even at moderately reduced electric field. On the left-hand side the breakdown voltage rises steeply as pd decreases, since at small pd (i.e low density of neutrals and short gaps) the possibilities for ionizing collisions are very limited, and a strong field is required to achieve the necessary amplification. Hence the

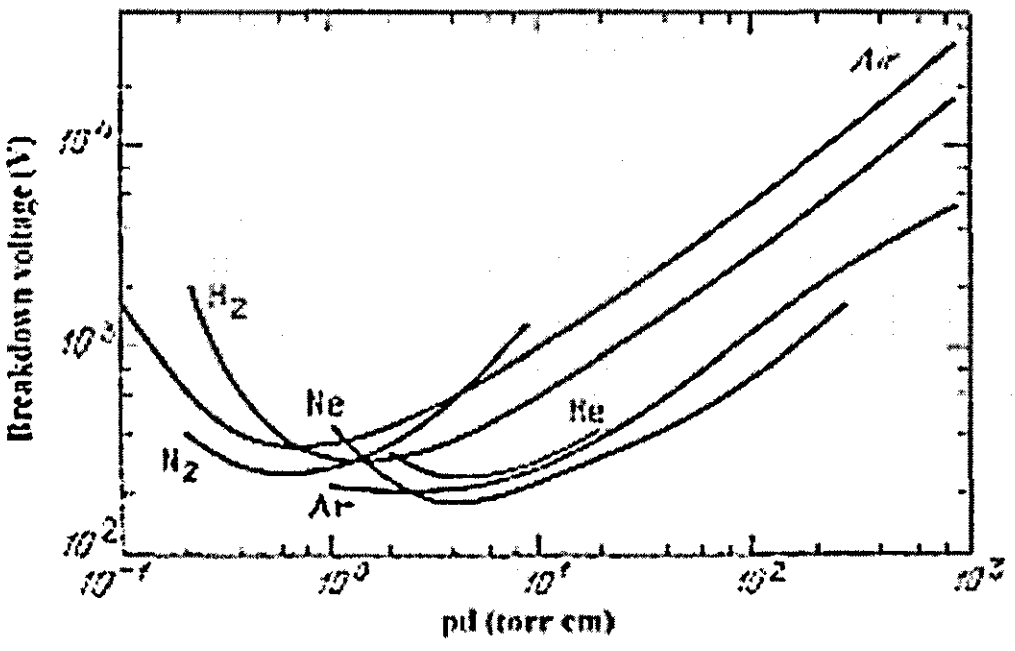

Figure 2.1: Experimentally obtained Paschen curves in various gases [46].

breakdown voltage exhibits a minimum at which the ionizing capability of electrons is a maximum, and around this point the conditions for breakdown are most favorable because the conditions for multiplication are optimal. Paschen curves like those presented in Fig. 2.1 have been experimentally obtained for planar electrode geometry [46] and relatively low pressures, and in particular situations they therefore serve only as a guide line.

If the electrode gap is not too large and the electric field is homogeneous, the Townsend mechanism dominates even at high pressures, for pd values up to about 1000 torr·cm. For large gaps and high pressures a strongly conductive channel is formed, and the conditions which are responsible for the breakdown are dominated by the spark mechanism [46].

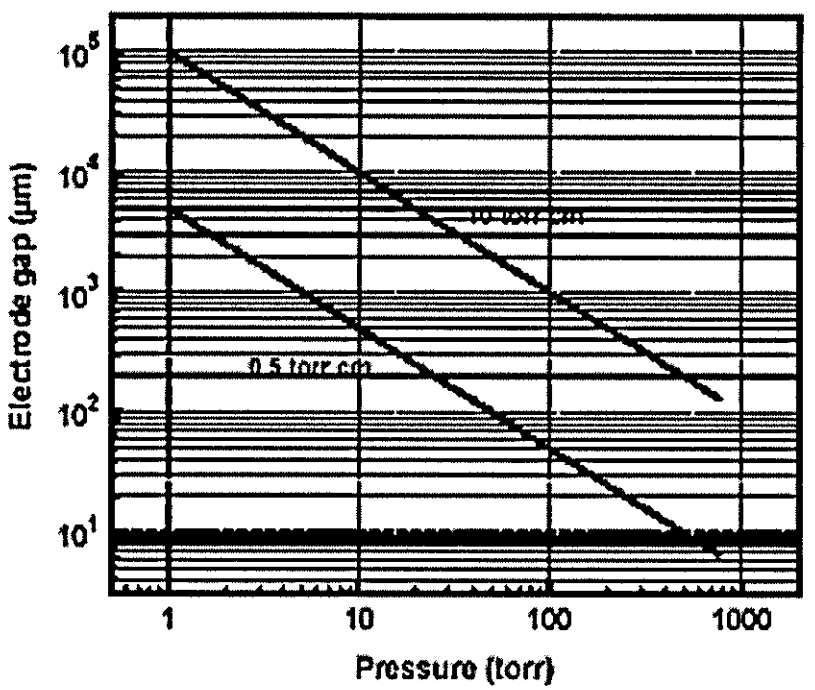

Figure 2.2: Electrode gap as a function of pressure at constant pd.

For high-pressure operation, the electric field necessary to induce breakdown can be achieved either by increasing the applied voltage or reducing the dimensions between the electrodes. The use of moderate voltages offers advantages in respect of potential applications. If a Townsend breakdown mechanism is assumed, one way to generate high-pressure plasma is to apply the scaling law *pd* = *constant* [46]. This dependence is plotted in Fig. 2.2 for values of the product pd corresponding to the minimum ignition potential. In order to produce breakdown at atmospheric pressure at moderate applied voltage, the distance between the electrodes has to be about 100 µm [46].

The minimum values of the voltage and the product pd to induce breakdown are dependent on the gas (α) and the cathode material (γ). From Fig. 2.1 it can be concluded that, in either noble gases or in air, and for copper electrodes, the voltage required for breakdown is less than 500 V at pd products ranging from 0.5 to 10 torr·cm.

2.3 Theory of non-thermal plasma

It has been mentioned before that plasma processing can be categorized as either thermal or non-thermal. A thermal plasma contains electrons, ions and neutrals in thermodynamic equilibrium. Such plasmas are formed in the reduced field E/p or E/n regime, in areas of high pressure or low field. Since the background gas is usually at a very elevated temperature (1000s of K) such plasmas are also called 'hot' plasmas [50], and flames and high pressure DC arc discharges are typical examples. No work has been done to date using thermal plasmas for ozone production, because the efficiency is often very low. Considerable energy is dumped into the background gas, increasing the temperature inside the discharge chamber and leading to decomposition of the ozone.

On the other hand, non-thermal plasmas are those in which the mean electron energies are considerably higher than those of the components of the ambient gas. This kind of plasma is termed a 'cold' or low temperature plasma (LTP), with most of the electrical energy going into the production of energetic electrons rather than into gas heating [4,50]. Cold plasmas are characterized by electrons with kinetic energies much higher than those of the ions or molecules, and the electrons are short-lived under atmospheric conditions. They undergo collisions with the dominant bulk-gas molecules and have a mean energy between 1 and 20 eV. This is an energy range in which electrons can very effectively transfer their kinetic energy into internal energy of the molecules they interact with (i.e oxygen or air). The energy in the plasma is thus directed preferentially to the electron-impact dissociation and ionization of

the background gas to produce a mix of reactive species. This plasma is in the form of radicals, ions and secondary electrons that, in turn, initiate plasma chemical reactions even at relatively low temperatures [50,51], and it can be produced, for example, by a high voltage electrical discharge. Since the electrical energy is directed primarily into increasing the motion of the electrons, these can be used for a number of purposes, mostly dealing with initiating desirable chemical reactions in bulk gases or liquids, or on the surfaces of solids. Gas phase electrical discharges have in fact been used commercially for the production of ozone for many years.

2.4 Electrical Discharges in Ozone Production

Most common methods of producing ozone use an electrical discharge. The techniques widely employed produce much higher concentrations than the UV method, and they are more practical and efficient for large scale production.

Ozone is produced by the electric discharge occurring when a high-energy electric field exists between two conductors separated by a dielectric and a discharge gap, and with a gas containing oxygen passing between them. The high electric field causes an electron flow-through across the discharge gap, providing energy that dissociates the oxygen molecules and leads to the formation of ozone.

In an ozone generator, the feed gas (air or oxygen) passes between two closely space electrodes, one of which (usually the high-voltage electrode) is coated with a ceramic or glass dielectric to prohibit a complete breakdown. Normally a potential of around 10 kV is applied to the high-voltage electrode, resulting in the gas becoming partially ionised and a blue/violet glow appearing in the gap (silent or glow discharge). Such discharges consist of numerous randomly distributed low current micro-discharge pulses. Filamentary streamers are produced, 100 to 200 μm in diameter, emanating from the dielectric surface and being extinguished within 10 ns [8].

Because ozone formation only occurs within these micro-discharge channels, ozone production efficiency is dependant on the strength of the micro-discharge channels, which in turn are affected by the gap geometry, the electrode and dielectric properties, the voltage level, the pulse frequency etc. In weak discharges, a significant fraction of the energy is consumed by the ions, whereas, in stronger discharges, almost all the discharge energy is transferred to electrons responsible for the formation of ozone. The optimum is a compromise that avoids energy losses to ions but at the same time obtains a reasonable conversion efficiency of oxygen atoms to ozone [8].

The energy supply employed in commercial ozone generators varies with the design, and it can be either DC, AC or pulsed. Typical operating voltages are 5 to 40 kV at frequencies between 50 and 500 kHz [8,52]. Typically, high-frequency ozone generators operate at lower voltages, where the expected lifetime of the high voltage electrode system is virtually unlimited. Although a lower voltage decreases the ozone production rate, when combined with high frequency it can produce more ozone per unit electrode area.

Basically, the generation of ozone using an electric discharges can be categorized into several common discharge phenomena as follows;

i) Corona discharge.
ii) Dielectric barrier discharge.
iii) Surface discharge
iv) Atmospheric pressure glow discharge
v) Pulsed streamer discharge

and these are all dealt with below.

2.4.1 Corona discharge

Corona discharge is a localised discharge process using a DC voltage supply. Corona discharges are relatively low power (less than 100 W) and occur at or near atmospheric pressure. They are characterised by very low current (10^{-10} A – 10^{-5} A) and very high voltage (2 kV-5 kV) [47], and they normally take place in the Townsend dark discharge region [13]. The current that flows has a small component due to electron/ion drift across the gap, and a larger contribution due to displacement current. The corona is invariably generated by strong electric fields associated with small diameter wires, needles, or sharp edges on an electrode as shown in Fig. 2.3. The electron energy to cause ionisation is roughly between 3 eV and 5 eV [50].

The corona is weakly luminous, appearing as a faint filamentary discharge radiating outwards from the discharge electrode. In corona discharges at relatively low voltages the discharge is self limiting, due to the build up of space charge near the sharp electrode [53].

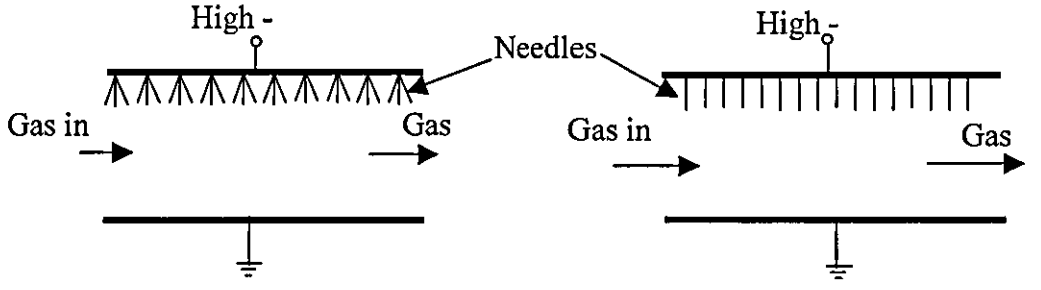

Figure 2.3 : Typical corona discharge arrangement, a multipoint-to-plane reactor .

This space charge soon disappears due to diffusion and recombination, and a new discharge pulse appears. The process is self-repetitive corona or a self-sustained partial breakdown of the gas in the highly non-uniform field around the stressed point, and it occurs in both positive and negative corona.

For positive corona in a point-to-plane electrode configuration in air, a steady current flows, which increases with voltage and can reach 5×10^{-4} A before the device begins to arc [47]. Electrons produced in the vicinity of the point, form avalanches towards the point. These give current multiplication, that increases rapidly with voltage, after which the current takes the form of pulses known as burst pulse corona with a repetition frequency about 1 kHz [53]. The average current then increases steadily with voltage until the discharge becomes self-sustaining. As the voltage increases, the pulses are connected with streamers starting from the point and moving towards the plate. Increasing the voltage further will increase the average current, and this will change the streamer to a glow-like discharge. The self-sustaining current is typically several microamperes, increasing with voltage until breakdown into a high-current discharge produces a spark [49]. This phenomenon can be clearly observed in Figure 2.4 [53].

For negative corona in the same geometry, the corona current again flows in pulses, which increase in repetition frequency with current at the rate of about 5 kHz per 1 μA at atmospheric pressure, the figure decreasing for lower pressures. Since negative corona depends upon secondary emission from the (cathode) point itself, a criterion for self-sustenance can be formulated in terms of γ and α -the latter being a function of distance. But it is not certain that the γ-process is essential to the pulses, since experiments have shown that the choice of electrode material does not appreciably affect results [49]. At high field strengths the pulses are irregular and separate glow-like structures are visible, known as trichel pulse corona, corresponding to the non-uniform appearance of corona on a negative wire, followed by pulseless corona (streamers) appearing between the surrounding glow and the point and spark discharge (Figure 2.4b) as the applied voltage is increased [49,53].

It is well known that the polarity of the discharge electrode has a great influence on the ozone generation rate, with very much higher rates associated with negative polarity [13,52]. This can be explained by the fact that the non-thermal plasma generated by negative corona is richer in energetic electrons

than that generated by positive corona [13,52]. Moreover, negative corona provides lower sparking potential than does positive corona and the current is relatively stable [53]. However, positive corona has longer current filaments than does negative corona, and its plasma volume is therefore greater.

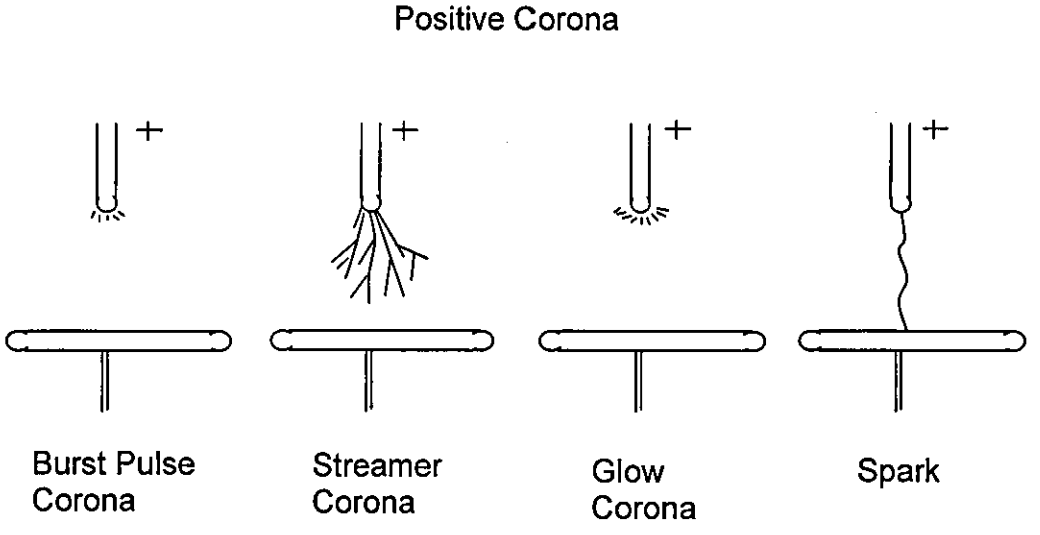

Figure 2.4: Point-to-point electrode configuration with, a) positive corona and b) negative corona. [53]

Unfortunately, although corona sources have the advantages of physical robustness, geometric simplicity, and an ability to operate at 1 atm and low input power, the energy efficiency is low by comparison with other discharge techniques, and it is therefore unsuitable for large scale industrial applications.

One reason for this is that the applied DC voltage is limited by the flashover voltage of the gap, which usually constrains the ratio of the electric field to the gas number density to a value too low to achieve high generation efficiency. This is known to be related to an inability to produce a range of energetic active species that generate free radicals such as ozone [17].

2.4.2 Dielectric barrier discharge

The most common method of ozone generation is by AC corona discharge , and is well known as a dielectric-barrier discharge. These discharges are characterised by the presence of one or two dielectric layers in the current path between metal electrodes, in addition to the discharge space. Different planar or cylindrical configurations are common, as shown in Figure 2.5, and although they can be operated between line and microwave frequencies, the typical operating range for most applications lies between 500 Hz and 500 kHz [8].

Gas spaces bounded by one or two dielectrics have practically the same breakdown voltage as if they were between metal electrodes. Typical gap spacings vary from less than 10 mm to several cm. For atmospheric pressure discharges gap spacings of a few mm are common, which require alternating driving voltages with amplitudes of typically 10 kV. Low loss dielectrics of high breakdown strength such as glass, quartz or ceramic plates or tubes are used, with metal electrode coatings applied to the outer surface [11].

In most gases at about atmospheric pressure, gas breakdown discharges are initiated in a large number of independent current filaments or microdischarges of submicrosecond duration per cm^2 [8]. Fast image intensifiers reveal that

each micro-discharge consists of a cylindrical current filament of about 100 μm radius in the discharge gap, which spreads into a surface discharge at the dielectric boundry [8]. In addition, the current densities can reach 1000 A/cm^2, with a total charge of 0.1 to 1 nC and an electron density of 10^{14} to 10^{15} cm^{-3} in a short micro-discharge channel of 1 to 10 ns duration [8,11]. This normally results in very little transient gas heating in the remaining channel. It is well known that the separation of the two electrodes, humidity, gas composition, gas pressure, thickness of the dielectric and the power supply all have a strong influence on the strength of the micro-discharges [3,50].

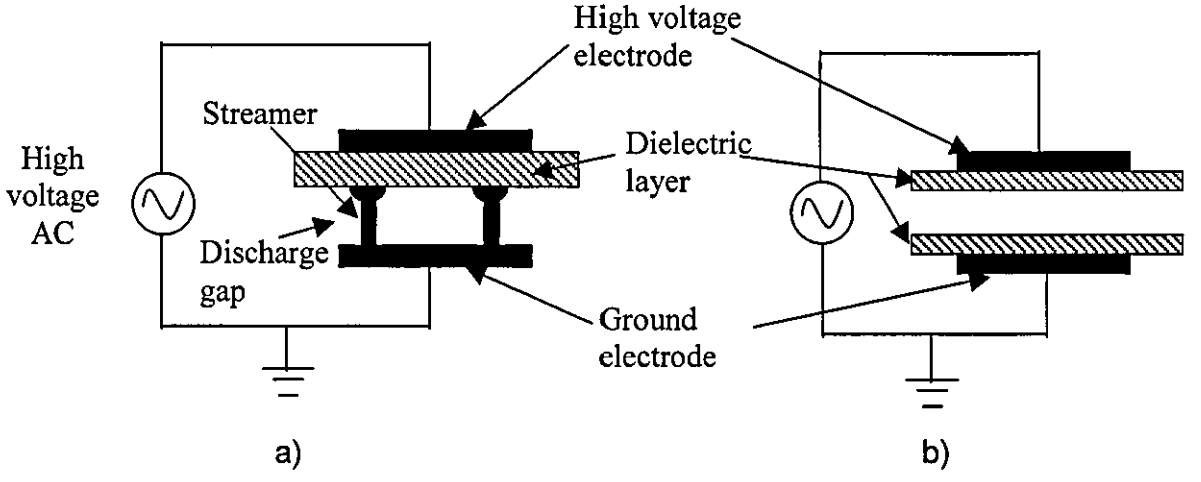

Figure 2.5: Dielectric-barrier discharge planar configurations [8]

Micro-discharge filaments can be characterized as weakly ionized plasma channels, with properties resembling those of transient high pressure glow discharges [8,11]. They ignite when the breakdown field is reached and are extinguished not far below the same field value, when electron attachment and recombination reduce the plasma conductivity. Due to charge build up on the dielectric, the field at the location of micro-discharges is reduced within a few ns after breakdown, thereby terminating the current flow at this location. The dielectric barrier limits the charge and energy deposited in a micro-discharge and distributes the micro-discharges over the entire electrode surface [8,11]. As long as the external voltage is rising, additional micro-discharges will occur at new positions, because the presence of residual charges on the dielectric

reduces the electric fields at positions where micro-discharges have already occurred. When the voltage is reversed however the next micro-discharges will form at the old micro-discharge locations. High-voltage low frequency operation thus tends to spread the micro-discharges, while low-voltage, high-frequency operation tends to re-ignite the old micro-discharge channels every half period.

2.4.3 Surface discharge

Surface discharge is a further localised discharge mechanism, similar to corona discharge. The basic configuration is a thin dielectric layer sandwiched between two metal electrodes, e.g with small but long high voltage electrodes in parallel (wires, bars, stripes) on one side of a dielectric layer and a plane counter electrode on its reverse side (Fig. 2.6). This interfacial phenomenon is featured by a very thin ionised atmosphere limited to the vicinity of the solid surface, and gas molecules can be directly excited in this region. Although the optimum thickness of the ionized region has not so far been confirmed, it is thought to be as small as that of the electrode [54]. Unlike other kinds of discharges, the ionized atmosphere is therefore limited to a very narrow region.

The potential distribution in a surface discharge is non-homogeneous, with the highest field strength being in the region where the surface electrode, dielectric and gas regions come together (i.e the triple junction line). With increasing distance from the triple junction line, the potential distribution and field strength along the dielectric surface decreases [15,54].

When a fast-rising voltage pulse is applied to the narrow electrode, a discharge will develop across the dielectric surface. It begins in the region where the surface electrode and dielectric meet, because of the high local longitudinal field in this region.

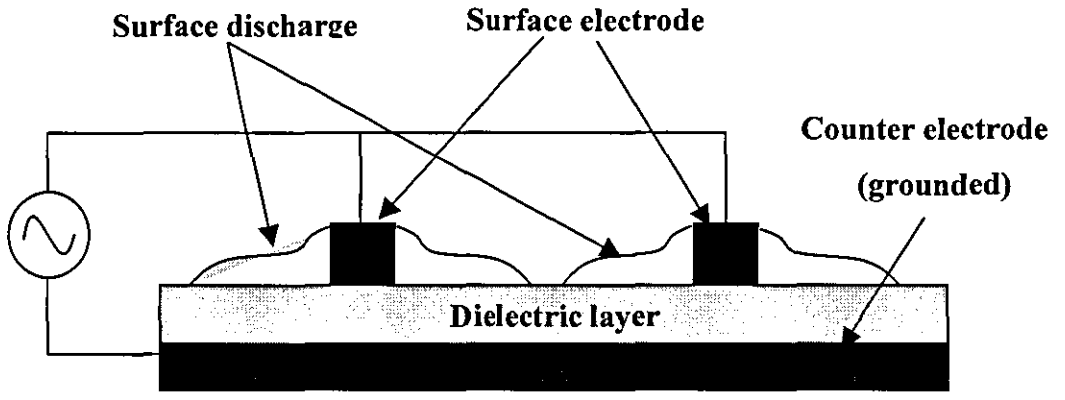

Figure 2.6: Configuration of the surface discharge device [15,54].

Because of the short rise time of the discharge pulses (in the order of several nanoseconds at atmospheric pressure) the shape and the rise time of the applied voltage have almost no influence on the properties of the discharge at any power supply frequencies [15,54].

The great advantage of this discharge technique is its cooling effect. In plasma chemical reactions such as ozone synthesis, heat is generated in either an endothermic or an exothermic reaction, which will increase the temperature inside the discharge volume and lead to destruction of the ozone. Removal of the heat produced by plasma is clearly an extremely severe problem during ozone synthesis, and the use of surface discharge is one promising solution [57]. As mentioned above, because the ionised gas is in close contact with a solid surface combined with a cooling system, the ionised atmosphere can effectively be cooled. However, a surface discharge technique still produces less ozone than other discharge techniques and needs further improvement to achieve an acceptable efficiency of ozone production. This is related to an inability to generate the high electric fields inside the discharge volume that can produce a range of energetic electrons to generate ozone. However, due to its cooling effectiveness, further research to improve the efficiency, including combination with other discharge techniques [6] is ongoing.

2.4.4 Atmospheric pressure glow discharge

Glow discharge is a plasma in which a partially ionized gas consists of nearly equal concentrations of positive and negative charges and a large number of neutral species. It is formed either in a cell filled with gas (inert or molecular) at low pressure or in a gas gap at atmospheric pressure, between two parallel plate electrodes covered with dielectric plates. By applying a potential difference between two electrodes, which can either be inserted into a cell or form the cell walls, a glow discharge plasma is created. Because of the potential difference, atoms of the discharge gas are ionized to yield free electrons and positively charged ions, which is called 'gas breakdown' [55].

Glow discharge can occur at either low pressure or at atmospheric pressure. The theory of the glow discharge in the low-pressure regime was developed at the beginning of the last century and is well established. Glow discharges have been used in many application, such as in the processing of materials ranging from silicon wafers to magnetic storage disks, light sources and thin film coatings [23,24]. Their advantages include a homogeneous discharge over a large volume, low breakdown voltage (500 V in helium), a high electron temperature capable of dissociating gas molecules (1–10 eV), low temperature and high concentrations of both ions and radicals [27,56,57]. To date, however, no work has been conducted on using low-pressure glow discharge for ozone generation. This may be due to a major practical limitation, in that the requirement for vacuum operation necessitates the use of expensive and complicated vacuum systems.

On the other hand, the production of atmospheric glow discharges has a long history. In 1933 Von Engle et al [28] reported producing such a discharge with bare electrodes in air and hydrogen, with both DC and audio frequency RF driving voltages. The discharge was however unstable in the glow-to-arc transition, required specially cooled cathodes, and could only be obtained at atmospheric pressure by slowly raising the pressure from vacuum level.

Recent development [24-29,58-60] have however, demonstrated a crucial advantage of atmospheric-pressure glow discharge over low-pressure glow discharge, in that complications introduced by the need for a vacuum are eliminated.

Glow discharge at atmospheric pressure is characterised by one single current pulse per half period of several ns duration and some tens of milli-ampere amplitude [58]. The amplitude of the positive current and the negative current pulse may be different, but the current waveform is the same. It is assumed [59] that the current pulse is due to a sudden discharge of the dielectric barrier as soon as the breakdown voltage of the gas gap is reached. The spatial distribution of the electric field and the ion and electron densities are similar to those in a low pressure glow discharge.

Atmospheric pressure glow discharges will provide interesting new possibilities if reliable control and average power densities comparable to those of filamentary discharges can be achieved. In practice however considerable research is still required to guarantee the production of a stable glow discharge at atmospheric pressure, and to ensure that it does not change to a filamentary condition. In general, the atmospheric pressure glow discharge is thought to be stable only if three simple requirement are fulfilled: (i) use of a source frequency over 1 kHz (ii) insertion of dielectric plates between the two metal electrodes, and (iii) use of a helium dilution gas [24,29]. However, available evidence [26,27,59,60] suggests that proper design of the discharge gap (less than 3 mm), replacing the plane electrode by a wire mesh, correct selection of the input voltage and dielectric barrier materials (Mylar, high purity alumina ceramic), as well as the gas flow rate (0.5–8 l/min), will enable a homogeneous discharge to be obtained, even with the use of air or oxygen as an input gas and a supply frequency of 50 Hz.

There are certain advantages that have been identified in using atmospheric pressure glow discharge for ozone generation, i) due to its homogeneity, the ionization process by electron impact takes place uniformly throughout the entire discharge volume, generating very many oxygen atoms which combine

with oxygen molecules to generate ozone, and ii) a low power consumption of less than 100 W. The literature reveals that use of this technique for ozone generation enables an increase in the production efficiency to about 10% in air and 15% in oxygen, which is higher than by the silent discharge technique [25].

2.4.5 Pulse streamer discharge

A pulsed streamer discharge is created by applying a series of fast-rising, high voltage pulses to a field-enhanced geometry, such as the coaxial wire-cylinder configuration of Fig. 2.7. The pulses are formed by charging a capacitor and quickly releasing the stored energy to the reactor in nanoseconds through a fast closing switch, such as a high-pressure hydrogen spark gap or a rotating spark gap [61]. Applying these pulses generates a number of streamers within the gas volume that emanate from the wire or electrodes to the cylinder.

The fast voltage rise times (less than 100–200ns) from the pulsed power supply result in high electric fields before the onset of corona, while the short decay times (less than about 1-10 μs) reduce the movement of ions, reducing the likelihood of sparks forming in the high fields [62]. The high electric fields (greater than 10–20 kV/cm) that exist at the onset of corona produce higher average electron energies than can be achieved in DC coronas, and are thought to lead to the formation of larger numbers of energetic species and free radicals than DC coronas [2,62]. This means that high electric fields can be applied during the duration of the pulses, without causing spark breakdown in the reactor. Higher electric fields thus indirectly produce a higher number of streamers, and a higher number of collisions with electrons to produce more atomic oxygen, which in turn will increase the production of ozone [4,7,19-21]. Since the reaction for ozone formation is separated from the decomposition reaction by a long pulsed interval, the efficiency of the ozone yields is high.

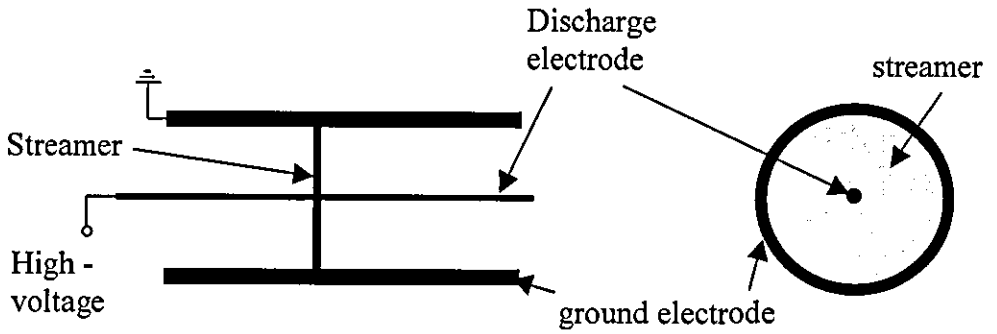

Fig. 2.7 : Typical pulse corona discharge from wire-to cylinder arrangement

Streamers yield good power efficiency due to the very short lifetime of the high voltage pulses, with or without the use of a solid dielectric between the electrodes [63]. The ions do not experience significant movement during this short lifetime and hence do not contribute to the power consumption. Chemically active species or radicals formed by high energy electrons contained within the discharge can then preferentially react with the background molecules, oxygen or air, to generate ozone [63].

A pulsed streamer discharge can be used to decrease ionic motion in the plasma. If the pulse is sufficiently short, only the electrons in the plasma respond appreciably to the field and the ions are effectively stationary. Since ionic motion does not assist most of the desired reactions, any energy added to this channel is wasted. As mentioned previously, the pulsed streamer discharge also decreases the probability of sparking at a given field strength. Electric fields above the DC critical sparking field can thus be applied to the gap without its breaking down (due to the limited time available for ion motion), thus generating higher average electron energies, higher electron densities, and higher radical densities [2,7,18]. Therefore, higher ozone production yields can be expected.

In general, the pulsed streamer discharge technique is a promising type of high-voltage discharge that can be controlled and has many interesting environmental applications. It is a non-thermal plasma processes in which a majority of the electrical energy goes into the production of energetic electrons,

rather than into gas heating. Since only the electrons, and not the back ground gas and ions are heated, the temperature inside the chamber can be maintained at ambient temperature and no cooling device is necessary [2,4,7,17-19].

2.5 Summary

To assist with a basic understanding of gas discharge, both thermal plasmas and non-thermal plasmas have been defined and the theory of non-thermal plasmas has been discussed. The different types of electric discharges commonly used for ozone generation has been explained. In this present study however, only atmospheric pressure glow discharge and pulse streamer discharge are be studied in term of their efficiency of ozone yields and ozone concentrations and the results of the study are discussed in later chapters.

CHAPTER 3

REVIEW ON THE EFFECT OF PRINCIPAL PARAMETERS ON OZONE PRODUCTION

3.1 Introduction

It is well known that the actual yield of ozone in any production process is far below the theoretical limit, and that this is influenced by several principal parameters. The effect of both the physical configuration and the electrical parameters therefore need to be studied to identify their effects on the ozone yield and concentration. This is undertaken in the present chapter, for both atmospheric pressure glow and pulsed streamer discharges.

3.2 Inlet gas quality (air or oxygen).

The preparation and nature of the feed gas to an ozone generator has an obvious influence on both the quality and the quantity of the generated ozone. For many older generators, efficiencies of between 40 and 100 g/kWh were reported [65], depending very much on the preparation and the nature of the feed gas and, of course, on the desired ozone concentration. Theoretically the generation efficiency that can be achieved using oxygen is 1220 g/kWh, against 400 g/kWh for pure air [8,64]. In practice, modern ozone generators approach values between 200 and 274 g/kWh in oxygen [2,3,10,17,18,65,66] and between 9 and 127 g/kWh in air [4,9,21,67] at low ozone concentrations.

The concentration of ozone in a generator can range between 8% and 20% (by weight) in oxygen [2,3,66] and between 3% and 6% in air [4,21,67].

The work presented in this thesis concentrates almost exclusively on ozone generation in dry air. Using air as a feed gas is inexpensive, although it gives only low yields and concentrations in comparison to pure oxygen. The experimental facilities available for a laboratory investigation inevitably produce smaller amounts of ozone than do commercial units, and the present aim is therefore to compare the effectiveness of the atmospheric pressure glow discharge and pulse streamer discharge in a small discharge chamber. Bottled compressed air that is 90% dry is adequate for the purpose and does not require a complicated air preparation system, unlike commercial systems in which incoming air must be properly conditioned to prevent damage to the generator. This preparation is critical to the efficient and reliable operation of commercial ozonators and, depending on the ozone capacity, it will be designed as either a low or medium pressure unit. The component of a unit are compressor(s), after cooler(s), refrigerant dryer(s), filters and heat regenerated adsorber dryer.

The requirements placed on such a treatment plant using an air-fed are :

i) Removal of dust particles.
ii) Compression to the required operating pressure i.e atmospheric pressure.
ii) Drying to a residual humidity corresponding to an atmospheric dew point of at least - 60°C

Moisture and particulate matter have a detrimental effect on both the generation cell electrodes and the dielectric material. Moist air will cause nitric acid to form, both decreasing the ozone production and corroding the generation cell components. Because ozone is such a powerful oxidizer, it will also oxidize nitrogen (N_2) in the air to nitric oxide (NO_2), and the moisture will reacts with this to produce both nitrous (HNO_2) and nitric (HNO_3) acids that are again highly corrosive to the electrodes, piping and other components of the ozonation system. The following reactions involving destruction of ozone have been reported as occuring in air feed systems [21,41]

$$N + O_3 \rightarrow NO + O_2 \quad (3.1)$$

$$NO_2 + O \rightarrow NO + O_2, \quad (3.2)$$

$$NO + O_3 \rightarrow NO_2 + O_2 \quad (3.3)$$

$$NO_2 + O_3 \rightarrow NO_3 + O_2 \quad (3.4)$$

$$N_2 + O_3 \rightarrow N_2 + O_2 + O \quad (3.5)$$

The supply gas used for ozone production (either air or oxygen) has a recommended maximum dew point of -60°C [68]. Moisture measurement is desirable in ozonizers because, at higher dew point temperatures, the efficiency of the ozonizer is reduced, and less ozone is produced from the same electrical discharge. For example, raising the dew point from -60°C to -50°C can mean as much as a 15% decrease in the production efficiency [67].

To eliminate problems due to moisture, the air is dried prior to entering the generator. This increases the concentration of oxygen and/or reduces the moisture content in the feed gas, improving the output capability of the ozone generator. It also helps to control the long-term maintenance costs. Air preparation systems fall in the two general categories described below:

i) Air dryer

Two basic types of air dryers are currently available: replaceable dessicant dryers that are relatively inexpensive but require regular replacement of dessicant and pressure-swing absorption dryers that produce drier air but are mechanical and require more maintenance. Air dryers do not significantly increase the output of the ozone generator, but they are effective in drying the feed gas to a dew point of -60^{o} C.

ii) Oxygen concentrators

Oxygen concentrators dry the feed gas to a -37.8 °C dew point and remove a large percentage of the nitrogen. This increases the concentration of oxygen, leading to an improved ozone output and concentration. Depending on the type of generator, the concentration of ozone by weight can be increased.

For efficient ozone generation, the final air supply must be filtered to remove particulate matter and any oil or hydrocarbons which may carry over from the compressed air system. Particles greater than 1 μm and oil droplets greater than 0.05 μm need to be removed [67].

However, for higher concentrations, oxygen is generally selected, which reduce the power consumption from 18-20 kWh/kg to 6-7 kWh/kg [64]. Many oxidation reactions require higher ozone concentration, in which cases oxygen fed generators are automatically selected. The main reactions in oxygen feed ozone generators are shown below [5]:

Creation	Destruction
$e + O_2 \rightarrow O + O + e$	$O + O_3 \rightarrow 2O_2$
$e + O_2 \rightarrow O + O^-$	$O + O + M \rightarrow O_2 + M$
$O + O_2 + M \rightarrow O_3 + M$	$O_3 + e \rightarrow O_2 + e$

(3.6)

Most ozone generators use either a bulk liquid oxygen supply (LOX) or a pressure-swing adsorbtion (PSA) oxygen concentrator. PSA oxygen concentrators have improved significantly over recent years and they now are able to provide reliably up to 95% oxygen purity. The equipment can also be very cost effective, in areas where liquid oxygen deliveries are expensive.

3.3 Electrical Parameters

3.3.1 High voltage input.

The effect of the amplitude of applied voltage on the ozone generation rate has been investigated for both pulse streamer discharge [4,21] and atmospheric pressure glow discharge [28] technique. The apparent effect of increasing the voltage is to increase the electric field strength inside the discharge volume, with this being expressed for a dielectric barrier discharge configuration [68] by.

$$E = \frac{V - (x\sigma / \varepsilon_o \varepsilon)}{d + (x / \varepsilon)} \qquad (3.7)$$

where

σ = density of the surface charge

ε_o = input gas permittivity

ε = dielectric constant

d = gap distance

x = thickness of the dielectric

V = applied voltage

Any increase in the applied voltage results in an increase in the electric field strength in the discharge volume. Gas breakdown will take place when the applied voltage reach an onset voltage which clearly depend on the gas pressure and gap space, as shown in figure 3.1 [69].

At the onset voltage, dissociation of oxygen molecules occurs and atomic oxygen is generated. This then recombines with oxygen molecules to produce ozone [69]. The ozone concentration will increase at a slow rate, up to a certain current density (or applied voltage). It then tends to increase more rapidly up to a certain limit, which depends only on the characteristics of the micro-discharge produced in the dielectric discharge.

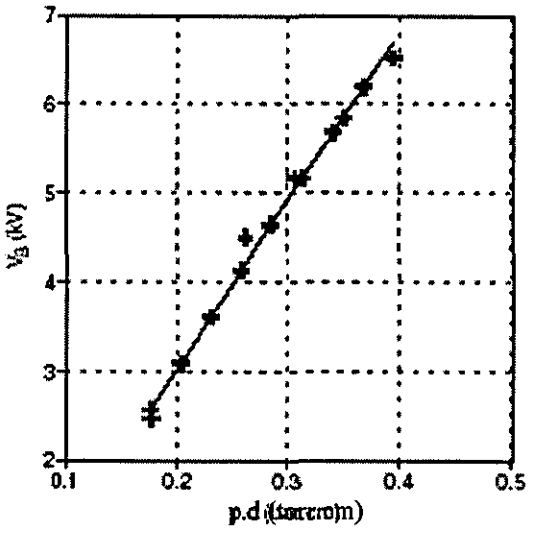

Figure 3.1: Relation between breakdown V_B and product pd, gap space d = 1.75 mm. [69].

The reduction in the rate of increase of the ozone concentration can be explained by noting that, as the concentration increases, the probability of its dissociation also increases. At higher applied voltage, the increased electric field strength leads to an increase in the electron energy. Instead of the reaction with the oxygen molecule continuing, the energetic electrons react instead with the generated ozone, resulting in a decrease in production. The ozone can be destroyed through collision with either electrons or atomic oxygen, according to the reactions [3,8,64,69];

$$e + O_3 \rightarrow O_2 + O + e \qquad (3.8)$$

$$O + O_3 \rightarrow O_2 + O_2 \qquad (3.9)$$

Atomic oxygen, which is the source of ozone, can be destroyed at high atomic oxygen density, according to the reaction

$$O + O + M \rightarrow O_2 + M, \qquad (3.10)$$

where M stands for a third body or the walls of the discharge cell. In addition, the energy dissipated in micro-discharge at high current density leads to an instantaneous local temperature rise, which may cause a significant dissociation of the ozone molecules.

The efficiency of the system (ozone yield) for ozone generation η, as given by Yagi and Tanaka [67] is

$$\eta = \left[\frac{C(O_3) f_r}{P}\right] \qquad (3.11)$$

where η is the efficiency (g/kWh), $C(O_3)$ is the ozone concentration (ppmv), f_r is the gas flow rate (l/min) and P is the electric power consumption in the discharge (kW). The parameters $C(O_3)$ and f_r are directly measurable, while parameter P is determined from equation (3.13) below or directly from the well-known Lissajous figure [64,70]

3.3.2 Applied frequency and pulse repetition frequency

Ozone generators are classified by the frequency of the power fed to the electrodes. Low frequency (50 or 60 Hz) and medium frequency (60 to 1,000 Hz) generators are most commonly used, although some high frequency generators are also available. In general, increasing the frequency improves the production rate of a generator, and properly designed corona discharge generators that utilize medium frequencies (300 Hz to 1000 Hz) are favoured because greater production is achieved with less electrode surface area and less energy consumption [5,11]. Modern high-power generators utilize thyristor-controlled frequency converters to supply square-wave currents in the medium frequency range between 500 Hz and 2000 Hz at voltages between 5

and 10 kV. The relatively low voltage results in less electrical stress on the dielectrics. Although medium and high frequency generators are efficient and can produce ozone economically at high concentration, they have limitations in that they generate more heat than do low frequency generators. Because of the adverse impact this has on ozone production, adequate cooling needs to be provided. Another limitation of medium and high frequencies is that they require a complicated power supply to step up the mains supply frequency, and both limitations involve a high cost of operation.

Any increase in frequency will produce an increase in power consumption, via an increase in current, and will lead to an increase in the gas temperature in the discharge channel. On the one hand, a frequency increase leads to a higher production of reactive species (because the discharge injected power increase), but on the other hand to a higher temperature of the medium. For a dielectric barrier discharge, the effect of frequency on the power consumption is given by [64]:

$$P = 4fC_D V_D (V_p - \frac{C_D + C_g}{C_D} V_D) \qquad (3.12)$$

$$P = 4fC_D V_D (V_p - V_{\min}) \qquad (3.13)$$

Where

$$V_{\min} = \frac{C_D + C_g}{C_D} V_D$$

or, with the abbreviations: $\beta = C_g/C_D$ and $V_{min} = (1 + \beta) V_D$, enables the power formula to be rewritten as

$$P = 4fC_D\left[\frac{1}{1+\beta}\right]V_{\min}(V_{p-}V_{\min}), \quad (V_p \geq V_{\min}) \qquad (3.14)$$

where

P = power dissipated

f = frequency

C_D = dielectric capacitance

V_{min} = minimum external voltage at which ignition occurs.

Vp = peak input voltage

It is clear from the above formula that the supply parameters f, Vmin and Vp affect the power dissipated. For a fixed Vmin and Vp, the power is directly proportional to both frequency f and electrode area A.

Operation at high frequency and low input voltage has the disadvantage of producing audible and irritating noise and, for an efficient system, both the optimum voltage and operating frequency need to be determined. An increase in operating frequency changes the discharge power, and to keep the power constant, the input voltage must be correspondingly reduced. Miller et al. [71] suggest that an operating frequency above 19 kHz at a fixed input voltage will reduce the ozone generation. The increase in frequency will increase the power consumption, resulting in an increase in temperature and decomposition of the generated ozone. Similarly, an increase in the input voltage at a fixed operating frequency value will decrease the ozone production.

On the other hand, the supply frequency plays an important role in maintaining the stability and homogeneity of the atmospheric pressure glow discharge. It was suggested [29] that the supply frequency should be higher than 1 kHz, in order to ensure a homogeneous glow in the discharge volume. However, in the present study, with a gap distance of 1.5 mm and 3 mm, soda lime glass as dielectric barrier and perforated aluminium inserted between the dielectric barrier and electrodes, a homogeneous glow discharge is produced even at a

frequency of 50 Hz and at atmospheric pressure. This has been proved from the Lissajous figure and by the existence of a single discharge current pulse in each half cycle of the input voltage given later in figure 4.6 and 4.9 in Chapter 4.

In the pulsed streamer discharge technique, the pulse repetitive frequency is generated by means of a rotating spark gap, as shown in figure 6.2, with the pulse frequency depending on the speed of the motor. It is reported [2,4,66], that the production yield and concentration of ozone are in a linear relationship to the pulse repetition frequency, and this was confirmed [4,19] as the case for all applied voltages. In the present study, a pulse repetition frequency of 50 pps is used throughout.

3.3.3 Pulse duration

In the pulse streamer discharge technique, the effect of pulse duration on the ozone generation rate and efficiency is important. It was suggested [2,17,18,65] that a very short duration pulse would be advantageous in increasing or maintaining the efficiency of generation. Research revealed [2,,4,17,19,66] that shorter duration pulses have a better efficiency of ozone generation than do longer ones. The efficiency increases as the pulse duration is reduced towards a certain value and remains more or less constant below this value. Pulse durations between 20 ns to 120 ns are common [4,65,66], with the 80 ns duration found in some experiment [65] giving a maximum value of ozone production yield of around 300 gO_3/kWh in oxygen.

Using pulses over 1 μs in width is inadvisable, since this is too long to allow the creation of atomic oxygen. This is probably related to the fact that, in the discharge region, ozone is both created and destroyed. The optimum pulse duration represent a compromise between the two mechanisms [2,17].

Because of cost and time constrainst on the development of a pulse supply with variable pulse duration, the present study considers only one duration.

The available duration of 120 ns (within the range as mentioned above) from previously set-up equipment was used throughout the investigation.

3.3.4 Polarity

The polarity of the input pulse voltage has an influence on the generation efficiency, with a short positive polarity pulse producing a more spatially extended and branched streamer discharge and giving a higher yields [16,72]. As reported by Masuda et al [73], in a wire-plane geometry in air more streamer channels were evident when the wire was fed with a short positive polarity pulses rather than short negative polarity pulses, and the former had more branching [72]. Furthermore, the positive streamers extended much further in the radial direction and generated slightly more than twice the total ozone density than negative streamer discharges [72,73]. Samaranayake et al [7] also reported that a short positive voltage pulsed applied to the central electrode of a spiral wire in a coaxial geometry was more effective in the production of ozone in dry air than was a negative pulse. Negative streamers were restricted to the region close to the wire and the effective volume of ozone production was thus smaller than for the positive streamer. Salam et al. [74] also reported that the ozone generated by positive pulses in a point-to-plane configuration is higher than that of negative pulses, irrespective of the direction of gas flow through the reactor.

Because of its advantages, the positive polarity discharge is always used by researchers in ozone generation, and this was maintained throughout the present investigation.

3.4 Physical Configuration

3.4.1 Discharge gap.

A discharge gap can be described as a space in which strong electric field exist. The normal length of a gap is between 0.1-16 mm, depending on the size and type of the discharge chamber with or without a dielectric barrier. In most previous designs, the discharge gap was between 0.1 mm and 2.5 mm with a dielectric barrier and between 8 mm to 16 mm without a dielectric barrier [8,64]. Varying the gap length is an attempt to vary the electric field in order to influence the ozone generation. An increase in the gap distance d (see equation (3.7)), will decrease the electric field strength, meaning that more energy is needed for the ionization process and a longer time for the ozone production. This reduction in the system capability may also cause an increase in the gas temperature, since the increase in gap length will increase the discharge volume, and the temperature increase (see equation 3.17) will decrease the ozone production.

However, with a longer gap the volume of the discharge increases, and the probability of the reaction e + O_2 → 2O + e and the radius of the micro-discharge will both increase. This is evident in the following empirical formula, in which the radius of the micro-discharge r is increases with increasing gap length d and decreases with increasing pressure p [69].

$$r(p,d) = \left[\frac{(d)^{1/2}}{p}\right]^{1/2} \qquad (3.14)$$

As the radius increases more oxygen atoms are generated, and the probability of ozone formation increases. Also as the gap d increases, the volume of the reactor discharge region increases.

Since decreasing the discharge gap will increase the electric field strength it is advantageous in suppressing the production of low-energy electrons. The value of the electric field in the gas gap determines the electron energy in the discharge, which is an important parameter that influences all electron collision phenomena. A shorter gap will generate a higher electric field, which in turn will give the advantage of producing a high ozone concentration by suppressing any increase in gas temperature and thereby suppressing the decomposition of generated ozone. The decreased gap will also increase the energy input into the discharge, because of the increase in discharge current due to the increased conductivity of the plasma discharge with an increasing number density of the streamer.

In most glow discharge applications, the gap distance is important in determining the stability and homogeneity of the glow discharge. This is normally achieved by reducing the gap length to less than 1 mm, but in some cases with a gap of 3 mm a glow discharge can also be obtained even with air as the medium [26,27]. However, a gap above 3 mm creates instability of the glow discharge, and tends to lead to a filamentary discharge [27].

On the other hand, in a pulsed streamer arrangement increasing the gap distance to several milli-meter can still generate streamer discharge with slightly lower electric field strength [4,17]. Nevertheless, for the purpose of comparison, the gap distance is kept constant at 1.5 mm and 3 mm in later consideration of both discharge techniques.

3.4.2 Dielectric material, thickness and dielectric constant.

The presence of a dielectric barrier influences the nature of the discharge, as it serves to distribute the micro-discharges evenly over the entire electrode area and to limit the charge and energy that can be fed into an individual micro-discharge [3,8,64]. It can also provide an effective series capacitor to the load, to stop any succeeding discharge and to help in preventing any arc development [20]. The material used in a discharge configuration influences

the ozone production, and the selection of a suitable material is quite important. For generating a glow discharge at atmospheric pressure, commonly used materials are Mylar or high purity alumina ceramic (Al_2O_3) [27,28].

Changing the capacity of the dielectric, e.g. by varying the thickness and/or the dielectric constant, will change the electric field strength within the discharge region [14]. An increase in the thickness increases the impedance of the active discharge reactor and tends to lower the discharge current, which is responsible for the generation of atomic oxygen [3]. On the other hand, an increase in the dielectric constant will produce an increase in the electric field strength (see equation 3.7). Therefore, the higher the dielectric constant and the smaller the dielectric thickness, the higher is the electric field strength and the discharge current. As a consequence the power in the discharge will increase at a constant applied voltage and will result in an increase in ozone production. Furthermore, the reduction of the thickness results in more intensive cooling of the discharge area and a reduction of the applied voltage for the same energy density [8]. Most technical ozone generators use glass tubes with a wall thickness of about 1.5 to 2 mm as a dielectric barrier. However, the use of high purity alumina ceramic (Al_2O_3) has the following advantages [75]:

a) High resistances to large temperature gradients and thermal shock.
b) High electrical, mechanical and chemical resistance, thus reducing the need for maintenance.
c) The comparatively high heat conductivity (20 to 28 Wm/K), enables the efficient cooling of the plasma chemical region of ozone generation.
d) Enabling the use of lower voltages as a result of the greatly reduce insulation thickness i.e 0.5mm. This will reduce the size and cost of the power supply.
e) The high dielectric constant (9-10) increases the electric field within the discharge region.

In the present study, soda lime glass with a thickness of 1 mm and a dielectric constant of 7.75 has been used as the dielectric material, due to the expense of high purity alumina ceramic.

3.4.3 Material of discharge electrode.

The material used for the discharge electrodes affects the ozone yield, due to different intensive oxidation processes at the electrode surface where higher electrical stresses occur. It is perhaps worth mentioning that the degree of oxidation of the discharge wire or electrode has an influence on the production of micro-discharges and was noted [16] as having an influence on the ozone generation rate, although the mechanism by which this occurs is not yet known. Oxidation is an electron extraction process from the surface region of the metal exposed to the oxidizing agent. It can be assumed that the degree of oxidation of the inner wire or electrodes affects the field emission and ultimately the discharge itself. Copper wire/electrodes are always used for the inner electrode and they are readily oxidized by ozone [72]. However, tungsten wires give a better oxidation process and produces higher stress at the electrode surface; which in turn will produce more micro-discharges around the electrode. By filling the entire discharge volume it increases the ozone yield [76].

3.4.4 Discharge chamber length

The dimension of the reactor is important in assessing the ideal size of the ozone tube, since different systems and configurations will have a different performance and capability. The normal length for a commercial ozone generator is between 1 m and 2 m [5]. Given the increasing performance of modern systems it is important to know the optimum length of the discharge chamber, so that the generated ozone is not decomposed back to oxygen atoms or molecules. It can be assumed that a short tube will supply a source of energetic electrons of low intensity, and a low ozone concentration and

generation rate are therefore to be expected. Furthermore, if all other parameters are kept constant a short active region implies a low input energy, which will be drained by the corona. In contrast, a long tube will supply a high intensity of energetic electrons, as well as a long active region of high input energy, and therefore a high ozone concentration and generation rate are to be expected.

The ozone yield is related to the concentration and energy input to the discharge. At a fixed applied voltage, the energy input increases with an increase in the reactor length, because the discharge current also increases with the increased length. This is related to the increased conductivity of the plasma discharge, with an increased number of streamers or micro-discharges in the longer reactor [8].

The increase in tube length will also increase the ozone concentration. The increase is related to the increase in the active discharge area, which leads to increases in both the number of micro-discharges and the residence time. In turn these lead to increasing dissociation of the molecular oxygen into atomic oxygen, and thus to an increase in the ozone concentration. It seems therefore that a longer discharge tube has the advantage of generating higher concentrations of ozone.

Unfortunately, there is a high probability in a long reactor that the ozone particles will be destroyed by energetic electrons and for their temperature to rise as they travel along the reactor. A longer discharge chamber means a longer residence time of the generated ozone and since the formation of ozone take approximately 10-100 μs after the dissociation of oxygen molecules to atomic oxygen [8], an increase beyond this formation time will have a detrimental effect on the generated ozone. Although the increase helps to increase the ozone concentration up to certain level, above this it will diminish the generated ozone.

An increased tube length will also increase the active discharge area, resulting in an increase in the gas temperature and a further decrease in the generated

ozone. It is suggested that the residence time should therefore not be too much longer than the ozone formation time, in order to minimize the destruction of ozone by electron bombardment and temperature rise. This is however based on the assumption that all other parameters (i.e pressure, flow rate and gap distance) are kept constant, and there is no way to tell in advance what the efficiency will be from knowledge of the length of the reactor, unless suitable experiments have been carried out.

The effect of discharge chamber length therefore becomes one of the focuses of the present study.

3.4.5 Gas flow rate/residence time

The gas flow rate plays an important role in the efficiency of ozone generation and its concentration. Since the time taken for oxygen molecules to dissociate into atomic oxygen is a few nanoseconds, while ozone syntheses at atmospheric pressure is within a few microseconds (say 10 μs) in oxygen and about 100 μs in air [8], the residence time of generated ozone inside the discharge chamber has to take into consideration if the generated ozone is not to be decomposed back to oxygen. The residence time of the gas can be determined either by increasing or decreasing the gas flow rate, as can be seen from the following equation [69]:

$$\text{Residence time, Rt (s)} = \frac{\text{Discharge volume, V (litre)}}{\text{Gas flow rate, fr (litre/s)}} \qquad (3.15)$$

In general, the ozone generation rate increases with an increasing gas flow rate, because, for higher flow rates, the shorter residence time results in the ozone spending less time in the discharge volume. Therefore, the amount of ozone destroyed by the discharge is reduced.

On the other hand, to obtain a higher concentration of ozone requires a reduced gas flow rate. This will increase the residence time and also the concentration of the ozone, and in an application requiring a high ozone concentration a low flow rate of input gas can be employed but will give a low ozone yield. Ideally, an ozone generator should combine a high generating efficiency with a high concentration. But these are conflicting requirements, since a high concentration will generate a lower yield and vice versa. To compensate for this, some generators operate in a medium range between 3 l/min to 5 l/min [4,66]. In the present study the gas flow rate used ranged between 0.2 l/min and 1 l/min.

The gas flow rate has two important effects: firstly it cools the gas by sweeping out the gas heated by the plasma and secondly by enhancing the ion diffusion it makes the current density distribution more uniform on the surface of the electrode or dielectric barrier. However, it sometimes also enhances a fluctuation of the plasma due to unstable flow of the gas. To prevent this, a stable gas flow rate needs to be monitored [71].

3.4.6 Temperature inside the discharge chamber.

At ambient temperature ozone is a gas, whereas at –76.7°C it condenses to a dark blue liquid and at –215.6°C it freezes. Ozone will decompose readily in the presence of certain catalysts or at temperatures exceeding 100°C [42]. At room temperature, ozone will revert to molecular oxygen within hours. In short, ozone is an unstable gas and very sensitive to temperature. Ozone destruction by decomposition increases as the gas temperature and ozone concentration increase. Bombardment by electrons can break ozone molecules apart, and they can recombine with each other as well as with oxygen molecules and oxygen atoms. This can be explained by the temperature dependencies of the ozone formation and destruction reactions [69]:

Formation: $O + O_2 + O_2 \rightarrow O_3 + O_2$, $k_f = 8.6 \times 10^{-31}.T^{-1.25}$ $cm^6.s^{-1}$

Destruction: $O_3 + O_2 \rightarrow O + O_2 + O_2$, $k_d = 73 \times 10^{-11} \exp(-11400/T)$ $cm^3.s^{-1}$

Where k_f, k_d and T are the reaction rate coefficient of ozone formation and destruction and the gas temperature respectively. It can be seen that an increase in gas temperature would reduce the reaction rate coefficient for ozone formation. On the other hand, the rate of ozone destruction increases when the gas temperature increases. It is important therefore to control the temperature inside the discharge chamber, both to obtain high production and to reduce the decomposition rate of the generated ozone. That is why most ozone generators use a cooling system that maintains the temperature inside the discharge volume within the stable range for ozone generation between 18°C and 27°C. The process gas temperature is the most important parameter influencing ozone generation, and the average increase of temperature ΔTg is determined by the balance between the discharge power not used for ozone formation and the heat removed by radial heat conduction to the cooled steel electrode. Thus [8]

$$\Delta T_g = \frac{dP}{3\lambda F}(1-\eta) \tag{3.16}$$

where d is the gap length, λ is the heat conductivity of the feed gas, P/F is the power density referred to the electrode area and η is the efficiency of ozone generation. If, on a time average, the power is evenly dissipated in the gap volume, the resulting radial temperature profile is a half parabola with a peak value at the (uncooled) dielectric tube [8]. The wall temperature Tw of the steel tube is determined by the temperature of the incoming cooling water, and the average temperature in the discharge gap from

$$T_g = T_W + \Delta T_g = T_W + \frac{dP}{3\lambda F}(1-\eta) \tag{3.17}$$

For example, with typical values of wall temperature, T_W = 20°C, d = 2 x 10^{-3} m, λ = 2.5 x 10^{-2} W/mK, P/F = 2 kW/m^2 and η = 10%, an average temperature of about 70°C is expected in the gap. Therefore, with a wall temperature of 20°C, the peak value at the dielectric tube reaches approximately 90°C. From equation (3.17), lowering T_W and using a smaller gap will reduce the gas temperature.

The common threshold value for gas temperature lies between 50 and 52 °C, beyond which the thermal decomposition of ozone appears to become dominant [8]. The ozone generation rate decreases substantially at high temperatures, with the effect being more pronounced in air supplied ozonizers since

i) the ozone generation reaction coefficients ($O + O_2 + M \rightarrow O_3 + M$) decrease with a temperature increase.

ii) the concentrations of N_2O_5 and N_2O do not depend on temperature because the generation rates of nitrogen atoms and excited nitrogen molecules both remain constant with temperature. Almost all nitrogen atoms are finally reduced to N_2O_5, and some of the excited nitrogen molecules are converted to N_2O. At high temperatures and/or high concentration of nitrogen oxides, the process of ozone decomposition can even exceed that of ozone generation, leading to a low ozone concentration.

However, in the investigation reported later the physical size of the experiment and the power involved were small. Thermal problems were often negligible, since heating of the small size of reactor was limited. Application of either atmospheric pressure glow discharge or short pulses of pulsed streamer discharge results in less energy being used to transport heavy ions across the gap, which will certainly reduce the generation of heat.

3.4.7 Wire mesh/perforated metal

Wire mesh appears to be very important in increasing the likelihood of the existence of a homogeneous glow discharge at atmospheric pressure. Research reported by Trunec et al. [28], shows that, without this mesh, a filamentary discharge was observed. They suggested that the mesh could influence the discharge by its electrical resistance, which is higher than that of the metallic electrode, and found that the mesh does not influence the electric field in the discharge gap. However, Tepper et al. [27] proposed that the mesh behind the barrier is responsible for charging the electret (the dielectric barrier). This was based on the standard technique of electret charging by injecting charge carriers in a corona discharge, and also that the charging of polymer electret foils through a wire mesh produces a uniform distribution over the foil surface.

In the present study, however, a perforated aluminium with diameter holes of 1.2 mm and an open area of 23% were used as a replacement for fine wire mesh. Initial studies showed [77] that a configuration with perforated zinc inserted between the dielectric barrier and electrode, at both sides of the discharge volume, generates the same characteristic of glow discharge at atmospheric pressure although with slightly low stability than when wire mesh is used.

3.5 Conclusion

Based on the mechanisms described, it can be concluded that the most obvious parameters that limit ozone concentration and generation are the kind of input gas, the gas flow rate (residence time) and the gas temperature inside the discharge volume. It is believed that monitoring these three parameters will help to improve the ozone concentration and generation.

Apparently the use of air, with its lower concentration of oxygen, combined with the detrimental action of the nitrogen oxides, will generate less ozone than will

pure oxygen. Air feed systems for ozone generators are complicated, as the air needs to be properly conditioned to prevent damage to the generator. The presence of moisture causes nitric acid to form, which will decrease the ozone production and corrode the generation cell components. To eliminate these problems, the air needs to be dried prior to entering the ozone generator. For higher concentrations and ozone yields, the use of pure oxygen is suggested [64].

The second problem that has to be overcome is the gas flow rate or gas residence time in the discharge volume. An increase in the residence time will increase the ozone concentration, but will decrease the ozone production. It is already known that at, higher flow rates, the generation rate is high at a low concentrations but, at a low flow rate, the ozone concentration is by contrast high and the generation rate is low. The gas flow rate or residence time plays an important role in determining the efficiency of ozone generation, which is also influenced by the pressure and the discharge configuration (i.e gap distance, tube length and effective area of the discharge). To obtain optimum generation efficiency, the gas flow rate needs to be monitored, but until now no specific value of gas flow rate have been reported for optimum efficiency. Different research and different types of configuration and system performance will have different optimum values of gas flow rate, and the optimum value for a given configuration will need to be determined.

The third and most crucial problem that limits ozone concentration and production is the temperature rise inside the discharge volume, since over 90% of the input electrical power is dissipated as unwanted heat [5]. This is one of the main reasons why the generation of ozone cannot reach the 100% efficiency that corresponds to a yield of 1220 g/kWh, since some of the factors involved in generating the ozone also contribute to the temperature rise. For example, an increase in applied voltage will initially increase the electric field strength inside the discharge chamber, resulting in an increase in ozone concentration and generation, but at some stage the increase will also increase the power consumption, leading to an increase in temperature. Similarly, an increase in frequency will result in an increase in power

consumption via an increase in current, and will lead to an increase in the temperature of the gas in the discharge channel. Although the frequency increase leads to a higher production of reactive species (because of the injected power increase), it also leads to a higher temperature of the medium. Since both input voltage and frequency are important parameters for ozone generation, and the effect of a temperature rise due to the increase of both parameters cannot be avoided, the problem must be solved properly to improve the efficiency of generation.

It can be said that the increase in temperature of an ozone generator presents the major problem that needs to be solved, stimulating a search for an effective technique or material to reduce or if possible to eliminate it. The first possibility is, of course, to provide an effective cooling systems that prevents any increase in wall temperature as well as gas temperature. However, this is still not sufficient to prevent a temperature rise in the gas, although it can prevent any temperature rise at the tube wall. The second possibilities are to control and manipulate several other parameters, such as the gap length, the gas flow rate and pressure, and the dielectric barrier thickness and material. For example, the use of a short gap is believed to suppress an increase in gas temperature [8]. Similarly, by controlling the gas flow rate, the temperature rise can be reduced by sweeping out the gas heated in the plasma. Since the system is intended to be operated at atmospheric pressure, there is no room for pressure to be used for controlling the gas temperature. This in fact has been done by reducing the gap. Lastly, use of a thin dielectric barrier, (e.g of high purity alumina ceramic) with a higher heat conductivity, will result in more intensive cooling of the discharge area. An alternative method is to use a short pulse with a sharp rise time, that is to use pulsed power as the input supply. This is believed to provide an effective way of keeping non-thermal conditions for both the electrodes and the gas. Pulsed streamer non-thermal discharges have been shown to be very effective for ozone production, without significantly raising the gas temperature or inducing arc breakdown [7].

However other parameters, such as dielectric constant, material and sharpness of the discharge electrode, as well as the use of wire mesh or

perforated material to generate homogeneous glow discharge are believed to increase ozone concentration and generation with less contribution to the gas heating. These possibilities need to be exploited to obtain the maximum benefit in the efficiency of ozone generation.

CHAPTER 4

GENERATION OF A HOMOGENEOUS GLOW DISCHARGE IN AIR AT ATMOSPHERIC PRESSURE

4.1 Introduction

In general, a glow discharge is found to be stable only in a low pressure discharge of less than a few mbar [26,60]. At atmospheric pressure, the gas discharges are normally unstable, and in most cases [27,78] they tends to change to a filamentary discharge, very dependant on the specific gas, the material of the dielectric barrier, the structure of the discharge electrode, the frequency, the gap spacing and the humidity of the gas [24,26,27,29,56,60,78-80].

However, several authors [24,29] claim to have obtained a stable glow discharge at atmospheric pressure and have suggested that their success is based on three simple requirements i) a source frequency above 1 kHz, ii) insertion of a dielectric plate (or plates) between the two metal electrodes and iii) use of helium dilution gas. The ability of helium to produce a stable glow discharge at atmospheric pressure is well known and is said to be related to its low dielectric breakdown voltage [46]. To obtain a glow discharge at atmospheric pressure the occurrence of small avalanches under a low field is required [81], and since the dielectric breakdown stress of helium at 1 atm is only about 300 V/mm, some 10 times lower than that for air, it is relatively easy to produce a glow discharge. Although helium is good for generating a homogeneous glow discharge at atmospheric pressure, it is however not practical for ozone generation, due to its high cost and the low efficiency of the process.

Another interesting result on stabilization of an atmospheric pressure glow discharge (APGD) was reported [26] in its appearance in air, argon and oxygen when using a 50 Hz source and with the use of a fine wire mesh as the discharge electrodes. These experiment have been repeated [27,29] with similar results, and it has also been found that a fine mesh electrodes [60] produces a more stable glow than does a coarse one. Since ozone is commonly generated in air or in oxygen, the possibility of an APGD in air and in oxygen is very important, and this has therefore become a focus of the present investigation.

In the present study, perforated metal sheet is used instead of fine wire mesh. The basis for this is that the sheet consists of a series-parallel arrangement of small holes with sharp edges, which is expected to produce a higher local electric field strength than does a fine wire mesh (see Figs. 4.1a) and 4.1b)). The higher local electric field in the gap may be sufficient to cause ionization of the gas in the vicinity of the sharp edges. This in turn will produce more micro-discharges near the electrodes, and further will provide a discharge that fills the entire volume of the discharge chamber. If a dielectric barrier is present, the increase in field strength will lead to an increased number of micro-discharges of nanosecond duration [8]. Each micro-discharge consists of a thin almost cylindrical channel, with an intense spot at the metal electrode and spreading into a glow discharge on the dielectric surface.

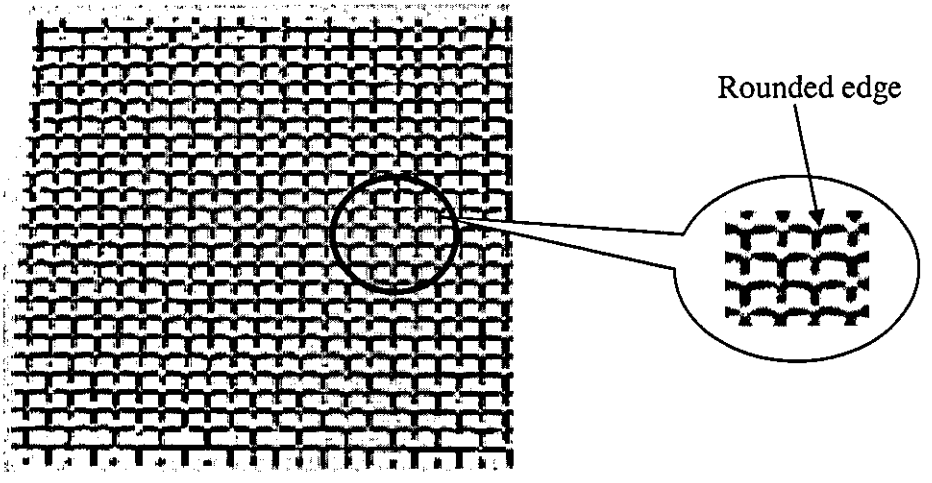

a) Fine steel wire mesh

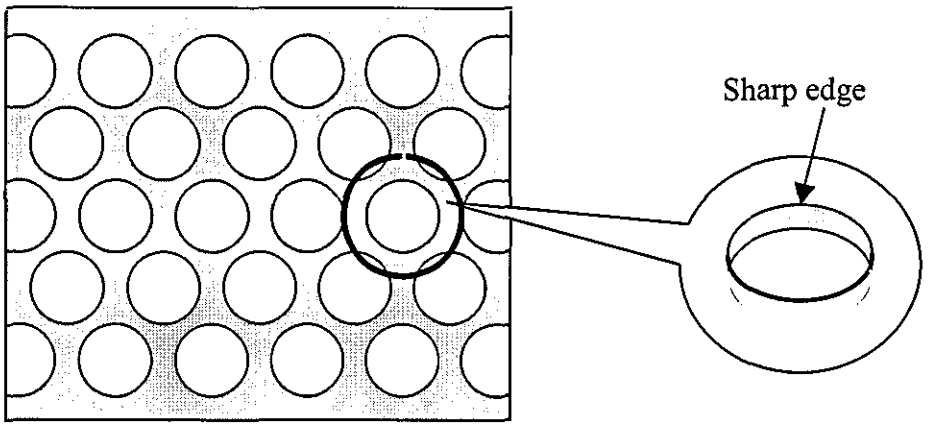

b) Perforated metal sheet

Figure 4.1: Physical structure of a) fine wire mesh and b) perforated metal electrodes.

Additionally, a greater perforation density with small diameter holes may produce the same effect as a fine wire mesh, at both low and high voltages [77]. However, with a higher concentration of holes and a sharper edge, the smaller diameters are expected to provide a higher electric field for charging the dielectric surface than does the wire mesh.

It is also expected that the physical structure of perforated metal such as the shape and diameter of the holes, and the metal thickness will all have an influence on the breakdown mechanism and the discharge stability, and certainly needs further investigation. However, a detailed investigation of these effects was not included in this study, due to budget and time constraints, and is left for future researchers. Since one of the present objectives is to use and evaluate the effectiveness of APGD for ozone generation, the study is restricted to round holes of different diameters and the results are presented later.

4.2 Preliminary experiment

In order to investigate the performance of perforated metal, a preliminary experiment was conducted involving a comparison between perforated zinc and a fine steel wire mesh. The results [77] showed that the perforated zinc produced a similar effect to that of the fine steel wire mesh but with slightly less stability. There was an indication of the influence of the material, hole shape and diameter on the discharge stability and this therefore needs further investigation. Based on this finding, a second preliminary experiment utilizing perforated aluminium with round holes of different diameter was carried out and the results compared to those for a fine steel wire mesh. Perforated aluminium was used, since it has a better oxidation process than does perforated zinc and it may therefore produce a higher stress at the electrode surface. This in turn will produce more micro-discharges near the discharge electrode, and is expected to enhance the discharge stability. Since the aim of this experiment was to identify the effect of the material and the hole diameter on the discharge stability, before conducting a further comparison with a fine steel wire mesh, only round holes in perforated aluminium were investigated. A series of tests was performed and analysed, and it was found that perforated aluminium with smaller diameter holes (1.2 mm) produced a better stability than when bigger holes (3.0 mm) were used, following the same pattern as a fine steel wire mesh, where a fine mesh produces a better stability than does a coarse one [60]. It became evident that the material and the hole diameter have an influence on the discharge stability, indicating an ability to provide a similar function to a fine steel wire mesh in producing a stable glow discharge. However, these preliminary results are not presented here, since they were used merely as guidelines for the latter comparative study (section 4.3).

4.3 Comparative study between fine wire mesh and perforated aluminium

Based on the results obtained previously, a further comparative study was made between perforated aluminium with small diameter holes and a very fine steel wire mesh, in order to determine the best discharge stability of the two electrodes structure. Perforated aluminium with a hole diameter of 1.2 mm (which is the smallest readily available) and a hole density of about 42 per cm^2 and fine steel wire mesh with a wire diameter of approximately 35 μm, and 325 meshes per inch were compared. Table 4.1 summarizes the major parameters of the investigation.

It was anticipated that the larger perforation density of perforated aluminium would provide a better stability of the glow discharge than that of the fine wire mesh.

Electrode structure	**Hole diameter (mm)**	**Wire mesh diameter (μm)**	**Number of perforation per cm^2**	**Distance between axes (μm)**	**Pitch distance (mm)**
Perforated aluminium	1.2	-	42	-	1.7
Wire mesh	-	35	134	40	-

Table 4.1: Summary of electrode shape parameters

4.3.1 Electric field modelling

Before conducting a comparative study between the wire mesh and perforated aluminium it was necessary to estimate the electric field strength on both electrode structures, in order to identify the effect of the field strength on the discharge stability. It has been reported that the ionization rate in the discharge chamber depends on the local field strength [81], with a higher field strength producing a higher ionisation rate. A higher local electric field is also believed to have an effect on the glow discharge stability, and due to the sharp edges of the perforated metal a high electric field can be achieved locally. Electric field computations for both geometries were carried out using simulation software (Ansoft-Maxwell 2D student version), a complex code able to simulate electromagnetic fields between static conditions and high frequencies. For the present purpose only the electrostatic field module was used. In the first step of this, a grid is created that describes the geometry in which the electric field is applied and the potential difference and the electrical characteristics (dielectric constant) of the medium are then defined. Based on the discrete grid, the Maxwell equations are solved at each point within the software and the solution is displayed in graphical form. The resulting electric field distributions in both fine wire mesh and a perforated aluminium at input voltage of 3 kV and gap spacing of 0.3 mm are presented in Fig. 4.2 a) and b) respectively.

Table 4.2 show simulated values of the maximum electric field strength between the gaps for different wire sizes of a steel mesh. The results show that an increase in the diameter of the wire (reducing the number of wires per cm^2) results in a reduction in the electric field strength at the same input voltage. For an input voltage of about 3 kV an electric field strength around 31.47 kV/mm is achieved, corresponding to an average electron energy of about 21.9 eV.

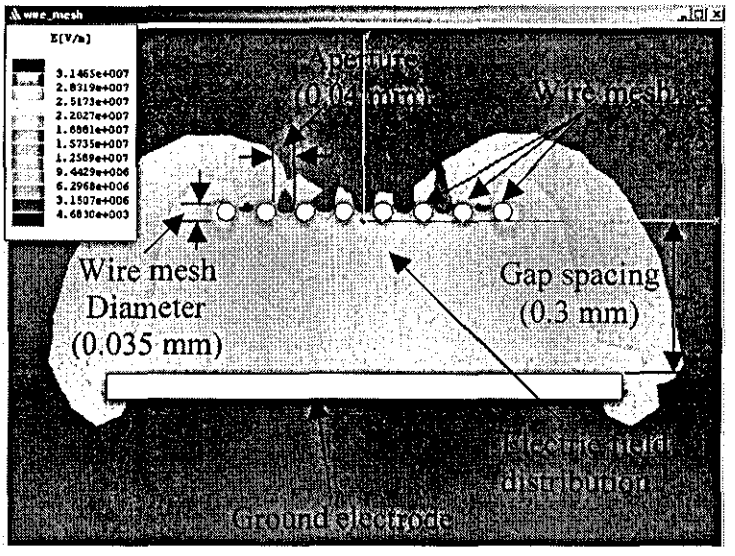

a)

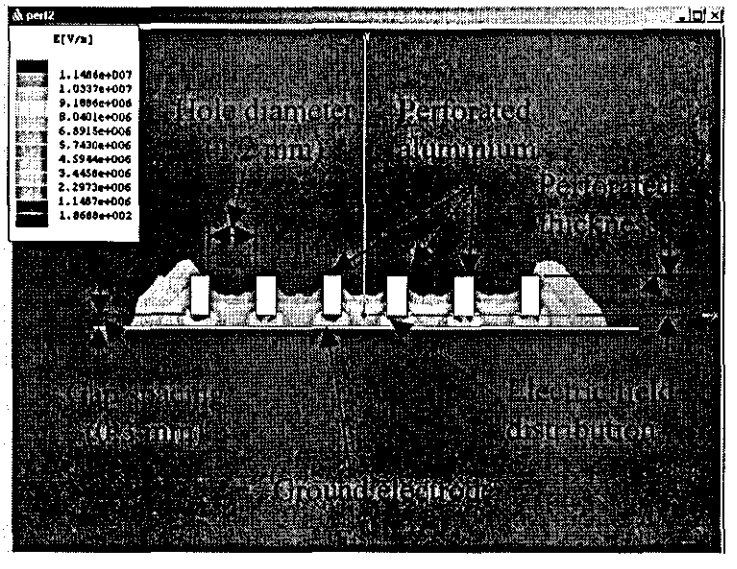

b)

Figure 4.2: 2D simulation of electric field strength and distribution for a) stainless steel wire mesh and b) perforated aluminium using Ansoft-Maxwell 2D program.

Input Voltage (kV)	Electric field strength (kV/mm) (#325,0.035mm)	Electric field strength (kV/mm) (#200,0.050mm)	Electric field strength (kV/mm) (#80,0.12mm)	Electric field strength (kV/mm) (#30,0.28mm)
3	31.47	27.38	18.30	14.88
4	41.95	36.50	24.40	19.85
5	52.44	45.63	32.41	24.81
6	62.93	54.75	38.89	29.77
7	73.42	63.88	45.37	34.73

Table 4.2: Maximum electric field strength at different input voltages and wire mesh sizes

Table 4.3 show simulated values of the maximum electric field strength between the gaps for perforated aluminium of different hole diameters. The results show that a decrease in the hole diameter results in an increase in the electric field strength at the same input voltage. For an input voltage of about 3 kV, an electric field strength around 11.49 kV/mm is achieved, corresponding to an average electron energy of about 9.9 eV.

Input Voltage (kV)	Electric field strength (kV/mm) (hole = ∅1.2 mm pitch = 1.7 mm)	Electric field strength (kV/mm) (hole = ∅1.5 mm pitch = 2.5 mm)	Electric field strength (kV/mm) (hole = ∅2.0 mm pitch = 3.5 mm)	Electric field strength (kV/mm) (hole = 3.0 mm pitch = 5.0 mm)
3	11.49	11.28	11.18	11.03
4	15.31	15.04	14.91	14.71
5	19.14	18.79	18.64	18.38
6	22.97	22.55	22.37	22.06
7	26.80	26.31	26.09	25.73

Table 4.3: Maximum electric field strength at different input voltages and hole diameter of perforated aluminium sheet.

It was concluded from the above results that the wire mesh generates a higher electric field strength, which is in contradiction to the initial assumption that the perforated aluminium would produce the higher value because of it sharp edges. Further verification of the effect of the two different electrode structures on the glow discharge stability therefore needs to be obtained experimentally.

4.3.2 Experimental set-up and procedure

Fig. 4.3 shows the experimental arrangement used to compare the two different electrodes structure, using either a plane-to-plane configuration with perforated aluminium sheet with 1.2 mm diameter holes and 23% open area or a fine steel wire mesh sheets of #325 numbers of meshes per inch and 0.035 mm wire diameter. A double barrier arrangement was adopted, with both sides having one electrode sheet (20 mm in length and 20 mm in width) located between the aluminium foil and dielectric barrier.

The aluminium foil serves as a high voltage electrode on one side of the reactor chamber and as the ground electrode on the other side. Mica sheet 130 μm thick was used as the dielectric barrier, to permit the charge build-up that maintains the plasma from one half-cycle of the supply to the next [12, 13].

The gap spacing and the air flow rate were kept constant at 1 mm and 1 l/min respectively, and a voltage between 1 and 20 kV at a frequency of 50 Hz was used to supply the APGD reactor. Dry air supplied by BOC with a relative humidity below 20% was used as the input gas. A 240 V/20000 V, 5 mA, 50 Hz step-up transformer provided the high AC voltage to the electrodes, with the primary voltage controlled by a Variac to give an input to the transformer between 0 and 240 V.

The voltage is measured by means of a high-voltage probe (Tektronix P6015A, 1000x) and the charge signal is obtained with the aid of a 0.22 μF capacitor connected in series to ground (see Fig. 4.3).

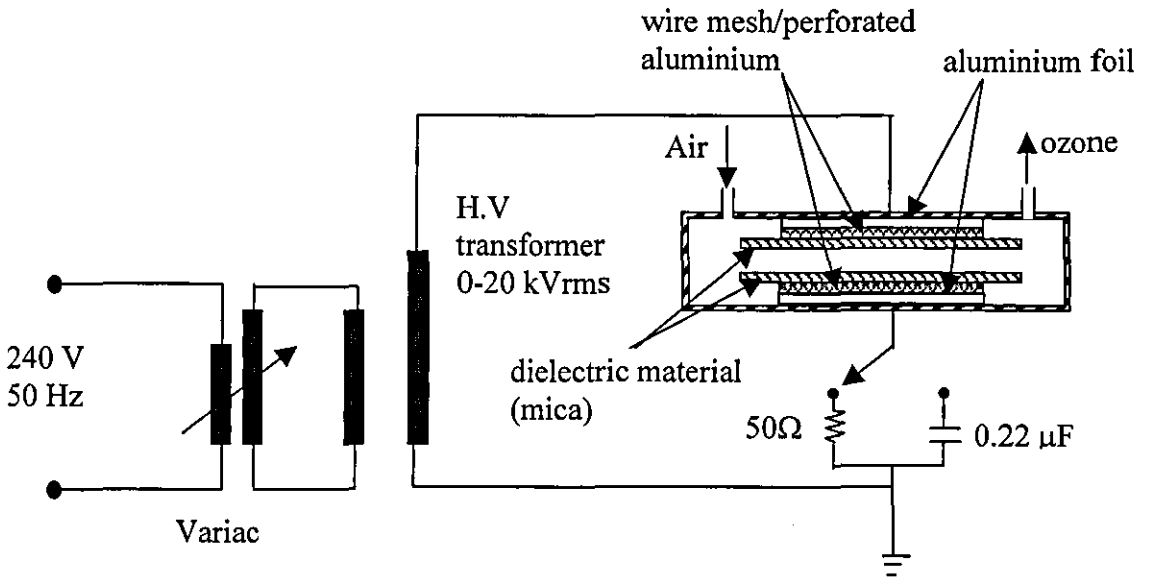

Figure 4.3: Experimental arrangement for comparison of the glow discharge stability.

The discharge current is measured using a Pearson Rogowski current monitor (Model 2877) through a 50 Ω resistor connected in series to ground (see Fig. 4.3). The output signals are measured by a digital oscilloscope (LeCroy 9344) with a bandwidth of 500 MHz and a sample rate of 1 GS/s.

4.4 Results and discussions

Visual observations indicated that the discharge was similar when the fine wire mesh was replaced by perforated aluminium. It is therefore difficult to differentiate the stability of the glow discharge between the two configurations. Because of this, two common discharge behaviour techniques were adopted [24,27,29] i) observation of the behaviour using voltage-charge Lissajous figures and ii) observation of the characteristics of the discharge current. The discharge behaviour was observed with mesh (#325, 0.035 mm) and perforated aluminium (1.2 mm diameter holes) respectively, at supply voltages of 1.2, 1.4, 1.6 and 1.8 kV for 1 mm gap distance and at supply voltages of 2.8, 3.2, 3.6 and 4.0 kV for 3 mm gap distance. The results are discussed later.

4.4.1 Voltage-charge Lissajous figure

Observation of the Lissajous voltage-charge figure (Okazaki et al 1993) [26] was used to distinguish between glow and filamentary discharges, using the circuit shown in Fig. 4.4. The attenuated high voltage is fed between point X and earth, and the capacitor voltage between point Y and earth. The values of resistors R1 and R2, and of capacitor C, are selected to provide the same voltage/division on the X and Y axes of the oscilloscope CRO.

The appearance of two voltage lines, as the top and bottom of a parallelogram, was taken as an indication of the existence of a glow discharge. The appearance of a staircase-like waveform, with or without continuous connecting lines, was taken as an indication of the existence of a filamentary discharge and a mixed glow-filamentary discharge respectively, as established by previous researchers [24,26,29]. The resulting Lissajous figures are shown in Figs.4.5 and 4.6.

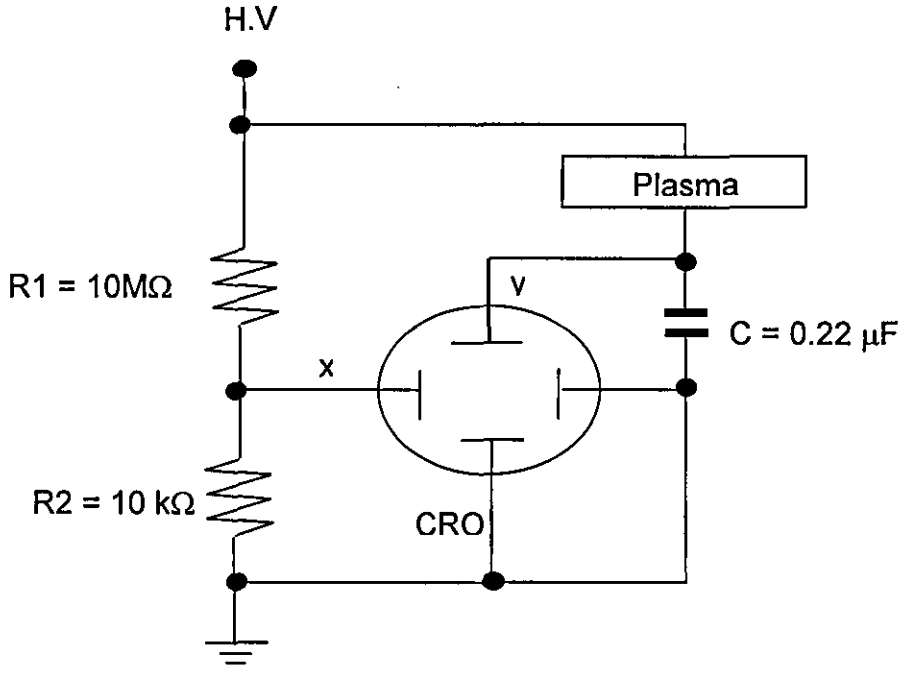

Figure 4.4: Circuit to measure Lissajous voltage-charge characteristics [26].

Fig 4.5 shows the effect of different values of applied voltage when using wire mesh (#325, 0.035 mm) electrode. It can be seen in Fig. 4.5(a) that, at a voltage as low as 1.2 kV, the Lissajous figure appears as only two straight lines, indicating the existence of the glow discharge. Increasing the voltage to 1.4 kV and then to 1.6 kV produces a mixed glow-filamentary discharge, as is indicated in both Figs 4.5(b) and 4.5(c) by the appearance of a staircase-like region in the waveforms. Finally, Fig. 4.5(d) shows that a change from a mixed glow–filamentary to a filamentary discharge appears at voltages of 1.8 kV and above, as is indicated by the existence of continuous connecting lines in the staircase-like regions.

Fig 4.6 shows Lissajous figures at different value of applied voltage when using perforated aluminium (1.2 mm, 23% open area) electrodes. The two long lines in Fig. 4.6(a) demonstrate that at 1.2 kV a pure glow discharge is produced. At a voltage of 1.4 kV, a slight change toward a mixed glow-filamentary discharge is produced as is evident in Fig. 4.6(b). Increasing the supply voltage to 1.6 kV, Fig. 4.6(c), results in an increased glow -filamentary discharge, shown by the existence of an extended staircase-like region in the waveform, and this continues up to 1.8 kV as is evident from Fig. 4.6(d). Unlike the results of Fig. 4.5, no pure filamentary discharge now occurs at a voltage of 1.8 kV. Increasing the voltage further to 2.0 kV, results in the discharge becoming entirely filamentary. However, for comparative purposes, all the results for the gap spacing of 1 mm in this study are shown up to a maximum of 1.8 kV.

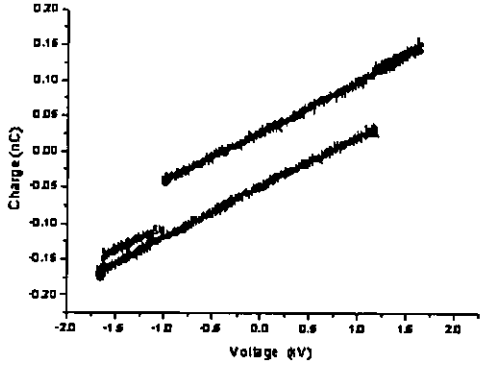

(a)

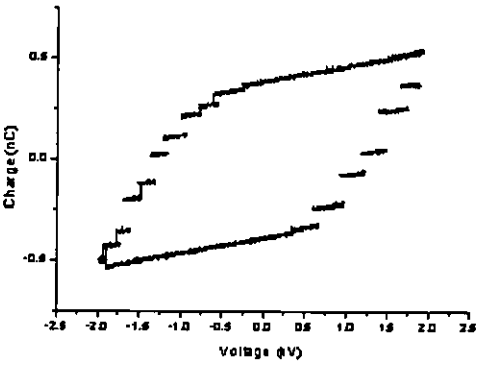

(b)

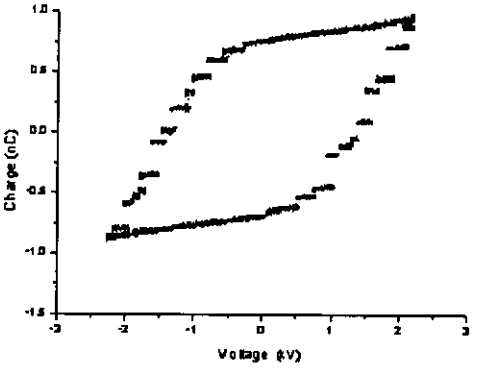

(c)

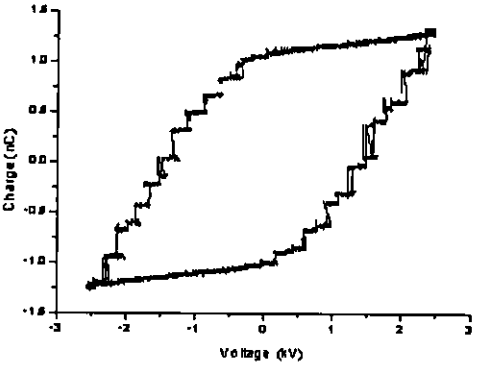

(d)

Figure 4.5: Voltage-charge Lissajous figure for fine steel wire mesh (#325, 0.035 mm) at (a) 1.2 kV, (b) 1.4 kV, (c) 1.6 kV, (d) 1.8 kV. Gap distance d = 1 mm, gas flow rate fr = 1 l/min, pressure p = 1 bar.

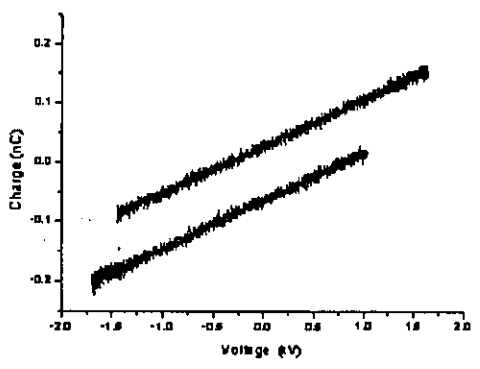

(a)

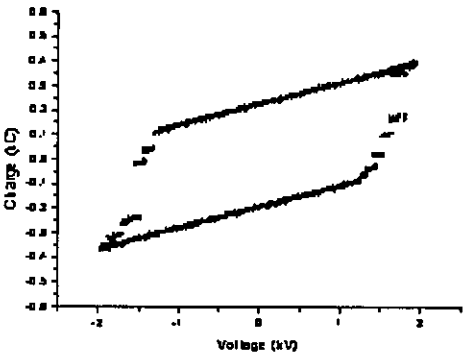

(b)

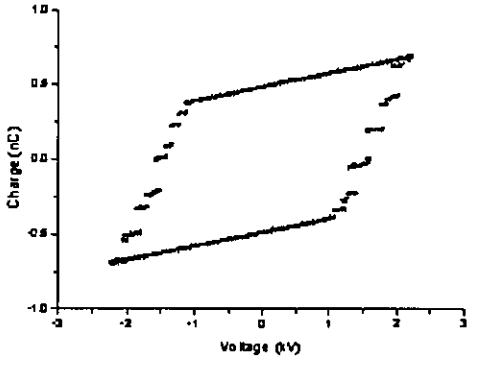

(c)

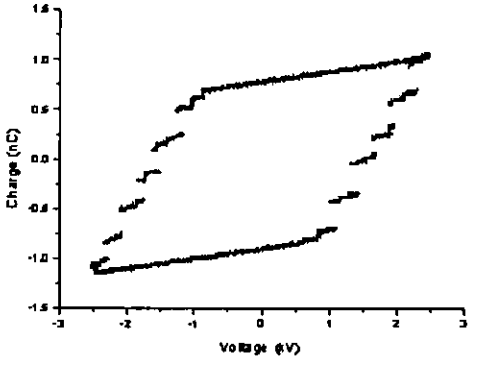

(d)

Figure 4.6: Voltage-charge Lissajous figure for perforated aluminium (1.2 mm diameter, 23% open area) at (a) 1.2 kV, (b) 1.4 kV, (c) 1.6 kV, (d) 1.8 kV. Gap distance d = 1 mm, gas flow rate f_r = 1 l/min, pressure p = 1 bar.

4.4.2 Characteristic of applied voltage and discharge current

Observation of the voltage and discharge current waveform (Okazaki et al 1993) provides an alternative method of detecting the existence of glow discharge, and was used to verify the result obtained from the Lissajous figure. The circuit arrangement is shown in Fig. 4.7. A glow discharge is characterised by the appearance of a single current pulse in each half period of the supply voltage, whereas the existence of a filamentary discharge is indicated by the appearance of several current pulses in each half cycle of input voltage as established by several researchers [24,26,29]. There are no specific characteristics given previously and associated with a mixed glow-filamentary discharge. However, in most experiments conducted in this study it was found that, when the results in Lissajous figure contain a staircase-like region without continuous connecting lines, the discharge current waveform exhibits several current pulses in one half cycle of the input voltage and a maximum of two current pulses in the other half cycle. This feature has therefore been used as an indication and confirmation of the appearance of a mixed glow-filamentary discharge.

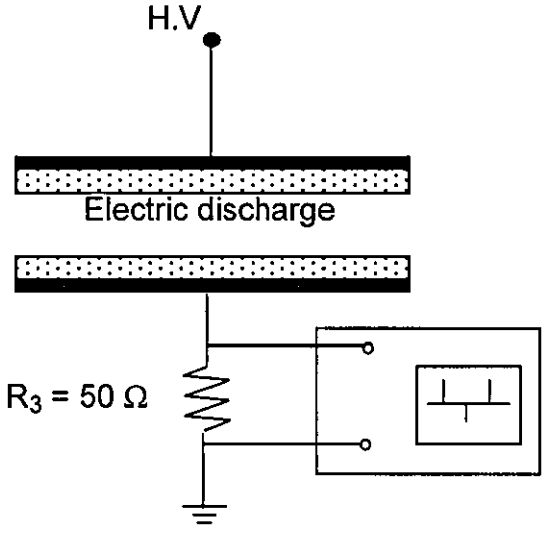

Figure 4.7: Circuit to record discharge current waveform [26].

Typical oscillograms of the applied voltage and the discharge current over an entire voltage cycle for the four different electrode shapes investigated are shown in Figs. 4.8 and 4.9.

Fig.4.8 shows results obtained for the APGD in air when using wire mesh (#325, 0.035 mm) electrodes. At 1.2 kV, the discharge current profile is clearly characterised by one pulse per half cycle, indicating the existence of a pure glow discharge. Increasing the voltage to 1.4 kV and then to 1.6 kV generates a mixed glow-filamentary discharge as shown in both Fig. 4.8(b) and 4.8(c) by the presence of several pulses in the positive half cycle, but only a single pulse in the negative half cycle. Increasing the input voltage to 1.8 kV changes the glow-filamentary discharge to a filamentary discharge alone as shown in Fig. 4.8(d) by the existence of several pulses in both the positive and negative half cycles, although with very small amplitudes.

Fig.4.9 shows the voltage and discharge current waveforms of the APGD produced by perforated aluminium (1.2 mm diameter, 23% open area) electrodes. Figs. 4.9(a) and (b) shows that at both 1.2 kV and 1.4 kV the discharge current waveform exhibits a single pulse per half cycle and only a glow discharge is produced. Fig. 4.9(c) shows the discharge current waveform beginning to contain several pulses in one half cycle of the input voltage and a maximum of two current pulses in the other half cycle when the input voltage is increased to 1.6 kV, and when the input voltage is further increased to 1.8 kV this becomes evident in both positive and negative current pulses of Fig. 4.9(d). This shows that a mixed glow-filamentary discharge is produced at both input voltages without changing to a filamentary discharge, confirming the findings from the Lissajous figure.

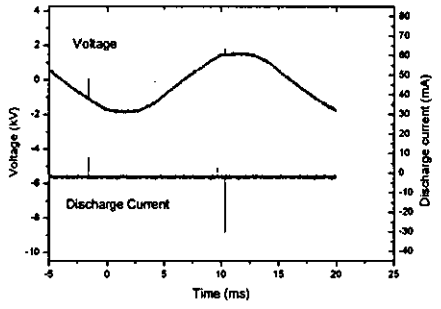

(a)

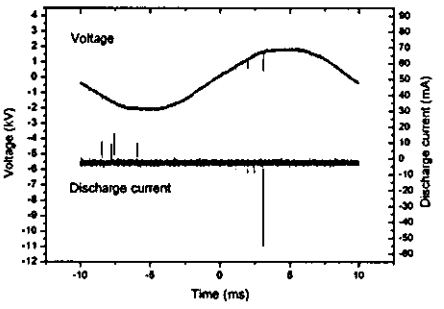

(b)

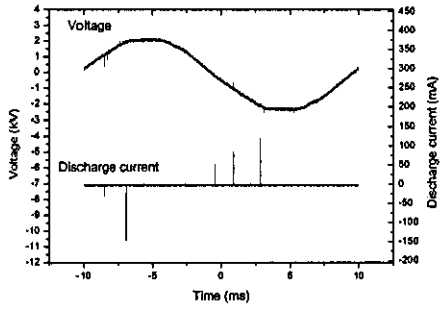

(c)

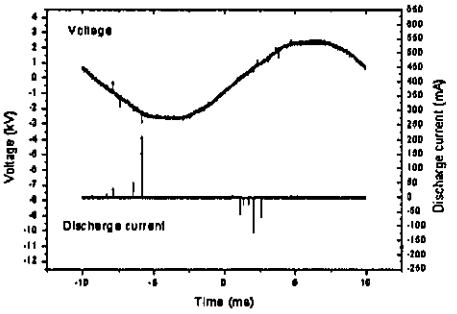

(d)

Figure 4.8: Voltage and discharge current waveform for steel wire mesh (#325, 0.035 mm) at (a) 1.2 kV, (b), 1.4 kV, (c) 1.6 kV, (d) 1.8 kV. Gap distance d = 1 mm, gas flow rate fr = 1 l/min, pressure p = 1 bar

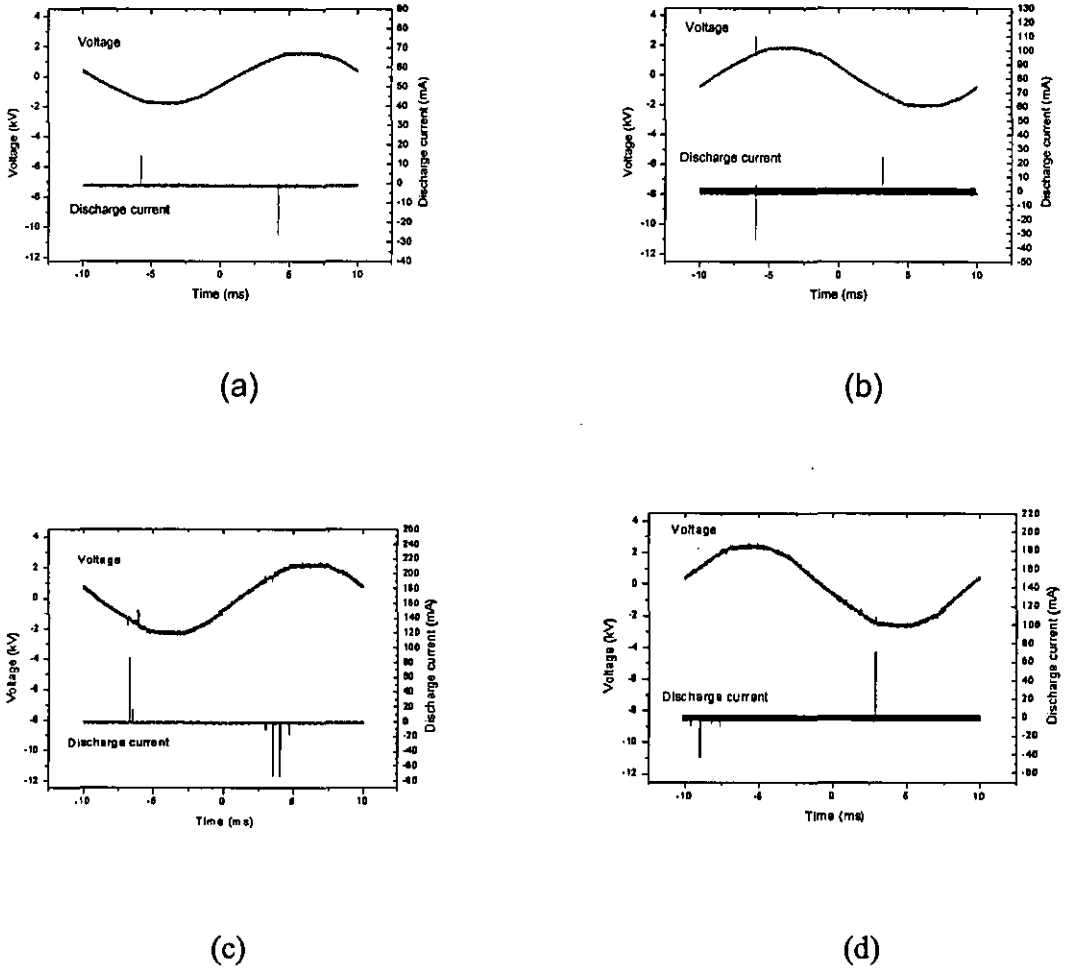

Figure 4.9: Voltage and discharge current waveform for perforated aluminium (1.2 mm diameter, 23% open area) at (a) 1.2 kV, (b), 1.4 kV, (c) 1.6 kV, (d) 1.8 kV. Gap distance d = 1 mm, gas flow rate fr = 1 l/min, pressure p = 1 bar.

In order to investigate further the effectiveness of perforated aluminium over a fine wire mesh, a comparative study between two arrangements (a fine steel wire mesh and a small diameter of perforated aluminium) involving an increased gap spacing (3 mm) was conducted. The results obtained are shown in Figs. 4.10, 4.11, 4.12 and 4.13, and these confirm the results obtained previously with the gap spacing of 1.5 mm.

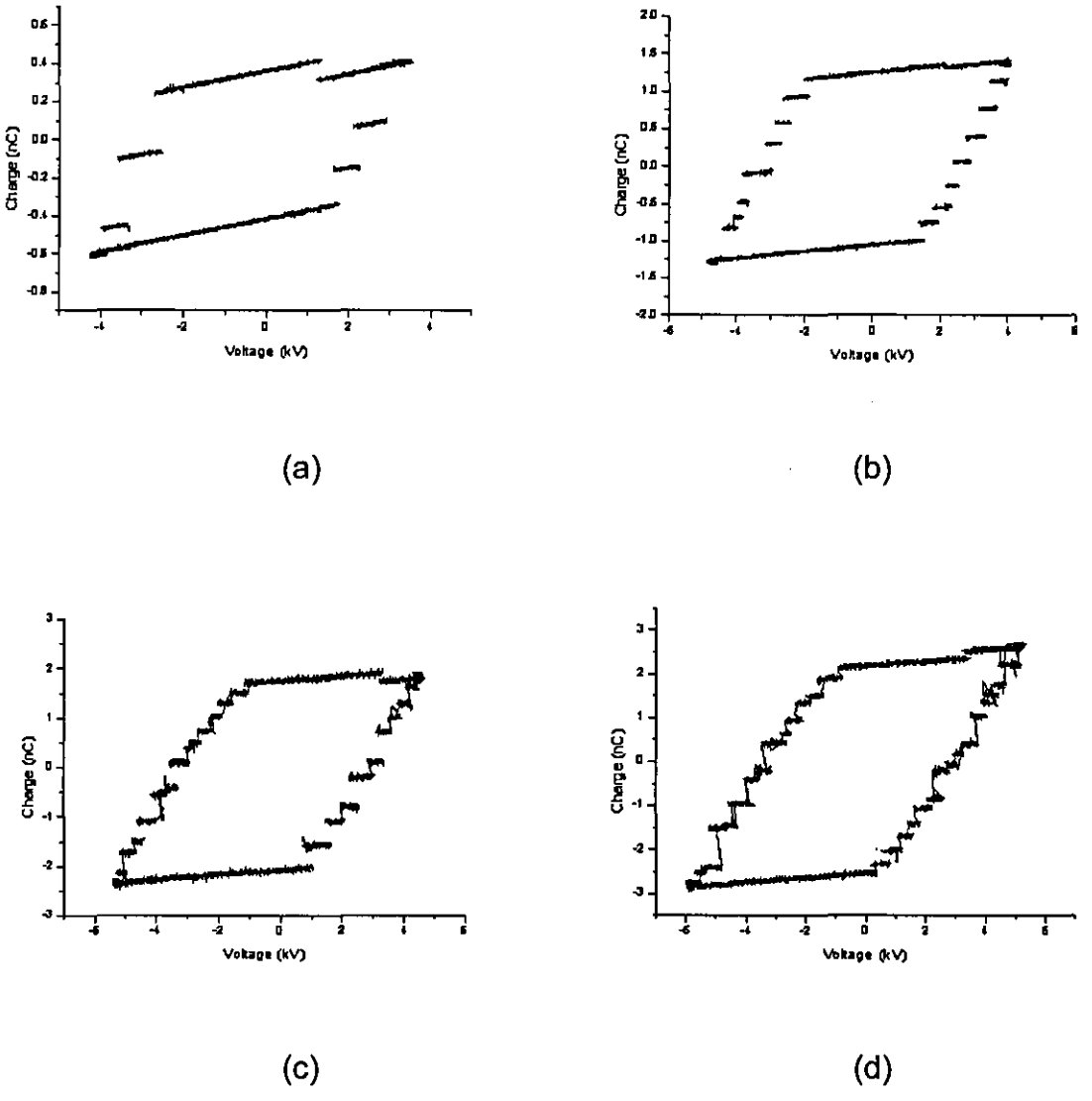

Figure 4.10: Voltage-charge Lissajous figure for fine steel wire mesh (#325, 0.035 mm) at (a) 2.8 kV, (b) 3.2 kV, (c) 3.6 kV, (d) 4.0 kV. Gap distance d = 3 mm, gas flow rate fr = 1 l/min, pressure p = 1 bar.

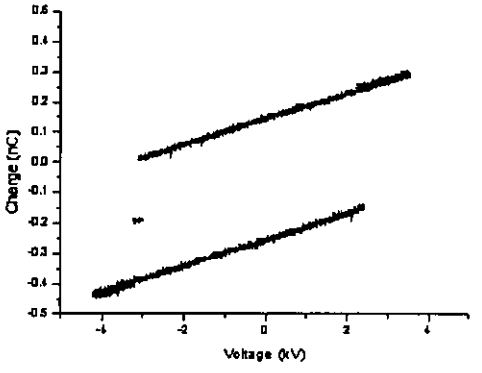

(a)

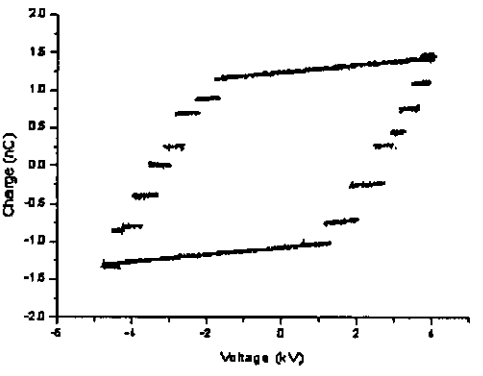

(b)

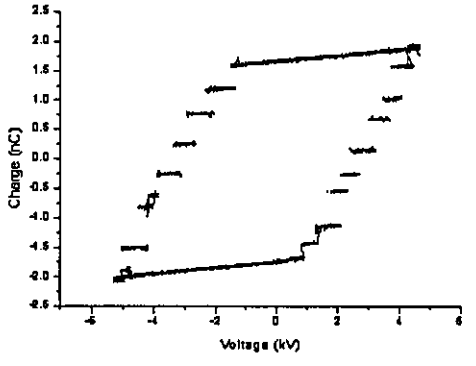

(c)

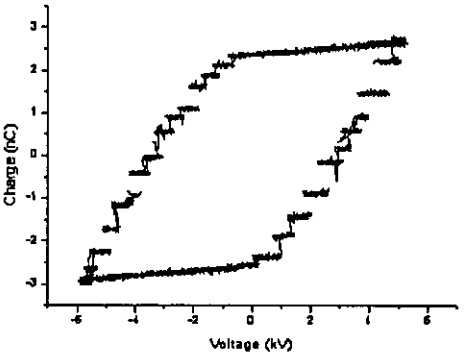

(d)

Figure 4.11: Voltage-charge Lissajous figure for perforated aluminium (1.2 mm diameter, 23% open area) at (a) 2.8 kV, (b) 3.2 kV, (c) 3.6 kV, (d) 4.0 kV. Gap distance d = 3 mm, gas flow rate fr = 1 l/min, pressure p = 1 bar.

Fig 4.10 shows the effect of different values of applied voltage when using steel wire mesh (#325, 0.035 mm) electrodes at a gap spacing increased to 3 mm. Fig. 4.10(a) indicates that at 2.8 kV, a slight glow discharge changing toward a mixed glow-filamentary discharge is generated. Increasing the voltage to 3.2 kV generates a mixed glow-filamentary discharge, as is evident from Figs. 4.10(b). Input voltage of 3.6 kV and 4.0 kV produce similar results, with the glow-filamentary discharge changing to a filamentary discharge, as shown in Figs. 4.10(c) and (d).

Fig 4.11 shows Lissajous figures at different value of applied voltage when using perforated aluminium (1.2 mm, 23% open area) electrodes at gap spacing of 3 mm. The two long lines in Fig. 4.11(a) demonstrate that at 2.8 kV a pure glow discharge is produced. Increasing the voltage to 3.2 kV and then to 3.6 kV generates a mixed glow-filamentary discharge as is evident from Figs. 4.11(b) and (c). At 4.0 kV, Fig.4.11(d) shows that the glow-filamentary discharge mixture has changed into a filamentary discharge.

Fig.4.12 shows results obtained for the APGD in air when using wire mesh (#325, 0.035 mm) electrodes at a gap spacing increased to 3 mm. As shown in Fig. 4.12(a), the discharge current waveform contains only a single pulse in one half cycle of the input voltage and a maximum of two pulses in the other half cycle at input voltages of 2.8 kV, indicating that a slight glow discharge changing toward a mixed glow-filamentary discharge is produced. Increasing the voltage further to 3.2 kV changes the discharge to a mixed glow-filamentary discharge as can be seen in Figs. 4.12(b). When the input voltage is increased to 3.6 kV, Fig. 4.12(c) shows that the discharge current waveform begins to exhibit several pulses in each half cycle of the input voltage. A similar effect appears when the input voltage is increased to 4.0 kV as can be seen from Figs. 4.12(d), indicating that only a filamentary discharge is produced.

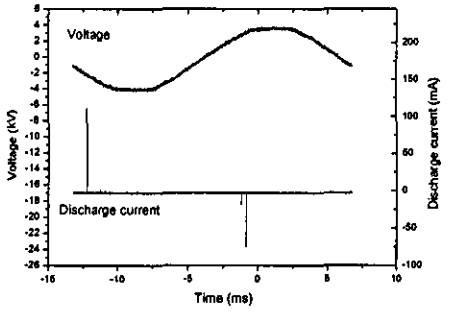

(a)

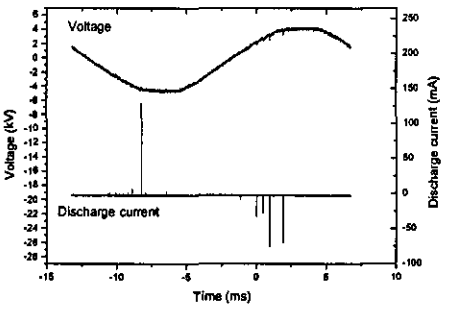

(b)

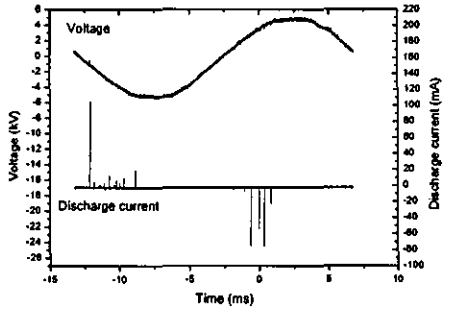

(c)

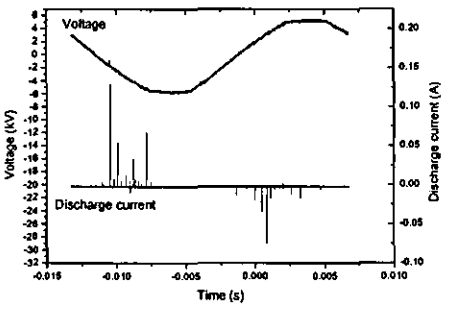

(d)

Figure 4.12: Voltage and discharge current waveform for steel wire mesh (#325, 0.035 mm) at (a) 2.8 kV, (b), 3.2 kV, (c) 3.6 kV, (d) 4.0 kV. Gap distance d = 3 mm, gas flow rate fr = 1 l/min, pressure p= 1 bar

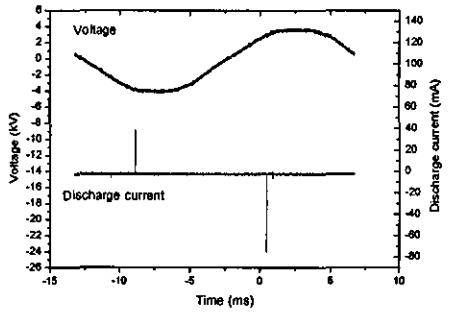

a)

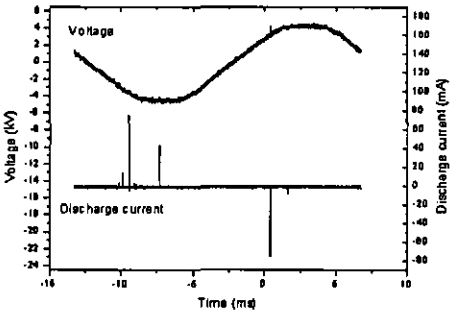

b)

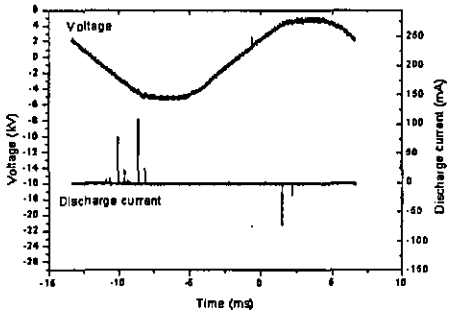

c)

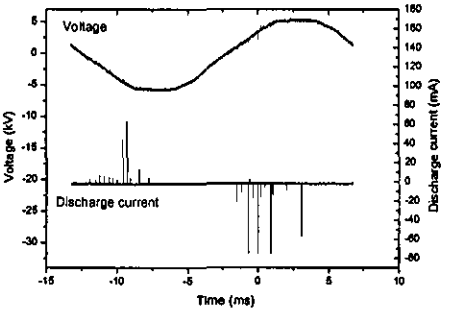

d)

Figure 4.13: Voltage and discharge current waveform for perforated aluminium (1.2 mm diameter, 23% open area) at (a) 2.8 kV, (b), 3.2 kV, (c) 3.6 kV, (d) 4.0 kV. Gap distance d = 3 mm, gas flow rate fr = 1 l/min, pressure p = 1 bar.

Fig.4.13 shows the voltage and discharge current waveform of the APGD produced by perforated aluminium (1.2 mm diameter, 23% open area) electrodes at gap spacing of 3 mm. Fig. 4.13(a) shows that at 2.8 kV, only a glow discharge is produced. Fig. 4.13(b) and (c) both show the discharge current waveform beginning to contain several pulses in one half cycle of the input voltage and a maximum of two current pulses in the other half cycle when the input voltage is increased from 3.2 kV to 3.6 kV, indicating that a mixed glow-filamentary discharge is produced. Increasing the voltage further to 4.0 kV changes the discharge into a filamentary discharge as seen in Fig. 4.13(d).

4.5 Discussion

In general, it has been found that perforated aluminium with small holes can generate a homogeneous glow discharge at atmospheric pressure in air at frequencies as low as 50 Hz, gap spacings of 1.5 mm and 3.0 mm and can produces an even more homogeneous glow discharge than does the fine wire mesh electrodes. This is clear by comparing the discharge behaviour of the two configurations using the Lissajous figures of Figs. 4.4 and 4.5 or the voltage and discharge current waveform of Figs. 4.7 and 4.8 for gap distance of 1 mm. The same advantages were evident when the gap distance was increased to 3 mm, as shown by the Lissajous figures of Figs. 4.10 and Fig. 4.11 or the voltage and discharge current waveform of Fig. 4.12 and Fig. 4.13. However, the maximum spacing between dielectric plates for a stable glow discharge was only 3.0 mm. Beyond that the glow was unstable and tended to generate a filamentary discharge, which is in general agreement with previous work [24,26,60]. Similarly, the stability of the glow discharge seems to depend on the applied input voltage. With the configuration used in this study, the maximum input voltages at which a stable glow discharge can be maintained were 1.6 kV and 3.6 kV for wire mesh at gap spacing of 1.0 mm and 3.0 mm respectively. Whereas, for perforated aluminium, the stability of the glow discharge can be achieved at a maximum applied input voltage of 1.8 kV and 4.0 kV at the gap spacing of 1.0 mm and 3.0 mm respectively, slightly higher than the wire mesh.

The reason why the glow discharge produced by the configuration with perforated aluminium has a better stability than the wire mesh is unclear, since the simulation results for the electric field strength obtained between the two materials showed that the wire mesh configuration produced a higher electric field strength than did the perforated aluminium. This indicates that the electric field strength does not influence the stability of the glow discharge, and is in general agreement with the finding in previous work [27].

However, it may be the shape and size of the holes, as well as the material used, which helps to distribute uniformly the electric field strength throughout the electrode surface, leading to a more uniform and stable glow discharge on the dielectric surface. The preliminary experimental results indicated that, with small diameter holes of perforated aluminium, the glow discharge produced is more stable than with bigger holes suggesting that the holes shape and diameter both have an influence on the glow discharge stability. It is expected therefore that with smaller diameter perforated holes of different shape (i.e of vee or cone form), a better stability of the glow discharge can be achieved

The effect of the material is also evident, when with the use of perforated aluminium a more stable glow discharge is produced than with perforated zinc or even the steel wire mesh. It can be expected that a better stability of glow discharge can be obtained with the use of perforated copper. This is because the copper has a better oxidation process and produces a higher stress at the electrode surface, which in turn will produce more micro-discharges around the electrode. This assumption provides the opportunity for future research.

4.6 Conclusions

The above finding can be summarised as follows:

i.) A homogeneous glow discharge can be produced using a perforated metal electrode configuration instead of the well established fine steel wire mesh (section 4.4).

ii.) Perforated aluminium with a small hole diameter can be used to generate a stable atmospheric pressure glow discharge in air at a frequency as low as 50 Hz (section 4.4 and 4.5).

iii.) The atmospheric pressure glow discharge generated by the perforated aluminium attached behind the dielectric barrier produced a better stability than when attached by the wire mesh (section 4.4).

iv.) The electric field strength does not influence the stability of the glow discharge, and this is in general agreement with the findings of previous work (section 4.3.1 and section 4.5).

v.) The stability of the glow discharge depends on the gap spacing and the applied input voltage, which is in general agreement with previous work (section 4.5)

vi.) The stability of the glow discharge depends on the hole shape and diameter of perforated sheet and the materials used. This was noted in from preliminary experiment and therefore needs further investigation (section 4.2).

vii.) Perforated copper with small diameter holes is expected to produce a better stability than aluminium, since it gives better oxidation process and produce more micro-discharges around the electrode (section 4.5).

With the above findings, the glow discharge produced by the configuration with perforated aluminium attached behind the dielectric barrier was used for ozone generation in the next experiment. The efficiency of the glow discharge system to generate ozone is evaluated and discussed in chapter 5.

CHAPTER 5

AN EXPERIMENTAL COMPARISON BETWEEN ATMOSPHERIC PRESSURE GLOW DISCHARGE AND PULSED STREAMER DISCHARGE FOR OZONE GENERATION IN AIR

5.1 Introduction

For many years ozone has been widely used in applications as diverse as the treatment of drinking and wastewater, and the decomposition of hazardous organic wastes, etc, due to its high oxidizing power. The recent rapid increase in the number of applications has led to the requirement for designing more efficient systems that can produce a high ozone concentration with a high generation efficiency, and this has become the focus of many researchers [1-4,36,37]. Industrial ozonizers based on electrical discharges have been in use for many years. Two of the most promising techniques that have become of considerable interest nowadays are atmospheric pressure glow discharge (APGD) and pulsed streamer discharge (PSD). A study of the relevant literature has confirmed that both of these techniques have the potential to generate ozone more efficiently and effectively than does the silent discharge [28,57]. The ability of the APGD to fill uniformly the entire discharge chamber leads to a better collision efficiency between electrons and molecules, and it appears to be good for generating ozone at high efficiency and concentration [25,28]. On the other hand, the particular features of the PSD with its fast rise time (< 60 ns) and short pulse duration (less than *1* μs) is the high efficiency for radical production [19,20]. This makes it suitable for chemical applications, with ozone generation being one of the best known examples.

This Chapter focuses on the experimental determination and comparison of ozone production efficiencies by both APGD and PSD in air at atmospheric pressure when performed in a single ozone reactor.

5.2 Experimental set-up and procedure

A schematic diagram of the ozone reactor used in both studies is shown in Fig. 5.1. Several such reactors were constructed with lengths ranging from 100 mm to 220 mm, but with a constant width of 16 mm. The change in length increases the effective area of the discharge electrodes from 1.60 $x10^{-3}$ m^2 to 3.52 x 10^{-3} m^2.

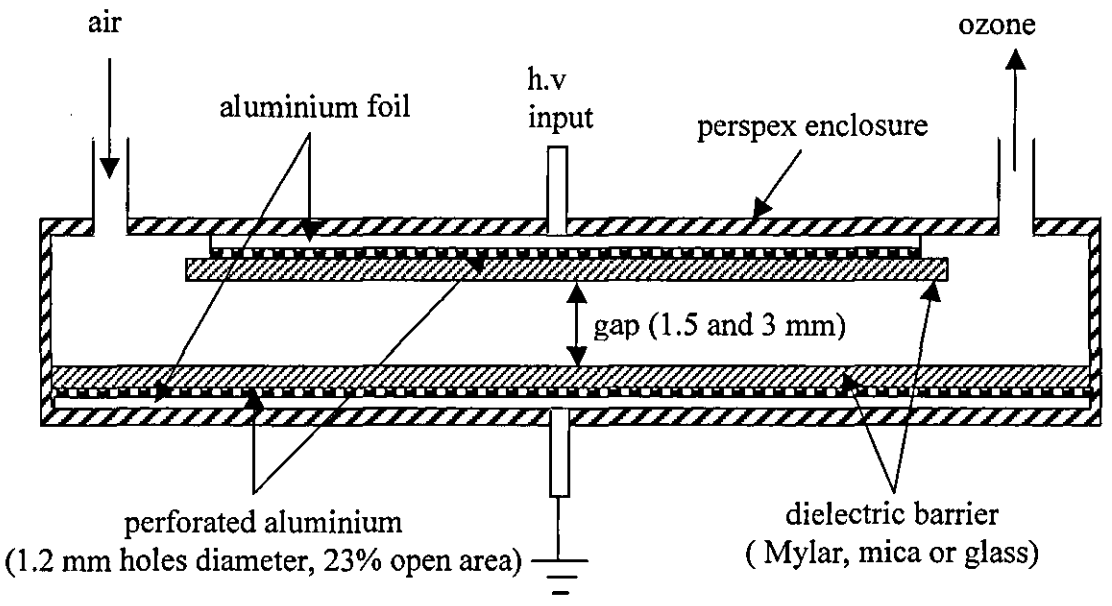

Figure 5.1: Schematic diagram of discharge plasma reactor.

Perforated aluminium (1.2 mm diameter holes, 23% open area) was used for the discharge electrodes and was placed each side of the discharge chamber between the dielectric barrier and the aluminium foil. Soda lime glass sheets with a relative permittivity of 7.75 and a thickness of 1 mm formed the dielectric barriers. The aluminium foil served as the high voltage electrode on one side of discharge chamber and as the ground electrode on the other side, as can be seen from Fig. 5.1.

The gap spacing was either 1.5 mm or 3 mm, with the greater spacing being that which maintained the existence of a glow discharge in the case of the APGD technique. Throughout the investigation the ozone reactor was fed by

cylinder dry air (supplied by BOC), with an oxygen content (by volume) between 17 to 21%. The air flow rate was varied between 0.2 l/min to 1 l/min and was monitored using a flow-rate meter, and the pressure of the dry air feed gas was kept constant at 1 bar. An ozone monitor (Ozone analyzer BMT 964 BT) recorded the ozone concentration on the basis of the ultraviolet absorption (254 nm) properties. Finally, the air-ozone mixture was passed through a catalytic ozone destroyer before being vented to atmosphere. The small scale of the experiment made the danger of ozone leakage into the environment negligible.

The applied voltage was measured by means of a high-voltage probe (Tektronix P6015A, 1000x), with the charge signal obtained with the aid of a 0.22 μF capacitor connected in series to ground. The discharge current was measured by a Rogowski coil/Pearson current monitor (model 2877, 1: 1 V/A). The output signals were measured by a digital oscilloscope (LeCroy 9344) with a bandwidth of 500 MHz and a sample rate of 1 GS/s.

5.2.1 Atmospheric pressure glow discharge mode

Throughout this study, the APGD was produced by applying a high-voltage 50 Hz A.C supply to a plane-to-plane discharge configuration using perforated aluminium, as described previously in Chapter 4 and shown in Fig. 5.1. One advantage of this system is that the glow discharge is produced in a small gap spacing (3 mm maximum) at low frequency (50 Hz) and a low input voltage (maximum 4.8 kV), which therefore utilise very little discharge power (maximum 330 mW). This results in a low gas temperature, which eliminates the need for a cooling system. Furthermore, the glow discharge was produced in air, which is one of the media used for the generation of ozone. Other advantages include a homogeneous discharge over a large volume, low gas breakdown voltage, high electron temperatures capable of dissociating gas molecules and high concentrations of both ions and radicals [29]. The ability of an APGD to fill uniformly the entire discharge chamber is expected to lead

to a better collision efficiency between electrons and molecules, and it appears to be very favourable for generating ozone at a high efficiency and concentration [25,28].

The system used to generate APGD uses the electrical circuit arrangement of Fig. 4.1 of Chapter 4. Table 5.1 summarizes the important experimental parameters.

Properties	Typical value	Unit
System geometry		
Plane-to-plane spacing	1.5 - 3	mm
Length	100 - 220	mm
Effective area	$1.60 \times 10^{-3} - 3.52 \times 10^{-3}$	m^2
Discharge volume	$1.6 \times 10^{-6} - 10.56 \times 10^{-6}$	m^3
Electrical properties		
Polarity	A.C	
RMS Voltage	1 - 20	kV
Current	5	mA
Frequency	50	Hz
Gas properties		
Gas type	Zero grade dry air	
Air flow rate	0.2 – 1.0	L/min
Gas residence time	0.072 – 3.168	s

Table 5.1: Summary of APGD experimental parameters

The discharge power can be estimated from a Lissajous figure (Appendix 5), with the applied voltage and charge from the voltage across the 0.22 μF capacitor displayed respectively on the x-axis and y-axis of an oscilloscope in the x-y mode. The area inside the closed curve is proportional to the energy dissipated in the glow discharge per cycle.

5.2.2 Pulsed streamer discharge mode

A PSD is created by applying a series of fast-rising (<60 ns) and short duration (120 ns) high-voltage pulses to a field-enhanced geometry, such as a plane-to-plane configuration. The use of short pulses is more advantageous for the efficient production of non-thermal plasmas than is the use of longer ones [17-20]. Short high-voltage pulses result in streamers with a short lifetime and allow the production of energetic electrons, and as a consequence less energy is transferred to the ions and the neutral gas [5,20]. In addition to eliminating the need for a cooling system to remove heat from the electrodes, this also reduces the cost of the energy consumed. A positive rather than negative polarity pulse was applied to the high-voltage electrode because, in this condition, the production of ozone is higher [7,16,72-74] (section 3.3.4, Chapter 3).

Fig. 5.2 shows a block diagram of the experimental PSD system. The system incorporates a Blumlein type pulse generator [82] (Fig. 5.3), which is used to generate a non-thermal plasma inside the ozone chamber. The switching system consists of the rotating spark gap shown in Fig. 5.4, driven by a DC motor with a rated speed of 4000 rpm. The discharge chamber is similar to that used for APGD (Fig. 5.1), and the experimental system also incorporated a measuring instrument and a dry air gas handling facility linked to a pressure regulator and flow rate meter (Fig. 5.2). Table 5.2 summarizes the important experimental parameters.

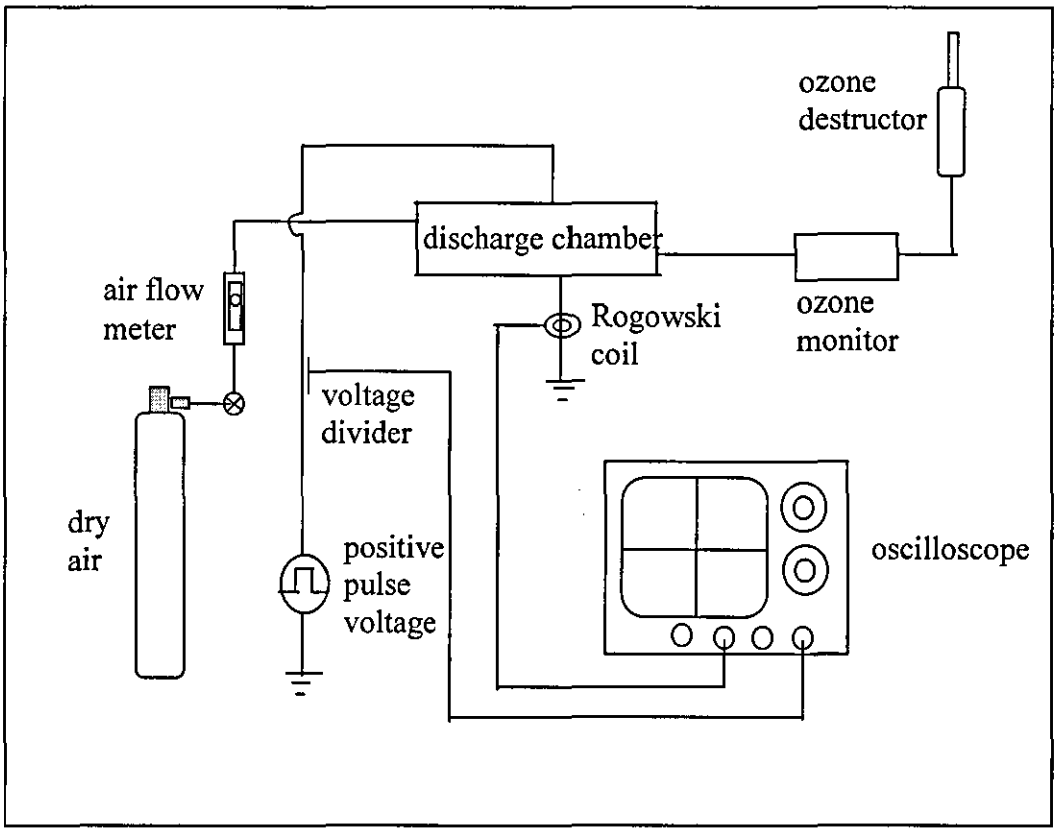

Figure 5.2: Experimental arrangement.

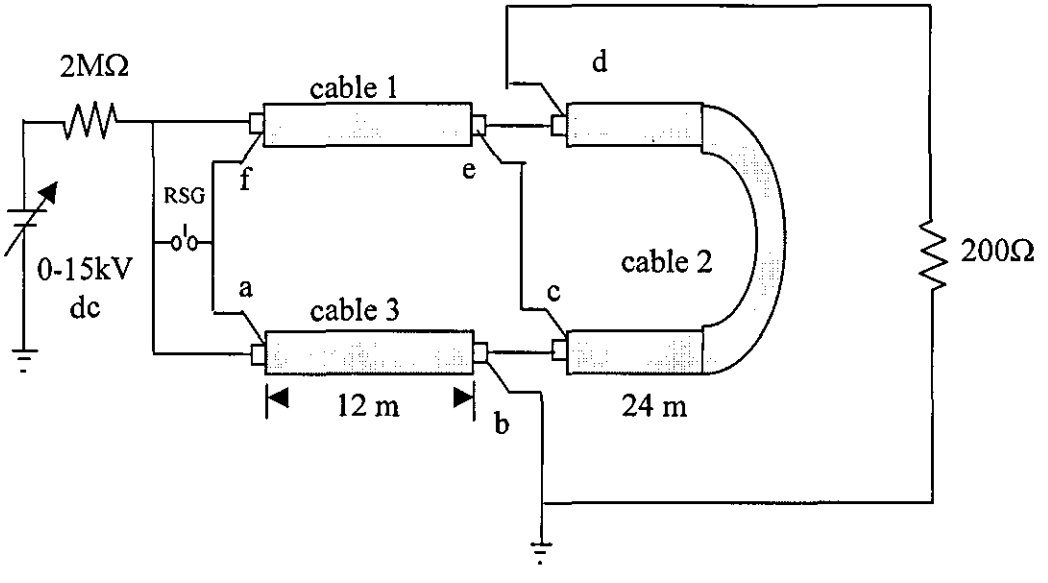

Figure 5.3 : Blumlein high voltage cable pulse generator [82].

Properties	Typical value	Unit
System geometry		
Plane-to-plane spacing	1 - 3	mm
Length	100 - 220	mm
Effective area	$1.60 \times 10^{-3} - 3.52 \times 10^{-3}$	m^2
Discharge volume	$1.6 \times 10^{-6} - 10.56 \times 10^{-6}$	m^3
Electrical properties		
Polarity	positive	
Peak Voltage	1 - 20	kV
Pulse duration	120	ns
Pulse repetitive frequency	50	pps
Gas properties		
Gas type	Zero grade dry air	
Air flow rate	0.2 – 1.0	l/min
Gas residence time	0.072 – 3.168	s

Table 5.2: Summary of PSD experimental parameters

As shown in Fig. 5.2, the pulse voltage is measured by a high-voltage probe (Tektronix P6015) and the discharge current by a Rogowski Pearson current monitor (model 2877, 1: 1 V/A). The discharge power (VI) is obtained automatically from the oscilloscope by multiplication of the measured voltage and current waveforms. The discharge energy per pulse ($\int VI\ dt$) is determined from the pulse voltage, discharge current and pulse duration. The energy per pulse is then multiplied by the pulse repetitive frequency to provide the average discharge power.

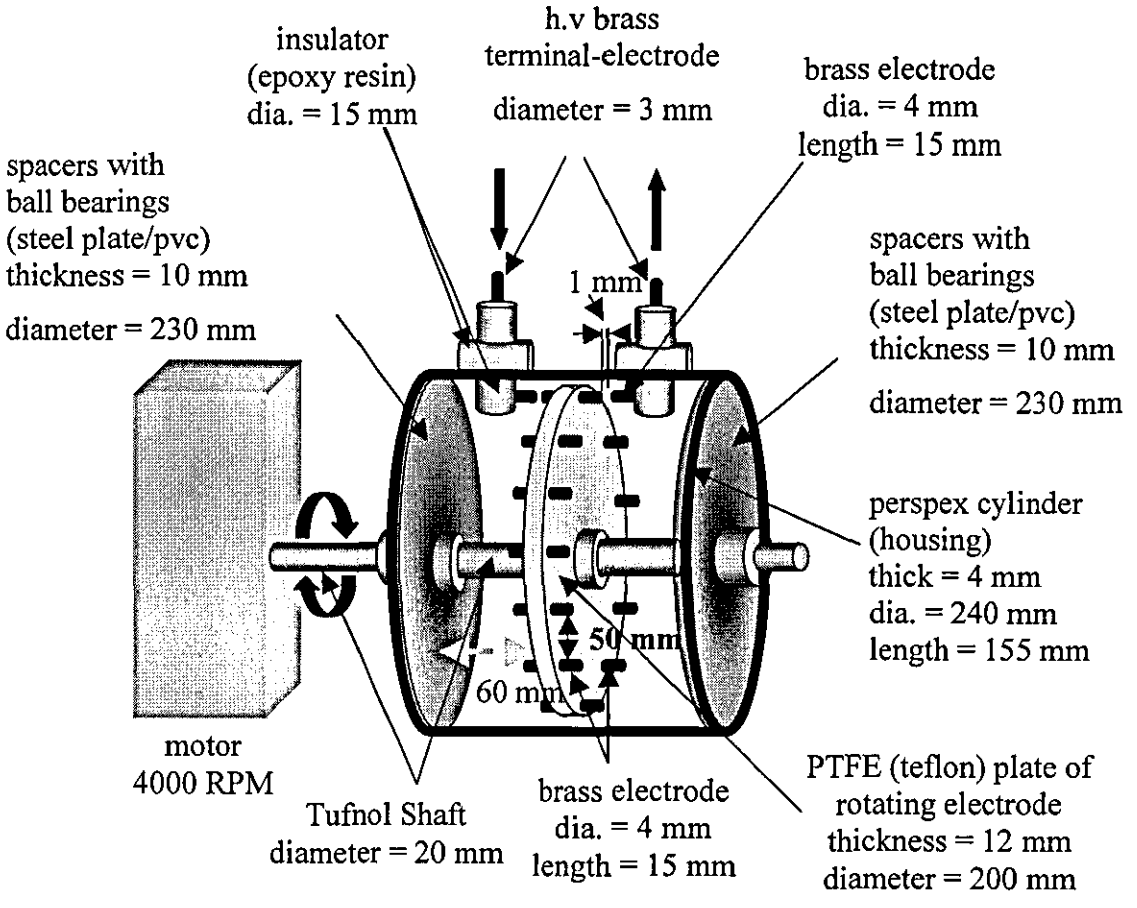

Figure 5.4: The rotary spark gap.

The pulse duration is defined as the full-width half maximum (FWHM) of the pulse voltage and Fig. 5.5 shows a typical voltage and discharge current waveform of the pulse, in which the FWHM of the applied voltage is approximately 120 ns. The peak voltage is about 14 kV and the peak current about 8 A. The small oscillations evident in the current waveforms of Fig. 5.5 may be attributed to both stray circuit inductance and reflected waves due to a slight impedance mismatch between the power supply and the reactor.

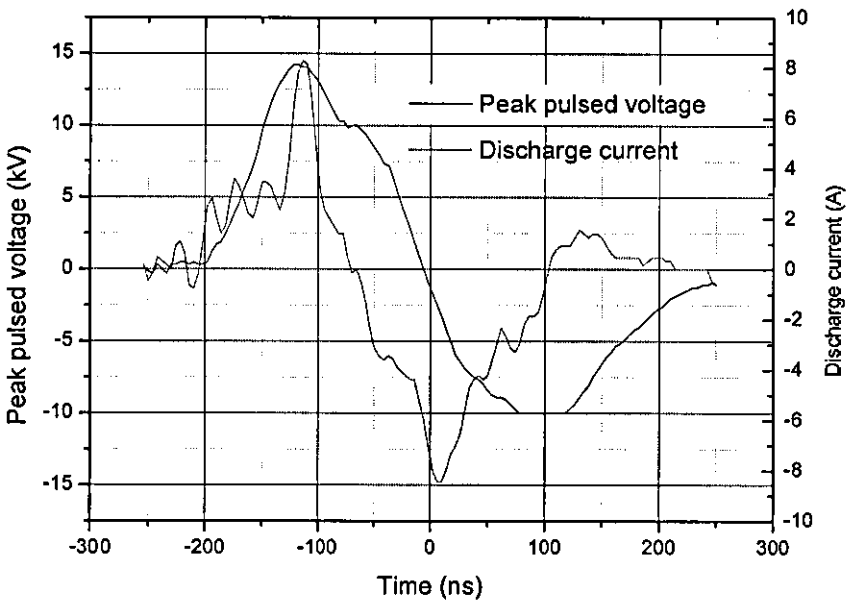

Figure 5.5: Typical pulse voltage and discharge current waveform. Gap spacing = 3 mm, peak pulsed voltage = 14 kV, air flow rate = 0.2 l/min, pulse repetitive rate = 50 pps, pulse duration = 120 ns and pressure = 1 bar.

5.3 Ozone Concentration Measurement

The ozone is detected through the absorption of UV at 254 nm, due to an internal resonance of the ozone molecule. Low pressure mercury lamps are used, so that only light at 254 nm is emitted. The sample gas flows into a transparent chamber/ optical cell, normally constructed from quartz, where the mass of ozone contained in a certain volume (g/m^3) is measured independently of the pressure and temperature of the gas mixture. The distance between the two sides of the measuring chamber defines the measurement range and the sensitivity of the instrument.

To enable the concentration to be calculated, the intensity of the light passing through the measurement chamber/optical cell is measured by a ultraviolet detector located at the opposite end of the optical cell. The reduction in

ultraviolet intensity at 254 nm caused by the presence of ozone in the sample cell is compared with a reference measurement of the generated UV intensity. From the ratio of the two values the concentration can be derived.

The degree of reduction depends on the path-length of the UV optical cell, the ozone concentration introduced into the optical cell, and the wavelength of the UV light, as expressed by the Beer-Lambert law [83]:

$$I = Io \exp (- \alpha LC) \qquad (5.1)$$

which can be simplified to enable direct calculation of the concentration through the equation:

$$C(O_3) = \frac{-\ln(I / I_o)}{\alpha_p L} \qquad (5.2)$$

where

$C(O_3)$ = Ozone concentration

I / Io = Transmittance of the ozone sample

α_p = Specific ozone molar absorption coefficient
= 308 cm^{-1} atm^{-1} at STP.

L = Path-length

The only routine test that must be made is to check the display for zero reading at zero ozone concentration. To achieve zero concentration, the instrument pathway has to be purged with pure feed gas or ambient air containing no ozone. This procedure was carried out regularly throughout the investigation, in order to ensure consistency of results.

5.4 Calculation of ozone yield

The efficiency of the system for ozone generation η in term of the yield in g/kWh was determined from [67]

$$\eta = \left[\frac{C(O_3) f_r}{P} \right] \tag{5.3}$$

where η is the efficiency (g/kWh), $C(O_3)$ is the ozone concentration (ppmv), f_r is the gas flow rate (l/min) and P is the discharge power (kW). The parameters $C(O_3)$ and f_r are directly measurable, while the parameter P in an APGD system is determined from equation (3.13, section 3.3.2, Chapter 3) or directly from Lissajous figure [64,70] (see Appendix 3). With a PSD system, parameter P is determined by multiplication of the pulse repetition frequency f (pps) and the input energy to the discharge per pulse E_r (J/pulse), which in turn is obtained as explained in Section 5.2.2.

5.5 Results and analysis

The performances of both APGD and PSD reactions were evaluated in term of their ozone concentration in volume per parts per million (ppmv) and their yield expressed in g/kWh. To ensure a correct measurement, the discharge was run continuously for at least 5 minutes, until a steady-state level was indicated by the ozone analyzer. After each measurement the discharge was turned off until the monitor recorded zero ozone level. The new discharge conditions and/or airflow were then fixed and the discharge turned on again for the new measurement

5.5.1 Atmospheric pressure glow discharge .

The measurement of ozone production was conducted before the glow discharge changed to a filamentary discharge, and recorded when the concentration has reached a steady-state value, typically after about 60 s to 90 s. This was to demonstrate the role played by the glow discharge at atmospheric pressure in the generation, which is the aim of this investigation. The transition from a glow to a filamentary discharge limits the input voltage to a certain maximum level. The maximum achievable values at gap spacings of 1.5 mm and 3 mm before a filamentary discharge appeared were 4.2 kV and 4.8 kV respectively, and a slight increase in the input voltage immediately resulted in a filamentary discharge at both gap spacings. Similarly, the maximum stable gap spacing between the dielectric plates was only 3.0 mm. Above that the unstable glow tended to form a filamentary discharge, which is in agreement with previous findings [24,26,27]. Since an objective of the study was to evaluate the performance of the APGD on ozone production, the ozone concentration when the glow change to a filamentary discharge is not recorded.

5.5.1.1 Ozone concentration

5.5.1.1.1 Effect of input voltage, air flow rate and/or residence time.

The effects of input voltage, air flow rate and gas residence time on ozone concentration as a result of the application of APGD to dry air for a chamber length of 160 mm are shown in Figs. 5.6, 5.7 and 5.8 respectively.

Fig. 5.6 shows the effect of the input voltage on the concentration at air flow rates of 0.2, 0.6 and 1.0 l/min, with all other parameters kept constant. At a gap spacing of 3 mm, the initial input voltage to start the glow discharge is about 3.8 kV, illustrating the advantage of the glow discharge in providing a low gas breakdown voltage. This input voltage produces approximately 490,

239 and 195 ppmv of ozone concentration at air flow rates of 0.2, 0.6 and 1.0 l/min. In general, the concentration increased linearly for all air flow rates as the input voltage is increased, and there is a rapid change in the magnitude and rate of increase of the concentration, especially at increasing gas flow rates. At a maximum input voltage of 4.8 kV (before the transition from a glow to a filamentary discharge occurs), the concentrations at 0.2 l/min, 0.6 and 1.0 l/min air flow rates were approximately 2050, 1039 and 674 ppmv (corresponding to about 0.31%, 0.16% and 0.10% by weight respectively), resulting in a total increment from the corona starting voltage of approximately 76.1%, 77.0% and 71.1% respectively.

Figs. 5.7 shows the effect of the air flow rates on the concentration at input voltages between 3.8 kV and 4.8 kV, and it can be seen that the concentration is higher for all input voltages at lower air flow rates and at higher gas residence times. The gas residence time is defined simply as the inverse of the gas flow rate (see equation (3.15), Chapter 3), which means that an increase in the air flow rate will decrease the gas residence time and vice versa. Fig. 5.7 shows that the concentration decreases rapidly as the air flow rate is increased from 0.2 to 0.6 l/min, and decreases gradually if is further increased to 1.0 l/min. By contrast, an increase in gas residence time from 0.461 s to 2.30 s results in an increased concentration, as is illustrated clearly in Fig.5.8. At the maximum input voltage of 4.8 kV, an increase in the air flow rate from 0.2 l/min to 1.0 l/min (decreasing the gas residence time from 2.30 s to 0.46 s respectively) has drastically decreased the concentration from 2050 ppmv (corresponding to about 0.31% by weight) to approximately 674 ppmv (corresponding to about 0.10% by weight). These changes have resulted in a reduction of about 79.6% in the concentration. Since the gap spacing (3 mm) and the chamber length (160 mm) were kept constant, the volume of the discharge reactor was also constant (7.68×10^{-6} m^3). Less energy is therefore deposited in the gas stream per litre of gas at a constant input voltage, resulting in a lower concentration as the air flow rate is increased.

The results in Figs. 5.6, 5.7 and 5.8 show that the APGD system generates a maximum ozone concentration of about 2050 ppmv (corresponding to about

0.31% by weight) at air flow rates as low as 0.2 l/min (2.30 s residence time) and input voltages as high as 4.8 kV. This is explained on the basis that, at a lower air flow rate, the background gas will have a longer residence time as well as an increased reaction time in the discharge zone. Furthermore, the characteristics of the glow discharge which uniformly fills the entire volume of the discharge reactor, make it possible for energetic electrons to dissociate more oxygen molecules to generate ozone. At longer residence times the probability of the dissociation of oxygen molecules into atomic oxygen increases, and hence the frequency of $O \rightarrow O_2$ attachment to generate (O_3) is increased. It can be concluded that the input voltage, air flow rate and gas residence time all have a great influence on ozone concentration. It can also be suggested that, at higher input voltages, the efficiency of the system used in this study is high at a low air flow rate of 0.2 l/min but low at higher air flow rates.

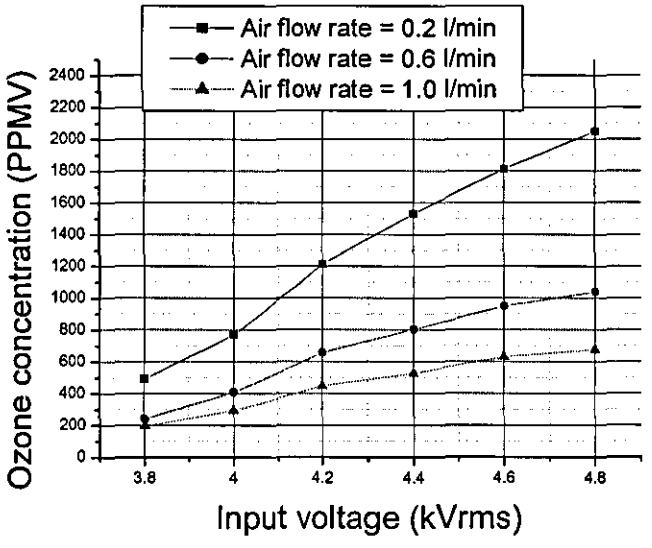

Figure 5.6: Effect of input voltage on ozone concentration at different air flow rates. Condition: dielectric material soda lime glass (ε_r=7.75), gap distance 3 mm, chamber length 160 mm, pressure 1 bar.

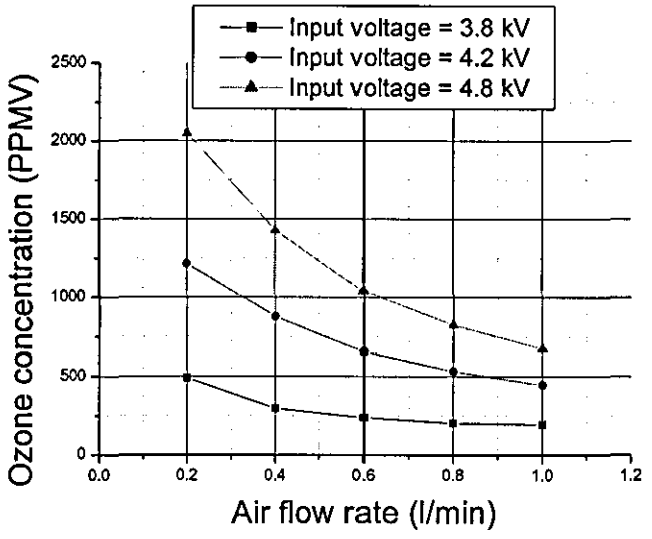

Figure 5.7: Effect of air flow rate on ozone concentration at different input voltage. Condition: dielectric material soda lime glass (ε_r=7.75), gap distance 3 mm, chamber length 160 mm, pressure 1 bar.

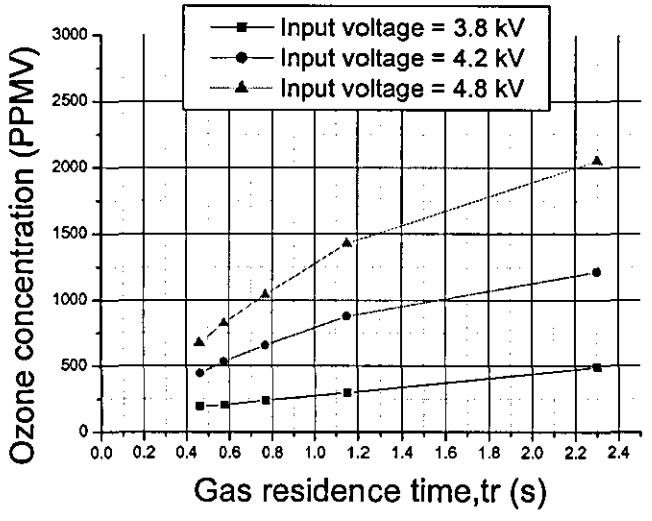

Figure 5.8: Effect of gas residence time on ozone concentration at different input voltage. Condition: dielectric material soda lime glass (ε_r=7.75), gap distance 3 mm, chamber length 160 mm, pressure 1 bar.

5.5.1.1.2 Effect of gap spacing on ozone concentration

The effect of reducing the gap spacing from 3.0 mm to 1.5 mm on the ozone concentration is shown in Figs. 5.9, 5.10 and 5.11, as a function of input voltage, air flow rate and gas residence time. Figs.5.9 and 5.10 show that, as the spacing decreases, the concentration becomes higher for a constant applied voltage and a low air flow rate. At an input voltage of 4.2 kV, a maximum concentration of about 1213 ppmv and 1516 ppmv is obtained at a low air flow rate of 0.2 l/min at gap spacings of 3.0 mm and 1.5 mm respectively. This result represents about a 19.97% increase in the concentration as the spacing is reduced from 3.0 mm to 1.5 mm, and this percentage is almost constant at increasing air flow rate, as is evident from Fig. 5.9. At the same, or even a lower gas residence time, the smaller spacing produces a higher concentration than the larger spacing, as can be seen in Fig. 5.10. For example, to obtain a similar concentration of 1200 ppmv, the spacing of 1.5 mm needs only about 0.78 s of gas residence time, whereas a spacing of 3.0 mm needs about 1.9 s. This is because, at a constant input voltage and a small gap spacing, the electric field strength and discharge current density are increased, increasing the reaction $e + O_2 \rightarrow 2O + e$ to result in the higher concentration. Furthermore, at the smaller gap spacing the corona starting voltage is lower and ozone production begins at a lower input voltage (3 kV at 1.5 mm gap spacing, Fig.5.11). These figures clearly indicate the advantages of the small spacing.

There is however a limitation to the maximum production of ozone at a small spacing, as is evident in Fig.5.11, Firstly, because the transition of the discharge from glow to filamentary limits the maximum input voltage to a certain value (4.2 kVrms in this case), thereby leading to a lower maximum concentration. Secondly, as the input voltage is increased, the concentration tends to saturate at an early stage and a lower concentration is generated than with a bigger spacing, as can be seen from Fig. 5.11. This is explained on the basis that, with a small spacing, electrons which gain more energy not only dissociate the oxygen molecules but also the generated ozone as the

input voltage is increased. At this stage, the rate of ozone formation is equivalent to the rate of its destruction, leading to saturation of the concentration. On the other hand, with a greater spacing a higher concentration can be obtained, and no sign of saturation is in fact observed until the discharge changes to a filamentary one, when the input voltage reaches 4.8 kV. At a greater gap spacing, a higher input voltage can be applied and an increased electron energy can be achieved. Furthermore, as the spacing increases the volume of the discharge and the residence time are also increased. Therefore, the probability of the reaction $e + O_2 \rightarrow 2O + e$ resulting to an increase in the concentration is also increased.

It can be concluded that the advantage of a small spacing over a large spacing in producing higher ozone concentration is limited, firstly by the change of the glow to a filamentary discharge at lower input voltage and secondly due to the lower saturation level. This indicates the limitation of the small gap spacing used in this study, in which the highest concentration that can be obtained at a spacing of 1.5 mm is approximately 1516 ppmv (corresponding to 0.23% by weight) at an input voltage of 4.2 kV and 0.2 l/min of air flow rate or 0.72 s of residence time. Whereas, at a spacing of 3 mm the maximum concentration obtained is about 2050 ppmv (corresponding to 0.31% by weight), which is 1.35 times higher than at the smaller spacing. This figure is obtained at the maximum input voltage before the glow discharge changed to a filamentary discharge (4.8 kV) and at 0.2 l/min air flow rate or 2.30 s of gas residence time.

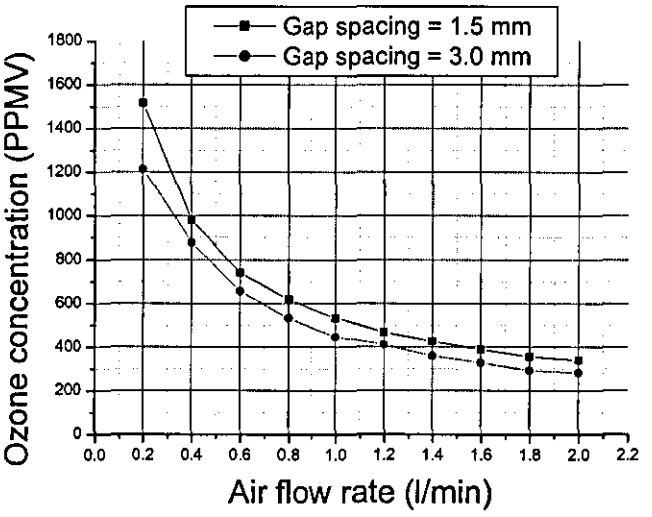

Figure 5.9: Effect of gap spacing on ozone concentration as a function of air flow rates. Condition: dielectric material soda lime glass (ε_r=7.75), chamber length 160 mm, input voltage 4.2 kV, pressure 1 bar.

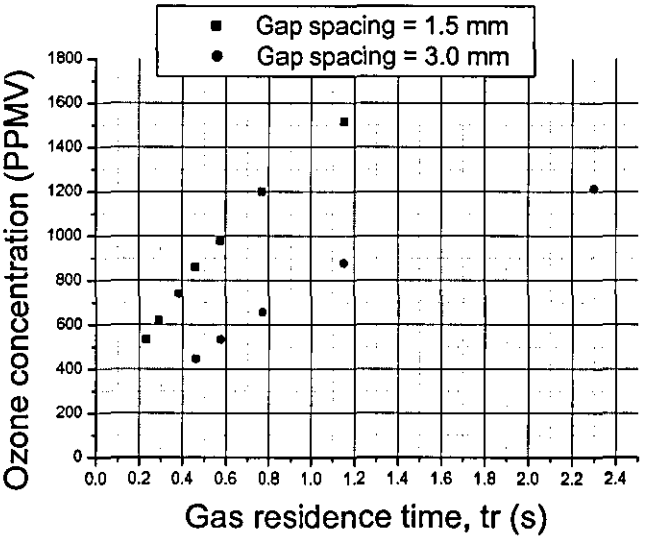

Figure 5.10: Effect of gap spacing on ozone concentration as a function of gas residence time. Condition: dielectric material soda lime glass (ε_r=7.75), chamber length 160 mm, input voltage 4.2 kV, pressure 1 bar.

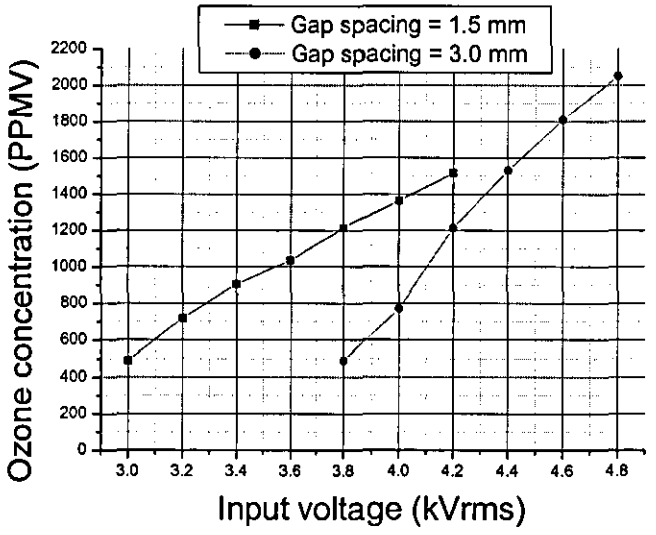

Figure 5.11: Effect of gap spacing on ozone concentration as a function of input voltage. Condition: dielectric material soda lime glass (ε_r=7.75), chamber length 160 mm, air flow rate 0.2 l/min, pressure 1 bar.

5.5.1.1.3 Effect of chamber length on ozone concentration

Figs. 5.12 and 5.13 show the effects of increasing or decreasing the chamber length on the ozone concentration as a function of input voltage and air flow rate, with all other parameters kept constant. A decrease in the chamber length from 160 mm to 100 mm results in a slight decrease in the concentration at a lower input voltage. However, at a higher input voltage of 4.8 kV the concentration decreases drastically from 2050 ppmv at 160 mm to 1648 ppmv at 100 mm, approximately a 19.61% reduction, indicating clearly the disadvantage of this length (see Fig. 5.12). Basically, the increase in input voltage results in an increase in the electric field strength but, with the chamber length decreased to 100 mm, the gas residence time is decreased from 2.3 s (160 mm) to 1.44 s (100 mm), leading to the lower concentration.

On the other hand, increasing the chamber length from 160 mm to 220 mm, results in a slight increase in the ozone concentration from 2050 ppmv to about 2355 ppmv at the maximum input voltage, approximately a 12.95%

increment as indicated in Fig. 5.12. Further, no sign of saturation can be observed for either chamber length, as the input voltage is still too low. As the chamber length is increased at a constant gap spacing (3 mm) the volume of the discharge reactor is also increased. The residence time of the gas stream in the discharge zone (2.30 s and 3.17 s for 160 mm and 220 mm respectively) and the discharge energy are also increased, resulting in an increased ozone concentration as the input voltage is increased, as can be seen in Fig. 5.12. However, it should be noted that as the discharge energy increases, the increase in the gas residence time not only results in an increased concentration but also in destruction of some of the generated ozone. This explains why increasing the chamber length from 160 mm to 220 mm provides only a very small increment in the concentration.

The effect on the concentration of changing the chamber length is shown in Figs. 5.13 as a function of the air flow rate. It can be observed that at a lower air flow rate, there is some difference in the concentration produced in the three chamber lengths of 100, 160 and 220 mm. However, at a higher air flow rate, the three curves are virtually identical, implying that the chamber length then has little effect on the concentration at an increasing air flow rate but a given input voltage. On the other hand, the effect of the chamber length on the concentration as a function of the residence time is more apparent, as can be seen from Fig. 5.14. It will be observed that at lower residence time, the shorter chamber length leads to a higher concentration than does the longer one. However, at an increased residence time, the longer chamber length produces a slightly increased concentration. It can be concluded that, for a constant input voltage and different chamber length, any increase or decrease in the air flow rate has little effect on the rate of increase of the concentration.

In general, since the gas input is measured in term of its flow rate, the use of the gas residence time serves only as a guideline to determine an optimum air flow rate for an ozone chamber, in order to obtain an optimum efficiency.

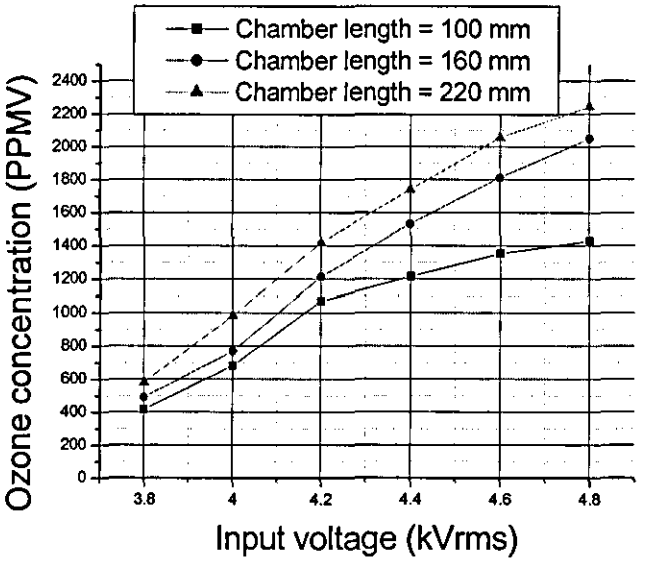

Figure 5.12: Effect of chamber length on ozone concentration as a function of the input voltage. Condition: dielectric material soda lime glass (ε_r=7.75), gap distance 3 mm, air flow rate 0.2 l/min, pressure 1 bar.

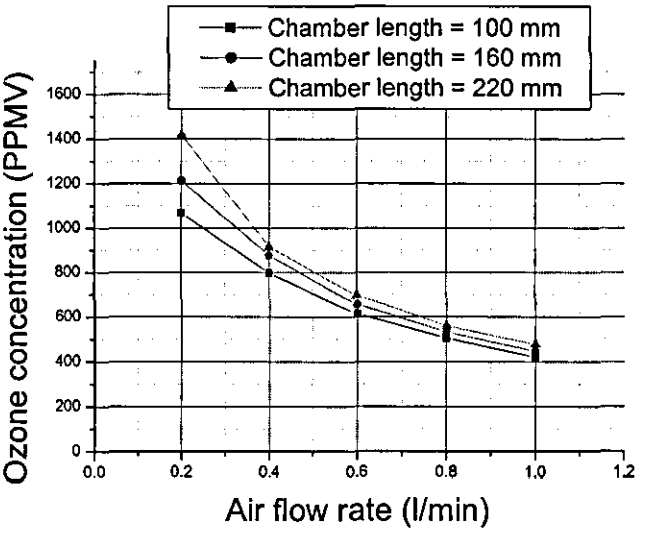

Figure 5.13: Effect of chamber length on ozone concentration as a function of the air flow rates. Condition: dielectric material soda lime glass (ε_r=7.75), gap distance 3 mm, input voltage 4.2 kV, pressure 1 bar.

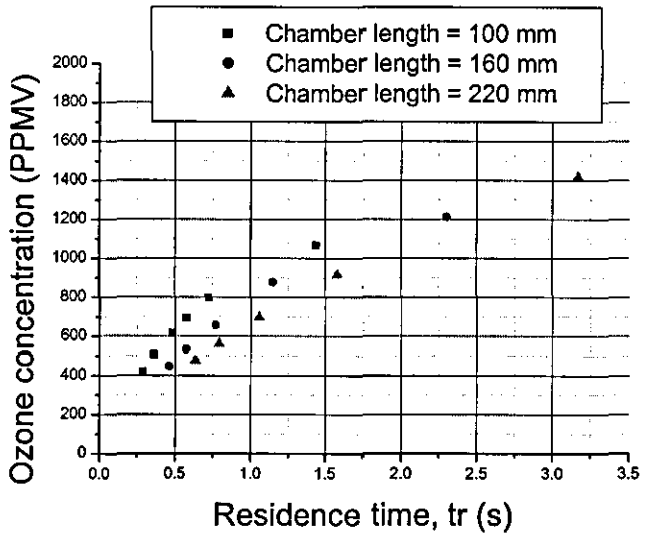

Figure 5.14: Effect of chamber length on ozone concentration as a function of gas residence time. Condition: dielectric material soda lime glass (ε_r=7.75), gap distance 3 mm, input voltage 4.2 kV, pressure 1 bar.

5.5.1.2 Ozone yield

5.5.1.2.1 Effect of input voltage, air flow rate and residence time on ozone yield.

The ozone yield in g/kWh of input energy to the gas is shown in Figs. 5.15, 5.17 and 5.18, as a function of input voltage, air flow rate and gas residence time at a fixed gap length of 3 mm and a chamber length of 160 mm. It can be observed that for all air flow rates the yield of ozone initially increases with an increasing input voltage, up to certain level. At an input voltage above 4.2 kV, the yield begins to decrease with any increase in the applied voltage, for all air flow rates, as can clearly shown in Fig. 5.15. This is because the rate of increase of the concentration with increasing voltage became less linear at higher voltages (see Fig. 5.6). The input energy to the discharge per cycle then increases at a higher rate than does the concentration of ozone (see Fig. 5.16), leading to a lower yield at higher voltages and therefore at higher

concentrations. The highest yield of 349.19 g/kWh was obtained at an air flow rate of 1.0 l/min and an input voltage of 4.2 kV.

Figs. 5.17 and 5.18 show the effect of air flow rate and gas residence time on the ozone yield at a fixed input voltage. It can be observed that either an increase in air flow rate or a decrease in gas residence time results in an increase in the yield at a fixed input voltage, with an input voltage of 4.2 kV producing the highest yield. At 0.2 l/min (2.3 s gas residence time) the yield at 4.2 kV is about 214.12 g/kWh. As the air flow rate increases to 1.0 l/min (the gas residence time reducing to 0.46 s), the yield increases to about 349.19 g/kWh. This represents an increment of approximately 38.7%, and indicates that the air flow rate and gas residence time have a considerable influence, as indeed is evident in Figs. 5.17 and 5.18.

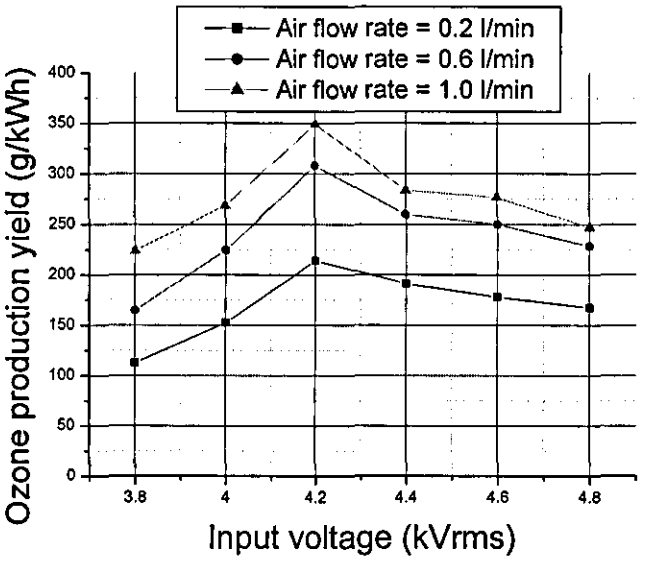

Figure 5.15: Effect of input voltage on ozone yield at different air flow rates. Condition: dielectric material soda lime glass (ε_r=7.75), gap distance 3 mm, chamber length 160 mm, pressure 1 bar.

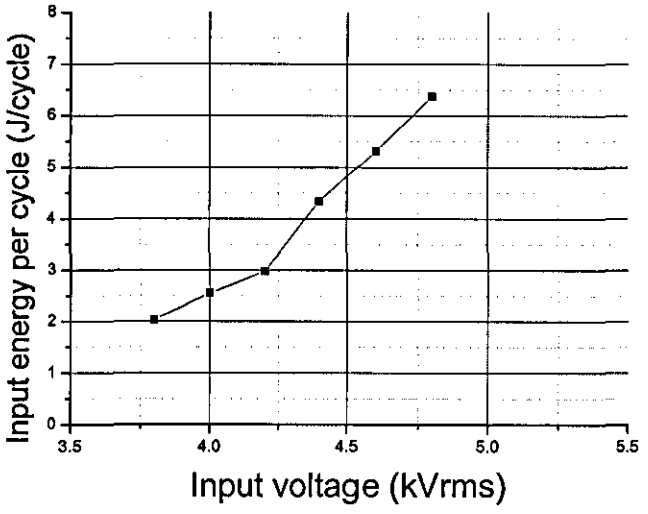

Figure 5.16: Effect of increasing input voltage on input energy to the discharge per cycle.

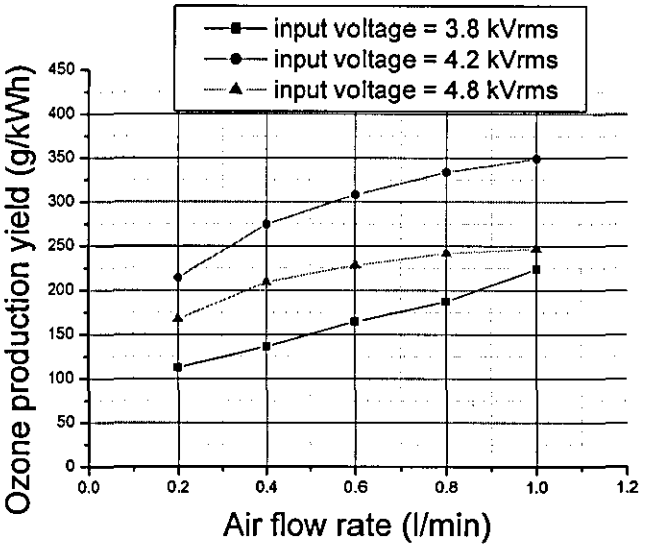

Figure 5.17: Effect of air flow rate on ozone yield at a fixed input voltage. Condition: dielectric material soda lime glass (ε_r=7.75), gap distance 3 mm, chamber length 160 mm, pressure 1 bar.

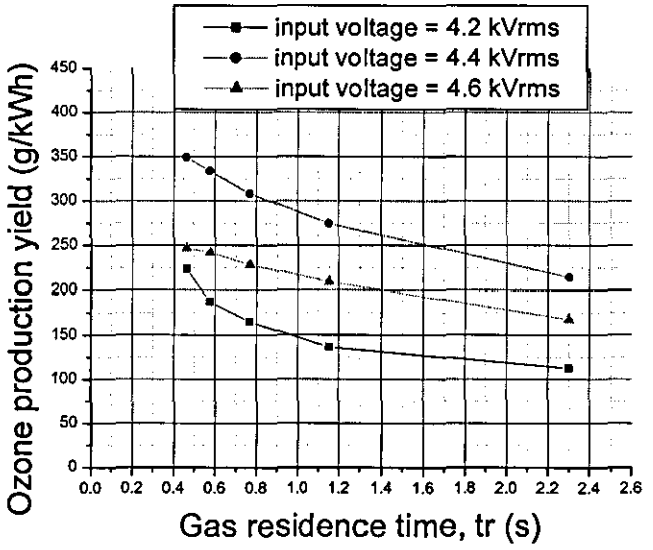

Figure 5.18: Effect of gas residence time on ozone yield at a fixed input voltage. Condition: dielectric material soda lime glass (ε_r=7.75), gap distance 3 mm, chamber length 160 mm, pressure 1 bar.

5.5.1.2.2 Effect of gap spacing on ozone yield.

The effect on the ozone yield of decreasing the gap spacing from 3.0 mm to 1.5 mm is shown in Figs. 5.19, 5.20 and 5.21 as a function of air flow rate, gas residence time and input voltage respectively. At a constant input voltage of 4.2 kV, decreasing the spacing from 3.0 mm to 1.5 mm results in a decrease in the yield. This occurs for all ranges of air flow rate and gas residence time as is clear from Figs. 5.19 and 5.20. At a low air flow rate of 0.2 l/min (2.3 s and 1.152 s gas residence time for spacings of 3.0 mm and 1.5 mm respectively), the yield fell from 214.12 g/kWh (3.0 mm gap spacing) to 147.75 g/kWh (1.5 mm gap spacing), a reduction of approximately 31%. The yield increases linearly as the air flow rate is increased for both spacing. At an air flow rate of 1.0 l/min (0.46 s and 0.23 s gas residence time for gap spacing of 3.0 mm and 1.5 mm respectively), it decreases from 349.19 g/kWh at 3.0 mm to 259.6 g/kWh at 1.5 mm spacing, a reduction of approximately 25.6%.

Fig.5.21 shows the effect of gap spacing on the yield as a function of input voltage, and decreasing the spacing from 3.0 mm to 1.5 mm is seen to result in a reduction in ozone yield. At a constant air flow rate of 0.2 l/min, the maximum yield with a spacing of 3.0 mm and obtained at an input voltage of 4.2 kV is approximately 214.12 g/kWh, whereas a decreased spacing of 1.5 mm results in a decreased yield, with the maximum of approximately 155.39 g/kWh now obtained at an input voltage of 3.2 kV, a reduction of about 27.4%. The efficiency of the yield is related to its dependence of the concentration (Fig. 5.11), and the dependence of the energy input into the discharge on the input voltage (Fig. 5.22) [4]. At a fixed input voltage and a constant air flow rate, the decreased gap spacing of the reactor results in an increased input energy to the discharge, as can be seen in Fig. 5.22. At a fixed input voltage, the discharge current increases with a decrease in the spacing, resulting in an increase in the conductivity of the glow discharge due to the higher electric field at a shorter spacing. At a point where the rate of increase of input energy into the discharge is higher than the rate of increase of ozone concentration, this may result to a decrease in the ozone yield.

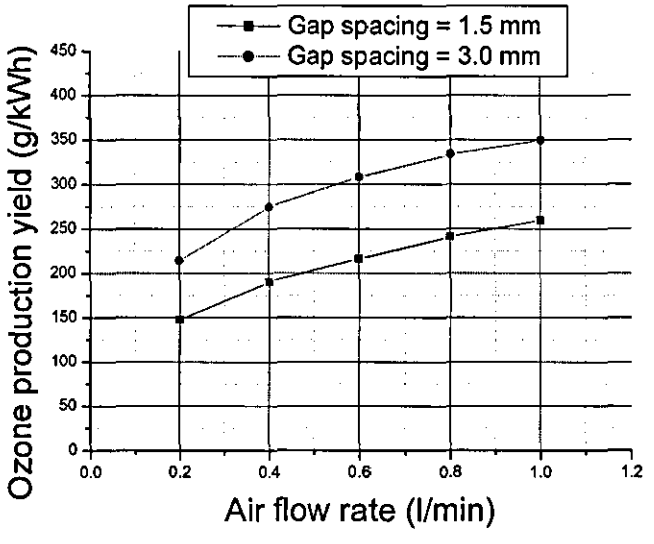

Figure 5.19: Effect of gap spacing on ozone yield as a function of air flow rate. Condition: dielectric material soda lime glass (ε_r=7.75), chamber length 160 mm, input voltage 4.2 kV, pressure 1 bar.

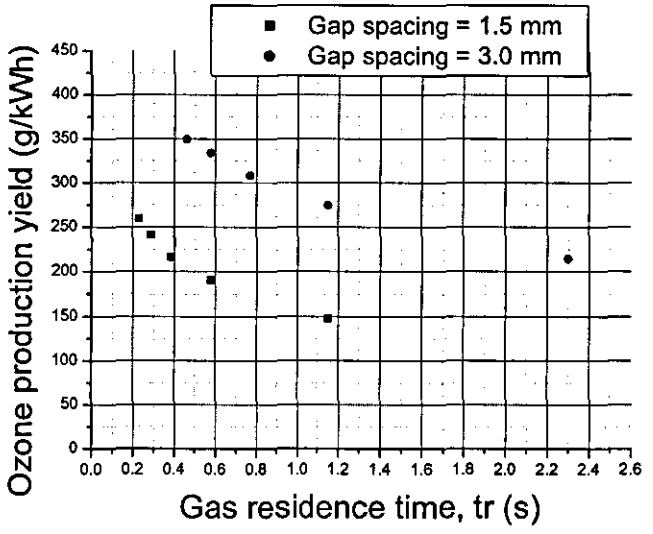

Figure 5.20: Effect of gap spacing on ozone yield as a function of gas residence time. Condition: dielectric material soda lime glass (ε_r=7.75), chamber length 160 mm, input voltage 4.2 kV, pressure 1 bar.

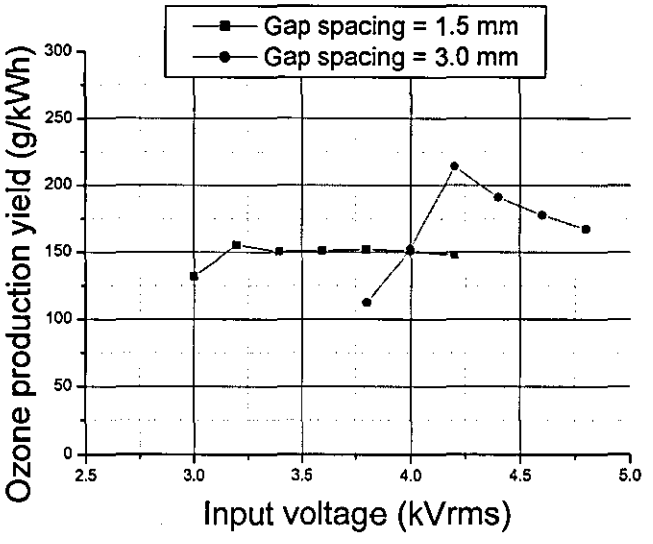

Figure 5.21: Effect of gap spacing on ozone yield as a function of input voltage. Condition: dielectric material soda lime glass (ε_r=7.75), chamber length 160 mm, air flow rate 0.2 l/min, pressure 1 bar.

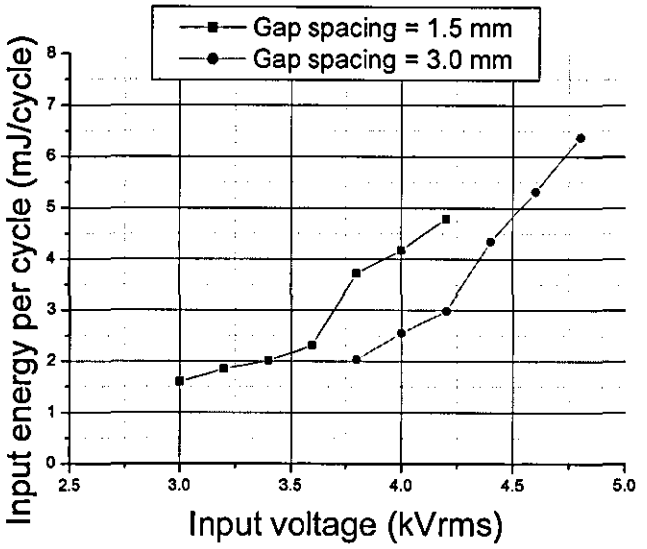

Figure 5.22: Effect of input voltage on input energy into the discharge per cycle at gap spacing of 1.5 mm and 3.0 mm.

5.5.1.2.3 Effect of chamber length on ozone yield.

The effect of varying the chamber length on the ozone yield is shown in Figs. 5.23, 5.24 and 5.25 as a function of input voltage, air flow rate and gas residence time.

Fig. 5.23 shows the effect of both increasing and decreasing the chamber lengtn on the yield as a function of the input voltage. It can be observed that an increase in the chamber length from 160 mm to 220 mm or a decrease to 100 mm, both result in a decreased yield. At a constant air flow rate of 0.2 l/min, the decreased length results in a reduced maximum yield, from 214.12 g/kWh (at 160 mm) to 158.01 g/kWh (at 100 mm), a reduction of about 26.2%. On the other hand, the increased length to 220 mm also results in a decrease in the yield to about 138.04 g/kWh (at 220 mm), a reduction of some 35.53%. This result is related to the dependence of the yield on the ozone concentration and the energy input to the discharge from the input voltage. It can be observed from Fig. 5.26 that, at a given applied voltage, an increased length result in an increase in the energy input to the discharge per cycle. A

decreased chamber length results in a decrease in the input energy (Fig. 5.26) and therefore to a reducing rate of increase in the ozone concentration with increasing voltage (Fig.5.12), leading to a lower yield. The result for an increased chamber length is explained in an opposite manner. Although the rate of increase of the concentration is high (Fig. 5.12) and is suppposed to generate a high yield, the energy input to the discharge per cycle is also increased (Fig. 5.26) as the length is increased. A higher rate of increase of input energy than of concentration will lead to a lower yield.

The effect of the chamber length on the ozone yield as a function of the air flow rate and the gas residence time is shown in Fig. 5.24 and 5.25. It can clearly be observed that as the air flow rate is increased and the gas residence time is decreased, the yield is also increased. This occurs at all ranges of the air flow rate and the gas residence time, and a length of 160 mm generates the highest yield. It can be suggested that, in this present study, a length of 160 mm is optimum for high efficiency generation.

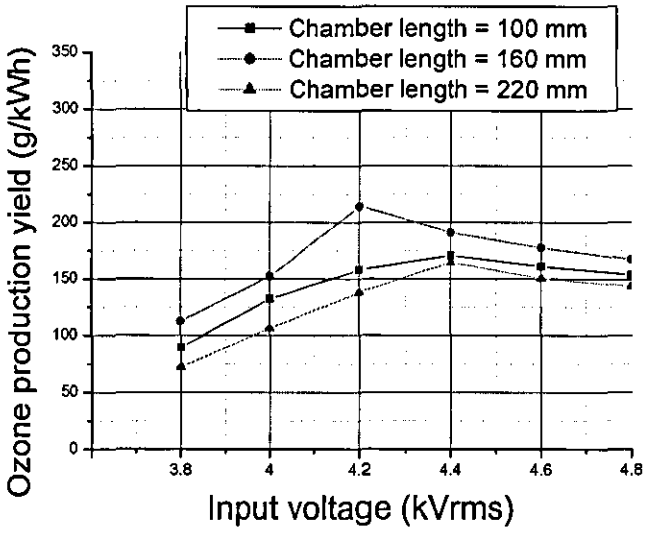

Figure 5.23: Effect of chamber length on ozone yield as a function of input voltage. Condition: dielectric material soda lime glass (ε_r=7.75), gap distance 3 mm, air flow rate 0.2 l/min, pressure 1 bar.

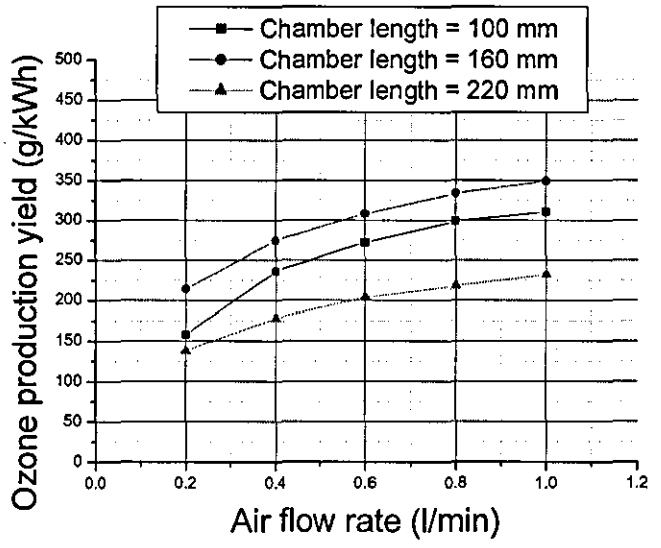

Figure 5.24: Effect of chamber length on ozone yield as a function of air flow rates. Condition: dielectric material soda lime glass (ε_r=7.75), gap distance 3 mm, input voltage 4.2 kV, pressure 1 bar.

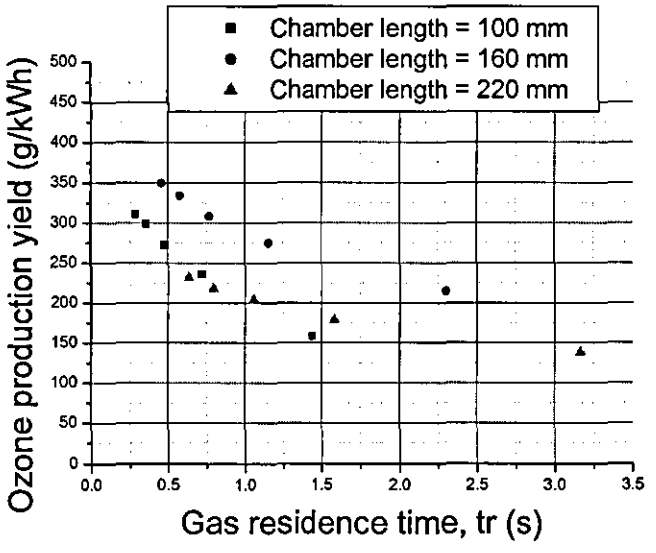

Figure 5.25: Effect of chamber length on ozone yield as a function of air flow rates. Condition: dielectric material soda lime glass (ε_r=7.75), gap distance 3 mm, input voltage 4.2 kV, pressure 1 bar.

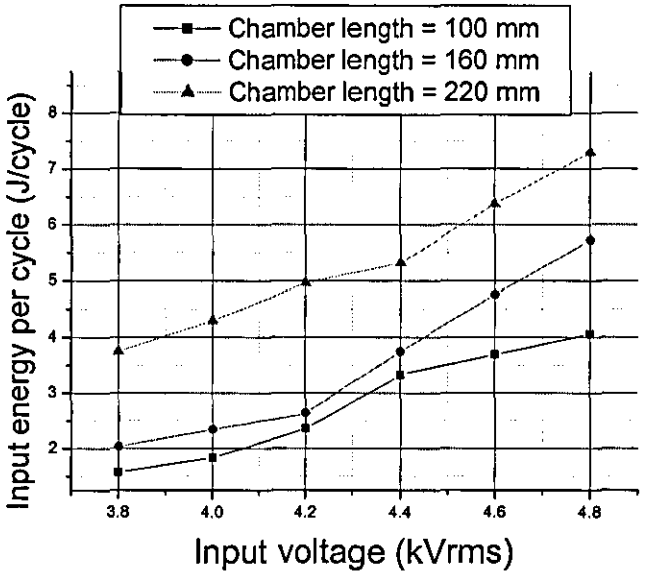

Figure 5.26: Effect of input voltage on input energy into the discharge per cycle at different chamber length.

5.5.2 Pulsed streamer discharge

Because of budget constraints, the Blumlein high voltage power supply was constructed with only a single pulse duration, in which with the circuit configuration shown in Fig. 5.3 it was used during an early investigations. The resultant pulse duration is 120 ns and this value was maintained thereafter, although some literature has reported [65] that a shorter pulse duration (80 ns) leads to a better efficiency of ozone generation. The pulse repetition frequency was fixed at 50 pulse per second (pps) for comparative purposes and a positive polarity was used throughout the investigation.

A typical pulsed voltage and the resultant current applied to the discharge reactor were shown in Fig. 5.5. All the measurements reported here were taken in the presence of streamers and before the discharge had transformed into an arc.

5.5.2.1 Ozone concentration

5.5.2.1.1 Effect of input voltage, air flow rate and/or residence time on ozone concentration.

The effect of applying a PSD on the ozone concentration in air is shown in Figs. 5.27, 5.28 and 5.29 as a function of pulsed voltage, air flow rate and gas residence time at atmospheric pressure respectively. A similar configuration was used as in APGD experiments, with the chamber length and gap spacing set at 160 mm and 3.0 mm. The pulsed voltage and air flow rate were varied between 13 to 18 kV and 0.2 to 1 l/min. It can be observed from Fig. 5.27 that the corona starting voltage in the PSD technique is higher than in the APGD technique, which started at about 13 kV, with breakdown occurring at any voltage above 18 kV. This illustrates one of the reasons why pulsed power is used, as it enables a higher input pulse voltage to be applied to a small gap spacing at a higher breakdown voltage, which can generate a higher electric field at the discharge electrodes. This results in an increase in the electron energy to dissociate the oxygen molecules and an expected higher ozone generation. In general, the results in Fig. 5.27 show that, as the applied pulse voltage is increased, the concentration also increases for all air flow rates, following the same trend as in the glow discharge experiment of Fig. 5.6, and which may be attributable to the use of the same discharge configuration in both experiments. At the corona (streamer) starting voltage, the concentration generated is approximately 554, 265 and 189 ppmv at air flow rates of 0.2, 0.6 and 1.0 l/min respectively, only slightly higher than the values obtained at the corona starting voltage in the glow discharge technique. As the voltage is increased, a higher concentration is observed at lower air flow rates and a decreased concentration at higher air flow rates, as is evident in Fig. 5.27. At the maximum pulse voltage of 18 kV before breakdown occurs, the ozone concentration at air flow rates of 0.2, 0.6 and 1.0 l/min were approximately 4281,1854 and 1219 ppmv (corresponding to about 0.64%, 0.28% and 0.18% by weight respectively), resulting in increments from the corona (streamer) starting voltage of approximately 87.1%, 85.7 % and 84.5% respectively. These high increments are related to the higher electron energy, due to the

higher input pulse voltage applied to the discharge chamber. This shows that the use of PSD generates a higher concentration and a greater increment at an increasing input voltage, confirming the advantage of PSD.

Figs. 5.28 and 5.29 show the effect of air flow rate and gas residence times on ozone concentration at a pulsed input voltage ranging from 13 kV to 18 kV. The results show that the concentration decreases with increasing air flow rates for all input voltages. As can be seen, the concentration is high at a low air flow rates (and at a longer gas residence time). At a flow rate of 0.2 l/min (2.3 s gas residence time), the highest concentration for 18 kV input pulse voltage is 4281 ppmv. However, as the flow rate is increased the concentration decreases, and at 1.0 l/min (0.46 s gas residence times) it has fallen to approximately 1219 ppmv at an input pulse voltage of 18 kV, representing about a 71.5% reduction in ozone concentration. However, the percentage reduction in concentration is less than in the glow discharge technique. It can be suggested that the PSD generates a higher concentration with a smaller reduction at increasing air flow rate than does the APGD technique with the same discharge configuration.

In general, it can be concluded that input voltage, air flow rate and gas residence time, all play an important role in determining the ozone concentration in both the APGD and the PSD reactors, especially at higher input voltages.

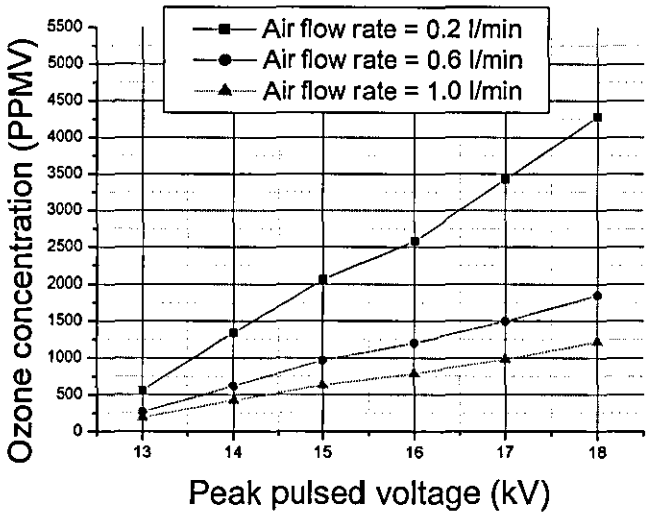

Figure 5.27: Effect of peak pulsed voltage on ozone concentration at different air flow rate. Condition: dielectric material, soda lime glass (ε_r=7.75), gap distance, 3 mm, chamber length, 160 mm, pressure, 1 bar.

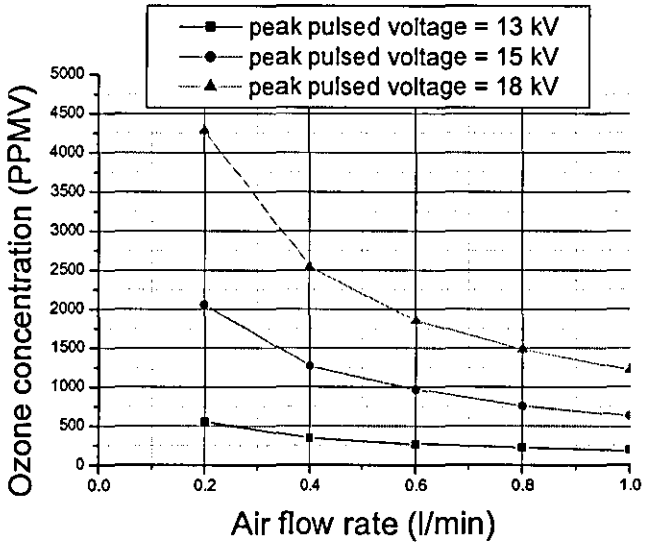

Figure 5.28: Effect of air flow rate on ozone concentration at different peak pulsed voltage. Condition: dielectric material, soda lime glass (ε_r=7.75), gap distance, 3 mm, chamber length, 160 mm, pressure, 1 bar.

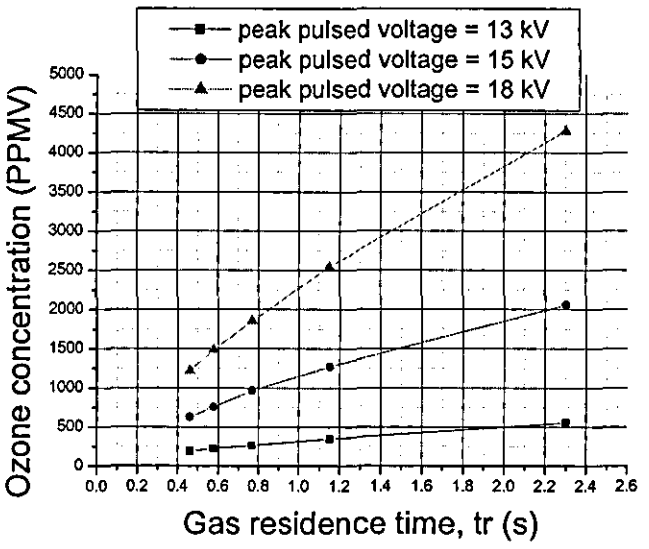

Figure 5.29: Effect of the gas residence time on ozone concentration at different peak pulsed voltage. Condition: dielectric material, soda lime glass (ε_r=7.75), gap distance, 3 mm, chamber length, 160 mm, pressure, 1 bar.

5.5.2.1.2 Effect of gap spacing on ozone concentration.

The effect of decreasing the gap spacing from 3.0 mm to 1.5 mm on the ozone concentration is shown in Figs. 5.30, 5.31 and Fig. 5.32 as a function of air flow rate, gas residence time and peak pulse voltage respectively. Fig. 5.30 shows that, at a constant pulse voltage of 15 kV, the concentration produced by a small spacing is higher than that by a longer spacing, throughout the range of air flow rate. The maximum concentration obtained at a low air flow rate of 0.2 l/min is about 2059 ppmv and 2538 ppmv at 3.0 mm and 1.5 mm gap spacings respectively. This represent about 18.9% of the increase when the gap spacing is decreased from 3.0 mm to 1.5 mm, and remains almost constant with an increase in the air flow rate, as is evident from Fig. 5.30. This is related to the increase in electron energy in the discharge volume with, as the gap spacing is decreased, the increase in the collisions between the oxygen molecules and energetic electrons generating more ozone. The advantage of a smaller spacing is more apparent when,

even at low gas residence times, it is noticed that a small spacing produces a higher concentration than does a greater one, as is seen from Fig. 5.31.

Fig. 5.32 shows the effect of decreasing the gap spacing from 3.0 mm to 1.5 mm on the concentration as a function of the peak pulse voltage, with all other parameters kept constant. It can be observed seen that, as the spacing is decreased to 1.5 mm, the corona (streamer) starting voltage has a lower value of about 11 kV, which has resulted in a decrease in the breakdown voltage to approximately 16 kV. The results again follow a similar trend to those obtained in APGD experiments. At a lower pulse voltage (up to a certain maximum level), the spacing of 1.5 mm generates a higher concentration than does a spacing of 3.0 mm. Above that the concentration tends to saturate, and to generate a lower concentration than does a spacing of 3.0 mm. The maximum concentration obtained with a 1.5 mm spacing is approximately 2848 ppmv, whereas at a spacing of 3.0 mm, the maximum concentration is approximately 4281 ppmv, about 33.5% higher. This is again explained by the higher pulse voltage that can be applied at the greater spacing, and indicates the limitation posed by the small spacing evident in Fig. 5.32.

It can be concluded that, at low input voltage, a small spacing of 1.5 mm is advantageous, since it can produce a higher concentration than the 3.0 mm spacing. However, at a higher input voltage the spacing of 3.0 mm is advantageous, giving the maximum achievable concentration of ozone about 4281 ppmv (corresponding to 0.64% by weight).

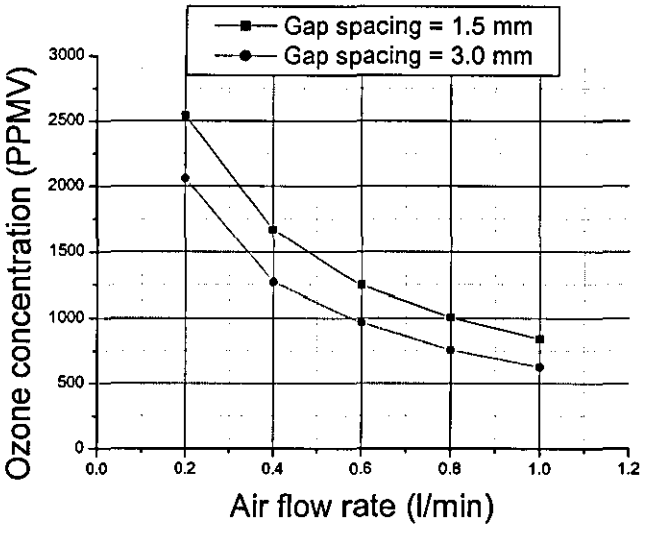

Figure 5.30: Effect of gap spacing on ozone concentration as a function of air flow rates. Condition: dielectric material, soda lime glass (ε_r=7.75), chamber length, 160 mm, peak pulsed voltage, 15 kV, pressure, 1 bar.

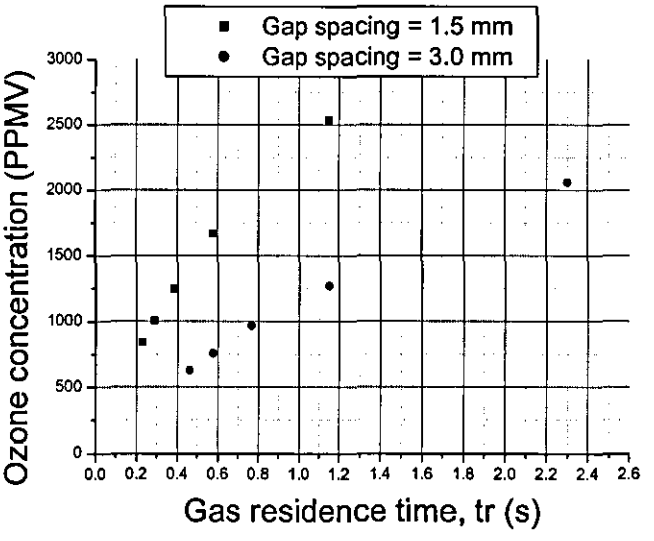

Figure 5.31: Effect of gap spacing on ozone concentration as a function of gas residence time. Condition: dielectric material soda lime glass (ε_r=7.75), chamber length 160 mm, peak pulsed voltage 15 kV, pressure 1 bar.

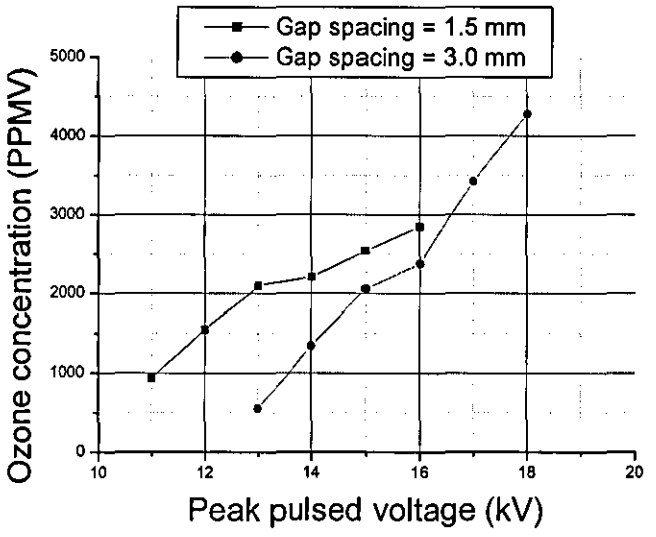

Figure 5.32: Effect of gap spacing on ozone concentration as a function of peak pulsed voltage. Condition: dielectric material soda lime glass (ε_r=7.75), chamber length 160 mm, air flow rate 0.2 l/min, pressure 1 bar.

5.5.2.1.3 Effect of chamber length on ozone concentration.

The effects of changing the chamber length on the ozone concentration is shown in Figs. 5.33, 5.34 and 5.35 respectively, as a function of the peak pulse voltage, air flow rate and the gas residence time, with all other parameters kept constant. It can be observed that at a low input pulse voltage the percentage difference in the production between the three chamber lengths is very small. As the input voltage is increased above 15 kV, the effect of the chamber length become apparent, with the longer chamber length producing the higher concentration. At an input voltage of 18 kV, a chamber length decreased from 160 mm to 100 mm results in a decreased ozone concentration, from 4281 ppmv (corresponding to about 0.64% in weight) to 2548 ppmv (corresponding to about 0.38% in weight), or about a 40.5 % fall. On the other hand, an increase in the chamber length from 160 mm to 220 mm results in an increased concentration. The highest concentration obtained in a chamber length of 220 mm and a maximum pulse voltage of 18 kV is about 5995 ppmv (corresponding to about 0.90% in

weight), representing about a 28.6% increment. This indicates that the chamber length has a great influence on the concentration, especially at an increased applied pulse voltage.

This phenomenon can be explained on the basis that, as the chamber length is increased at a constant gap spacing, the volume of the discharge reactor increases. The residence time of the gas stream in the discharge zone also increases, giving the greater concentration evident in Fig. 5.33. Typically the residence time at 0.2 l/min air flow rate increases from 1.44 s to 3.17 s, with a chamber length increased from 100 to 220 mm. The longer residence time results in an increased number of collisions between energetic electrons and oxygen molecules, and therefore a higher production of ozone. It should however be noted that, as the concentration increases at a higher applied voltage, the probability of its dissociation due to high electron energy also increases.

The effect of changing the chamber length on the concentration as a function of the air flow rate and/or gas residence time is shown in Figs. 5.34 and 5.35. It can clearly be observed from both these figures that the change in chamber length has a great effect on the concentration at a constant input pulsed voltage of 18 kV, with a longer chamber length generating a higher concentration. This condition occurs at all ranges of air flow rates as well as gas residence times. This suggests that, with the use of the PSD system, the increase in chamber length generates a higher concentration even at a lower gas residence time, indicating a clear advantage of a PSD system over an APGD system.

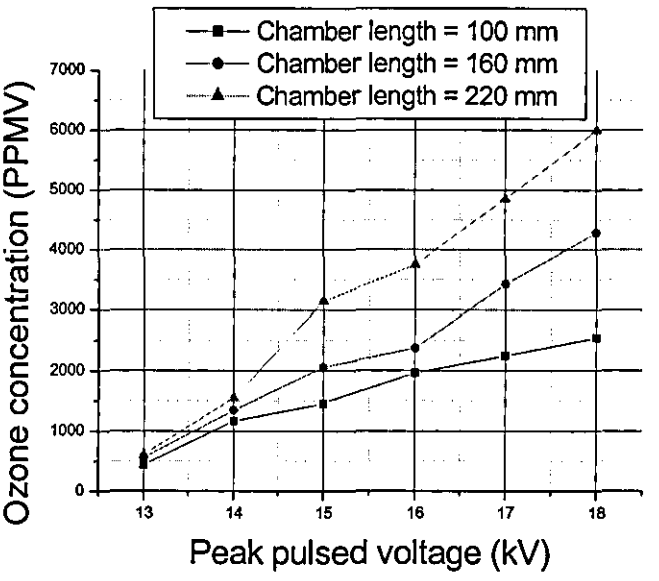

Figure 5.33: Effect of chamber length on ozone concentration as a function of peak pulsed voltage. Condition: dielectric material soda lime glass (ε_r=7.75), gap distance 3 mm, air flow rate 0.2 l/min, pressure 1 bar.

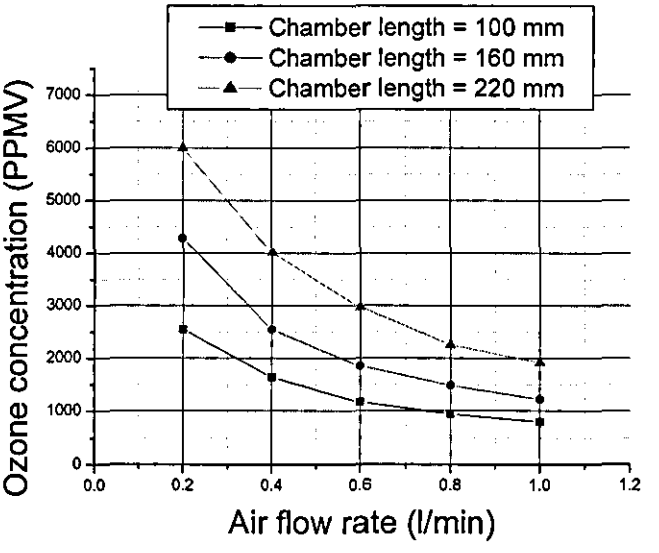

Figure 5.34: Effect of air flow rate on ozone concentration at a fixed chamber length. Condition: dielectric material soda lime glass (ε_r=7.75), gap distance 3 mm, peak pulsed voltage 18 kV, pressure 1 bar.

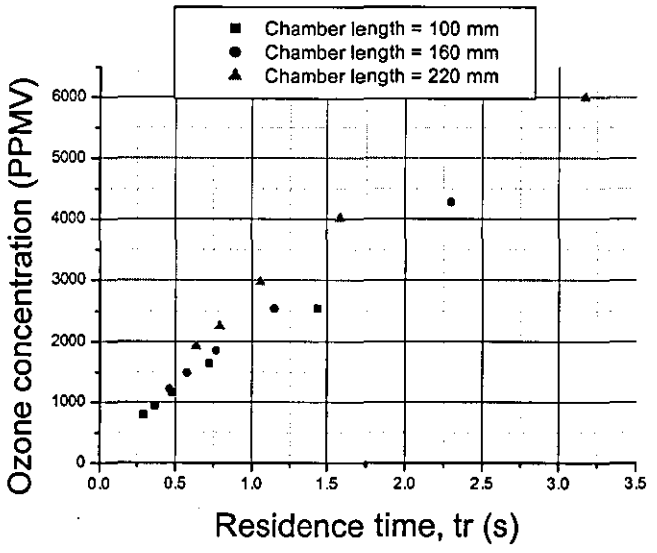

Figure 5.35: Effect of chamber length on ozone concentration as a function of gas residence time. Condition: dielectric material soda lime glass (ε_r=7.75), gap distance 3 mm, peak pulsed voltage 18 kV, pressure 1 bar.

5.5.2.2 Ozone yield

5.5.2.2.1 Effect of input voltage, air flow rate and residence time on ozone yield.

The effect of a PSD on the ozone yield at a chamber length of 160 mm and a gap spacing of 3.0 mm as a function of peak pulsed voltage, air flow rate and gas residence time was investigated, and the result obtained are presented in Figs. 5.36, 5.38 and 5.39. The yield increases to a maximum value as the voltage is increased up to about 15 kV, and then decreases for all air flow rates, as can be seen from Fig. 5.36. The highest yield of 144.01 g/kWh is obtained at an air flow rate of 1.0 l/min and a pulsed voltage of 15 kV. Above about 15 kV the rate of increase of the input energy to the discharge per pulse rises rapidly (Fig. 5.37) although the concentration increases almost linearly (Fig. 5.27). This results in a reduction in the yield with a further increasing voltage.

Figs. 5.38 and 5.39 show the effect of air flow rate and gas residence time on ozone yield at a fixed input voltage. It can be observed that an increased air flow rate results in an increase in the yield at a fixed input voltage, with a voltage of 15 kV produced the highest yield. At 0.2 l/min (2.3 s gas residence time) the yield generated at 15 kV is about 94.61 g/kWh. As the air flow rate is increased to 1.0 l/min (the gas residence time reduced to 0.46 s), the yield increase to about 144.01 g/kWh. This represents an increment of approximately 34.3% and indicates that the yield generated by the PSD configuration is lower than that by the APGD configuration.

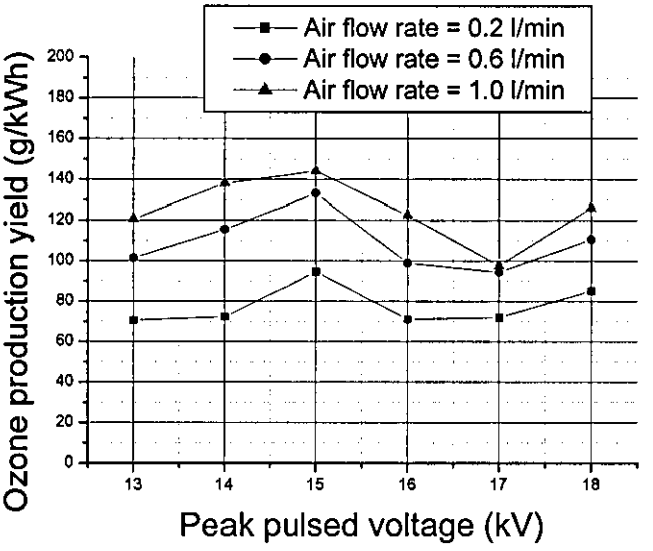

Figure 5.36: Effect of applied peak pulsed voltage on ozone yield at different air flow rate. Condition: dielectric material soda lime glass (ε_r=7.75), gap distance 3 mm, chamber length 160 mm, pressure 1 bar.

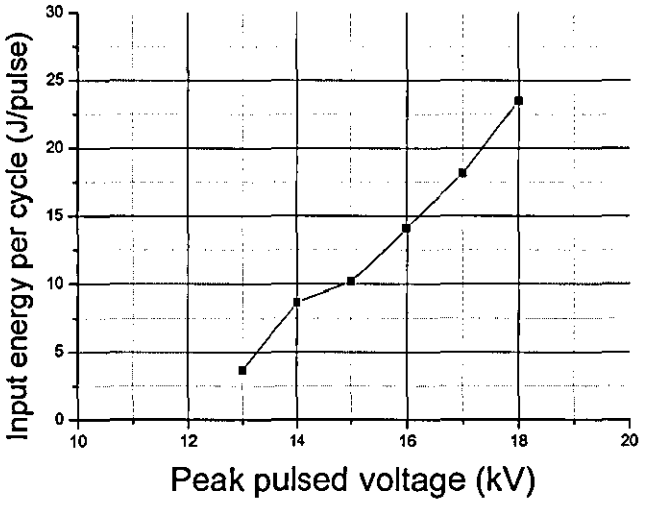

Figure 5.37: Effect of increasing the peak pulsed voltage on the input energy into the discharge per pulse.

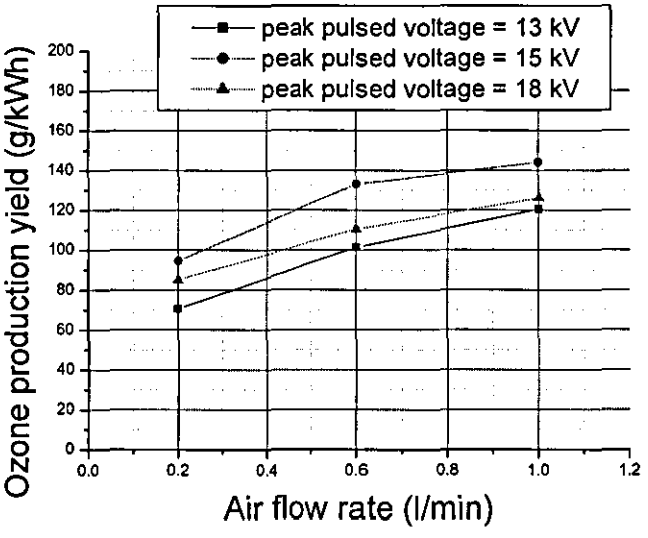

Figure 5.38: Effect of air flow rate on ozone yield at a fixed peak pulsed voltage. dielectric material Soda lime glass (ε_r=7.75), gap distance 3 mm, chamber length 160 mm, pressure 1 bar.

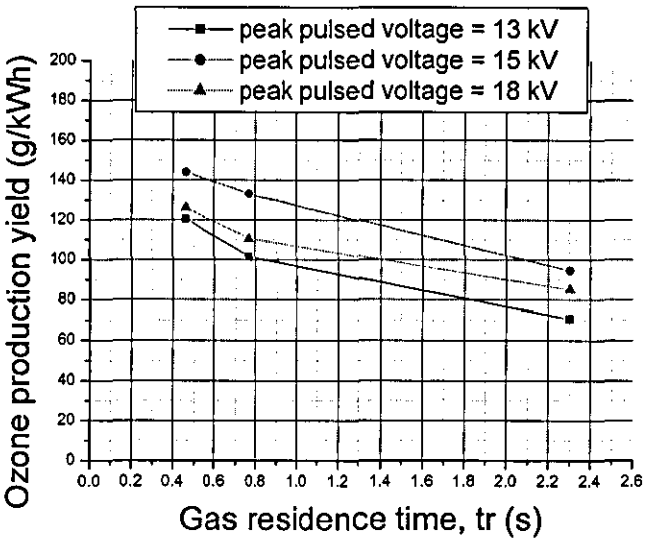

Figure 5.39: Effect of air flow rate on ozone yield at a fixed peak pulsed voltage. Condition: dielectric material soda lime glass (ε_r=7.75), gap distance 3 mm, chamber length 160 mm, pressure 1 bar.

5.5.2.2.2 Effect of gap spacing on ozone yield.

The effect of decreasing the gap spacing from 3.0 mm to 1.5 mm on the ozone yield is shown in Figs. 5.40, 5.41 and 5.42 as a function of air flow rate, gas residence time and input pulsed voltage respectively. At a constant input voltage of 15 kV, decreasing the spacing from 3.0 mm to 1.5 mm results in a decreased yield at an increased the air flow rate, as clearly seen in Figs. 5.40. At a lower air flow rate of 0.2 l/min (2.3 s and 1.152 s gas residence time for gap spacings of 3.0 mm and 1.5 mm respectively), the yield decreases from 94.61 g/kWh (3.0 mm gap spacing) to 72.16 g/kWh (1.5 mm gap spacing), a reduction of approximately 23.73%. The yield increases linearly as the air flow rate is increased, for both gap spacings. At an air flow rate of 1.0 l/min (0.46 s and 0.23 s gas residence time for gap spacings of 3.0 mm and 1.5 mm respectively), the yield is decreased from 144.01 g/kWh at 3.0 mm to 119.52 g/kWh at 1.5 mm gap spacing, a reduction of approximately 17%. This indicates that the reduced gap spacing results in a decreased yield.

The effect of decreasing the gap spacing from 3.0 mm to 1.5 mm on the ozone yield as a function of input voltage is more apparent, as is evident in Fig.5.43. At a constant air flow rate of 1.0 l/min, the maximum yield for a gap spacing of 3.0 mm and an input voltage of 15 kV is approximately 144.01 g/kWh, whereas at a spacing of 1.5 mm it has fallen to approximately 119.52 g/kWh, the reduction of about 17% indicating the disadvantage of the smaller gap spacing. The efficiency of the yield is related to its dependence on the concentration of ozone (Fig. 5.32) and the dependence of the energy input into the discharge on the input voltage (Fig. 5.43) [ ].

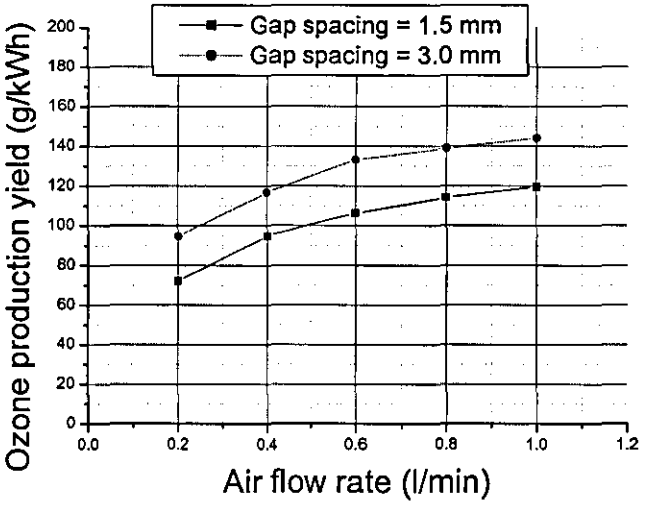

Figure 5.40: Effect of gap spacing on ozone yield as a function of air flow rates. Condition: dielectric material soda lime glass (ε_r=7.75), peak pulsed voltage 15 kV, pressure 1 bar.

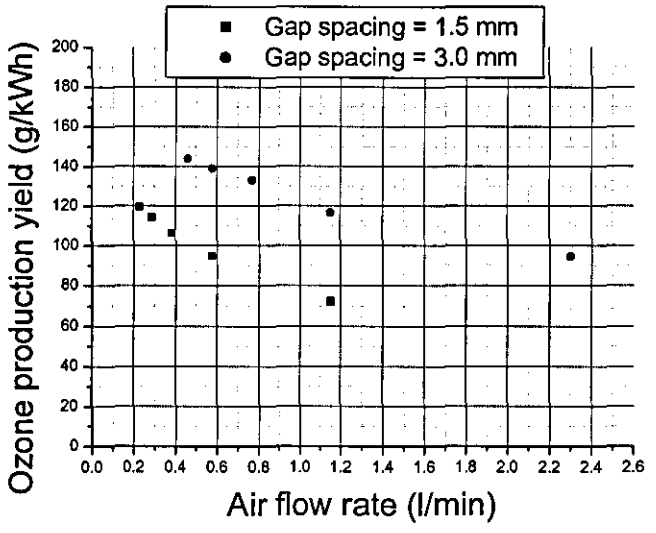

Figure 5.41: Effect of gap spacing on ozone yield as a function of gas residence time. Condition: dielectric material soda lime glass (ε_r=7.75), peak pulsed voltage 15 kV, pressure 1 bar.

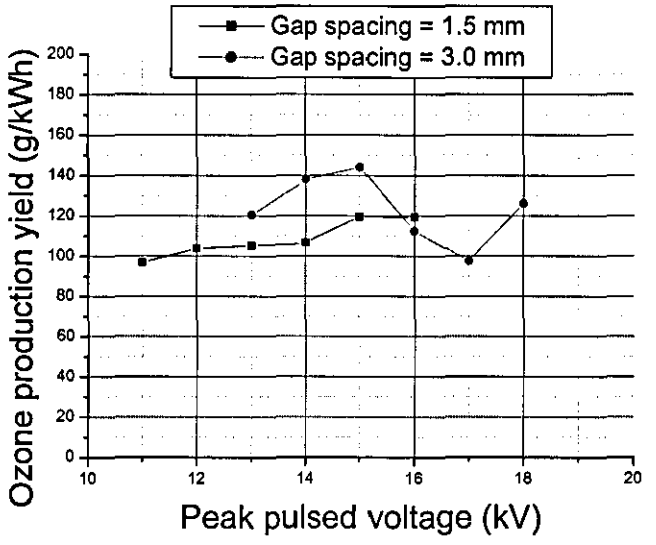

Figure 5.42: Effect of peak pulsed voltage on ozone yield at different gap spacing. Condition: dielectric material soda lime glass (ε_r=7.75), air flow rate 1.0 l/min, pressure 1 bar.

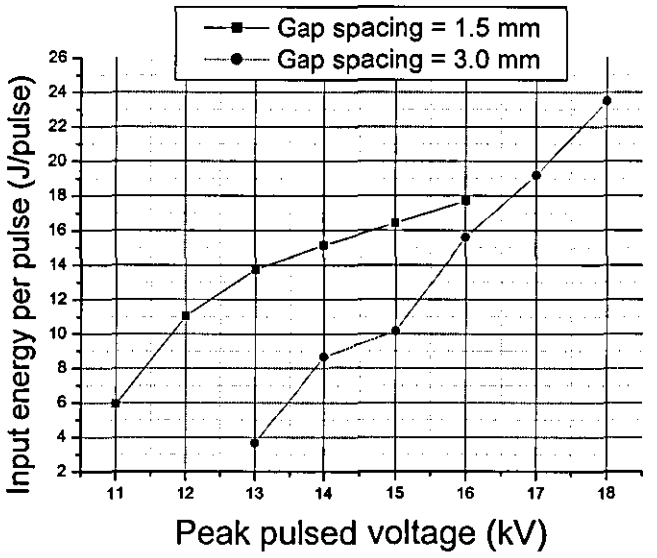

Figure 5.43: Effect of peak pulsed voltage on the input energy into the discharge per pulse at gap spacing of 1.5 mm and 3.0 mm.

5.5.2.2.3 Effect of the chamber length on ozone yield.

The effect of varying the chamber length on the ozone yield is shown in Figs. 5.44, 5.45 and 5.46 as a function of peak pulsed voltage, air flow rate and gas residence time.

The effect of both increasing and decreasing the chamber length is seen in Fig. 5.44. It can be observed that an increase or decrease in the chamber length from 160 mm to 220 mm or 100 mm, both result in a decreased yield. At a constant air flow rate of 1.0 l/min, the decrease results in a decrease in the maximum yield from 144.01 g/kWh to 120.32 g/kWh, a reduction of about 16.45%. Similarly, the increased chamber length results in a decreased yield to about 133.5 g/kWh, a reduction of about 7.3%. Fig. 5.47 show that at a fixed applied voltage, an increased chamber length results in an increased energy input to the discharge per pulse. On the other hand, a decreased chamber length results in a decreased input energy (Fig. 5.47), and therefore a lower concentration at increased voltage (Fig. 5.33), leading to a low ozone yield. On the other hand, the result of increasing the chamber length is

explained in an opposite manner. Although the rate of increase of concentration is high (Fig. 5.33) and is expected to generate a high yield as the chamber length is increased, the energy input to the discharge per pulse increases (Fig. 5.47) at a higher rate than the concentration, leading in fact to a low yield.

Figs. 5.45 and 5.46 show the effect of varying the chamber length on the yield, as a function of the air flow rate and gas residence time. It can be seen that as the air flow rate is increased, the yield also increases. The highest yield is obtained with a chamber length of 160 mm, an air flow rate of 1.0 l/min and a peak pulsed voltage of 15 kV.

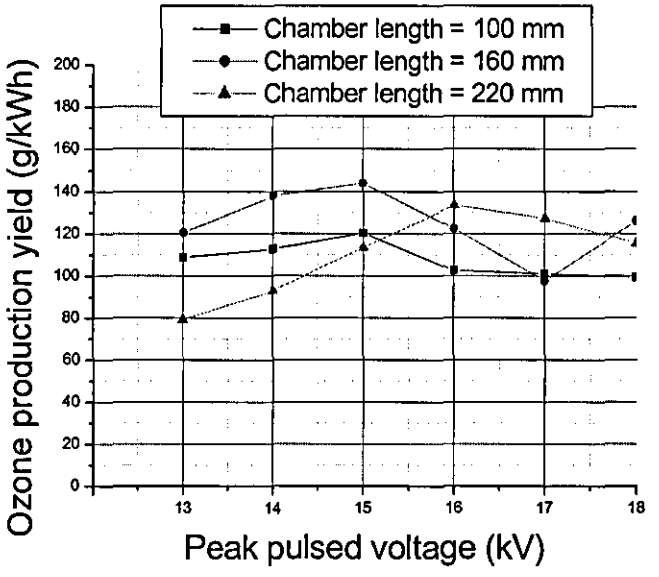

Figure 5.44: Effect of chamber length on ozone yield as a function of peak pulsed voltage. Condition: dielectric material soda lime glass (ε_r=7.75), gap distance, 3 mm, air flow rate, 1.0 l/min, pressure, 1 bar.

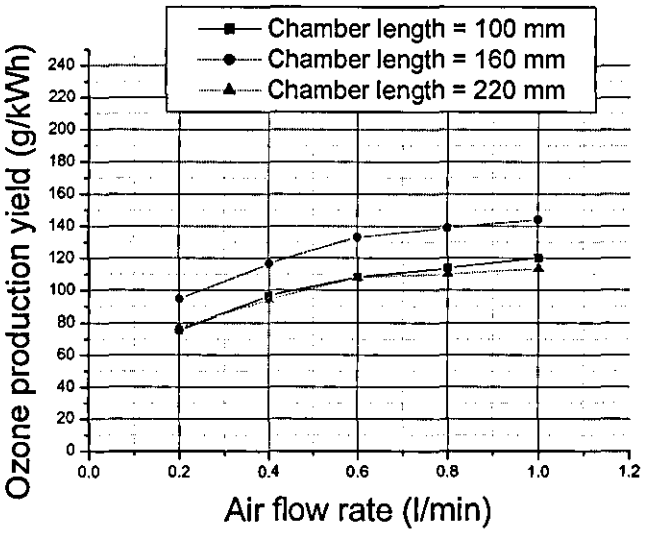

Figure 5.45: Effect of chamber length on ozone yield as a function of air flow rates. Condition: dielectric material soda lime glass (ε_r=7.75), gap distance 3 mm, input voltage 15 kV, pressure 1 bar.

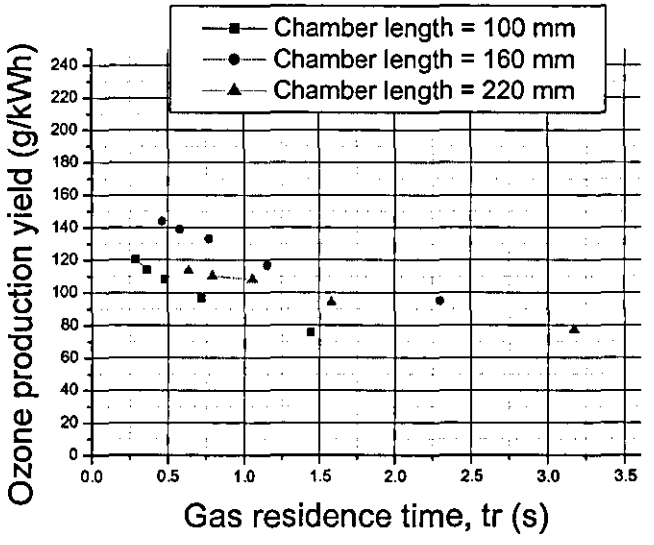

Figure 5.46: Effect of chamber length on ozone yield as a function of gas residence time. dielectric material Soda lime glass (ε_r=7.75), gap distance 3 mm, peak pulsed voltage 15 kV, pressure 1 bar.

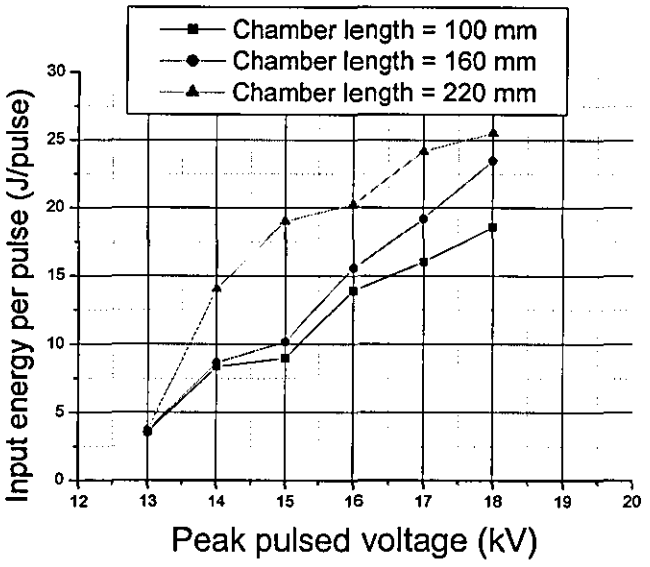

Figure 5.47: Effect of the peak pulsed voltage on the input energy into the discharge per pulsed at different chamber length.

5.6 Discussion

For the purpose of making a useful comparison between APGD and PSD, the effects of input voltage, gap spacing, chamber length, air flow rate and gas residence time have all been studied. This is based on the observation that the above parameters have in the past been shown to play an important role in determining the efficiency of ozone generation.

In general, the results for APGD and PSD follow the same trend as the selected parameters are changed. Although this may be attributed to the use of the same discharge configuration in both experiments, the amplitude and the rate of increase of ozone concentration and production yield are different.

The results of the comparison of the measured concentration in the APGD and PSD as a function of input voltage, air flow rate and gas residence time under the same discharge configuration are shown in Figs. 5.6, 5.7, 5.8, 5.27, 5.28 and 5.29. At a chamber length of 160 mm and a gap spacing of 3 mm,

both techniques show a similar trend. The ozone concentration increases with an increasing input voltage and longer residence time, but decreases at an increased air flow rate. At the corona starting voltage (3.8 kVrms for APGD and 13 kV for PSD) and a lower air flow rate of 0.2 l/min, the concentrations generated by APGD and PSD are slightly different, with APGD generating about 490 ppmv and PSD about 554 ppmv, some 11.4% higher. However, as the voltage is increased, up to the maximum input voltage achievable by both techniques, the concentration in PSD increases at a higher rate than that in APGD, from 554 ppmv to 4281 ppmv, an increment of about 87.06%. In the APGD technique, the rate of increase is lower, with the increase from 490 ppmv to about 2050 ppmv, representing an increment of about 76.1%. This indicates about a 52.1% difference in the maximum ozone concentration generated by the two techniques, with the maximum concentration generated by the PSD being twice that of the APGD. With the use of pulse power, a higher input voltage can be applied to the discharge chamber, resulting in a higher input energy into the discharge and a higher ozone concentration.

The comparison of the ozone yield in the APGD and PSD as a function of input voltage, air flow rate and gas residence time shows that the yield generated by a APGD is larger than that of the PSD technique, as can be seen from Figs. 5.15, 5.17, 5.18, 5.36, 5.38 and 5.39. At an increasing input voltage, the yield reaches a maximum at a certain value of input voltage before decreasing. On the other hand, the yield increases proportionally with an increased air flow rate and gas residence time as seen in Fig. 5.17, 5.18, 5.38 and 5.39. Fig.5.15 and Fig. 5.36 show that the ozone yield for APGD and PSD reaches a maximum at input voltages of around 4.2 kVrms and 15 kV respectively and begins to decrease as the input voltage is further increased, with the maximum yields being approximately 349.19 g/kWh and 144.01 g/kWh respectively. The approximately 58.8% higher yield in the APGD technique indicates that it produces a lower concentration but a higher yield. By contrast, the PSD system generates a high concentration but a low yield, which is related to the difference in the discharge power and input energy of the two system. Although the APGD produced a slightly lower ozone concentration, with a lower discharge power and rate of increase of energy

input to the discharge, it nevertheless produced a higher yield than did the PSD technique.

Comparisons between the ozone concentration produced by the APGD and the PSD as the gap spacing is varied are shown in Figs. 5.9, 5.11, 5.30 and 5.32. Although, at a constant input voltage, decreasing the gap spacing from 3.0 mm to 1.5 mm results in an increased concentration in both techniques (Figs. 5.9 and 5.30), at higher input voltages (Figs. 5.11 and 5.32) it has in fact reduced the maximum concentration. In the APGD technique, at a lower air flow rate of 0.2 l/min, a decreased gap spacing resulted in a decreased maximum concentration from 2050 ppmv (3.0 mm) to 1516 ppmv (1.5 mm), or about 26.05%. In the PSD technique, the decreased gap spacing resulted in a decrease from 4281 ppmv (3.0 mm) to 2848 ppmv (1.5 mm), or about 33.5%. This indicates that the ozone concentration generates by PSD technique is higher than that of the APGD, even at small gap spacing.

Figs. 5.19, 5.20, 5.21, 5.40, 5.41 and 5.42 compare the ozone yield produced by APGD and PSD when the gap spacing is changed. A decreased spacing results in a decreased yield in both techniques, for all air flow rates and gas residence times. In the APGD technique the maximum yield is reduced from 349.19 g/kWh (3.0 mm) to approximately 259.6 g/kWh (1.5 mm), or about 25.6%, slightly lower than the reduction in concentration. In the PSD technique, the reduced gap spacing has reduced the maximum yield from 144.01 g/kWh (3.0 mm) to 119.52 g/kWh (1.5 mm), approximately 17.0%, or almost twice that of the reduction in concentration. However, the ozone yield produced by APGD at 1.5 mm gap spacing is still higher than that of the PSD at 3.0 mm gap spacing, indicating that the APGD technique produces a higher yield even at a smaller gap spacing.

The comparisons between the ozone concentration produced by the APGD and the PSD, as the chamber length is varied (Figs. 5.12, 5.13, 5.14, 5.33, 5.34 and 5.35) show in general that an increased length results in an increased concentration and a decreased length results in a decreased concentration in both techniques. The highest concentration of 2355 ppmv

(APGD technique) and 5995 ppmv (PSD technique) was obtained at a chamber length of 220 mm.

On the other hand, an increase or decrease in chamber length resulted in a decrease in ozone yield for both techniques, indicating that the length of 160 mm used in the present study provides an optimum length for obtaining the highest yield.

However, the result presented for APGD technique does not take into consideration the effect of the sheath breakdown (the phenomenon that is most common in low and moderate pressure glow discharges). Recent research in rf APGD [84] has revealed that the sheath breakdown is responsible for the transition from an abnormal glow to the recovery mode within the glow discharge and is accompanied by a significant increases in the dissipated/discharge power (e.g 35 times). If this effect is taken into consideration, the increase in discharge power will reduce the ozone yield to a significantly lower value than the value that has been presented earlier. However, no such breakdown has been noticed in the present study, which may be due to the lack of realisation of the effect. In future research, this effect should be investigated and taken into consideration, especially when dealing with main frequency (50/60 Hz) APGD.

It can be noted that it is impossible to obtain the highest concentration and the highest yield at the same time, and one of these must be selected, depending on the specific application. The results presented in this study are applicable to a wide range of activities, including the pharmaceutical industry (maintaining the sterility of deionized water < 0.3 ppmv), turbidity (removal of the turbidity in water, 0.5 – 2 ppmv), deodorization (food hygiene, 6 ppmv), air purification (air cleaner, 40 ppmv), water purification (semiconductor industry, 1200 ppmv) [30,42,43] and all applications which need a concentration in the range up to 4,000 ppmv .

5.7 Conclusions

The efficiencies of the ozone production in the APGD and the PSD system were investigated and the results can be summarised as follows:

1. Both techniques were confirmed to be effective for ozone production in a discharge gap of 3.0 mm in air.

2. Input voltage, air flow rate and gas residence time all play an important role in determining the maximum ozone concentration in both techniques, especially at higher input voltage.

3. The maximum concentration generated by the APGD at a chamber length of 160 mm and a gap spacing of 3.0 mm is approximately 2050 ppmv, while it was about 4281 ppmv with the PSD.

4. The PSD system generates approximately twice the concentration of the APGD system.

5. With both techniques the concentration increased at a decreased gap spacing at constant input voltage. However, at higher voltages the decreased gap spacing results in a decrease in the maximum concentration in both techniques.

6. There is a limit to the maximum concentration obtainable at a small gap spacing.

7. At a constant air flow rate and higher voltages, a larger gap spacing generates a higher concentration than a smaller one.

8. The concentration generated by the PSD technique is higher than that of the APGD, even at a small gap spacing.

9. Both techniques generate a higher concentration at an increased chamber length.

10. The chamber length of 220 mm generates the highest concentration in both techniques.

11. The highest concentrations of 2355 ppmv (APGD technique) and 5995 ppmv (PSD technique) were obtained at a chamber length of 220 mm

12. The APGD technique generates a lower concentration but a higher ozone yield, while the PSD technique generates a higher concentration but a lower ozone yield.

13. The maximum yield generates by the APGD at a chamber length of 160 mm and a gap spacing of 3.0 mm was approximately 349.19 g/kWh, while it was about 144.01 g/kWh in the PSD.

14. The APGD system generates approximately a three times greater yield than does the PSD system.

15. The yield generated in both techniques decreased at a decreased gap spacing.

16. The yield generates by APGD technique is higher than that of the PSD, even at small gap spacing

17. The APGD and the PSD both generate a lower yield at increasing or decreasing chamber length.

18. The chamber length of 160 mm generates the highest yield at both APGD and PSD techniques.

CHAPTER 6

EFFECT OF CROSSED MAGNETIC FIELD ON OZONE PRODUCTION IN AIR

6.1 Introduction

When a magnetic field acts upon a discharge, various changes such as a change of radial ion and electron density and a marked alteration to the voltage-current characteristic takes place [85]. The application of a magnetic flux density B, perpendicular to the electric field E, creates a helical motion of the electrons inside the discharge chamber, due to gradient drift (gyration). This confines the electrons to the bulk plasma and the cathode region, thereby increasing the probability of ionisation [86]. This feature helps to increase the cooling effect and also lengthens the gas residence time in the discharge region. The electrons in the discharge region gain considerable energy, which in turn is responsible for the generation of a high density plasma [87]. This plasma, together with the helical electron motion and the increase in the gas residence time are believed to increase the rate of collisions between the electrons and the gas molecules and so generate more atomic oxygen. This phenomenon seemed to be very promising for increasing the production of ozone. To date, very little study on the application of its effect has however been carried out, although a study of the relevant literature [88] revealed that the use of AC corona subjected to a cross magnetic field produced very little change in the ozone production. Experiments were therefore performed to verify this conclusions.

This Chapter describes experiments to confirm (or reject) the previous findings, as well as to consider an alternative approach using AC and pulsed power supply. The ability of the plasma generated in the alternative approach to generate ozone when subjected to a cross magnetic field, is investigated. The results from both configurations are presented and discussed.

6.2 Experimental set-up and procedure

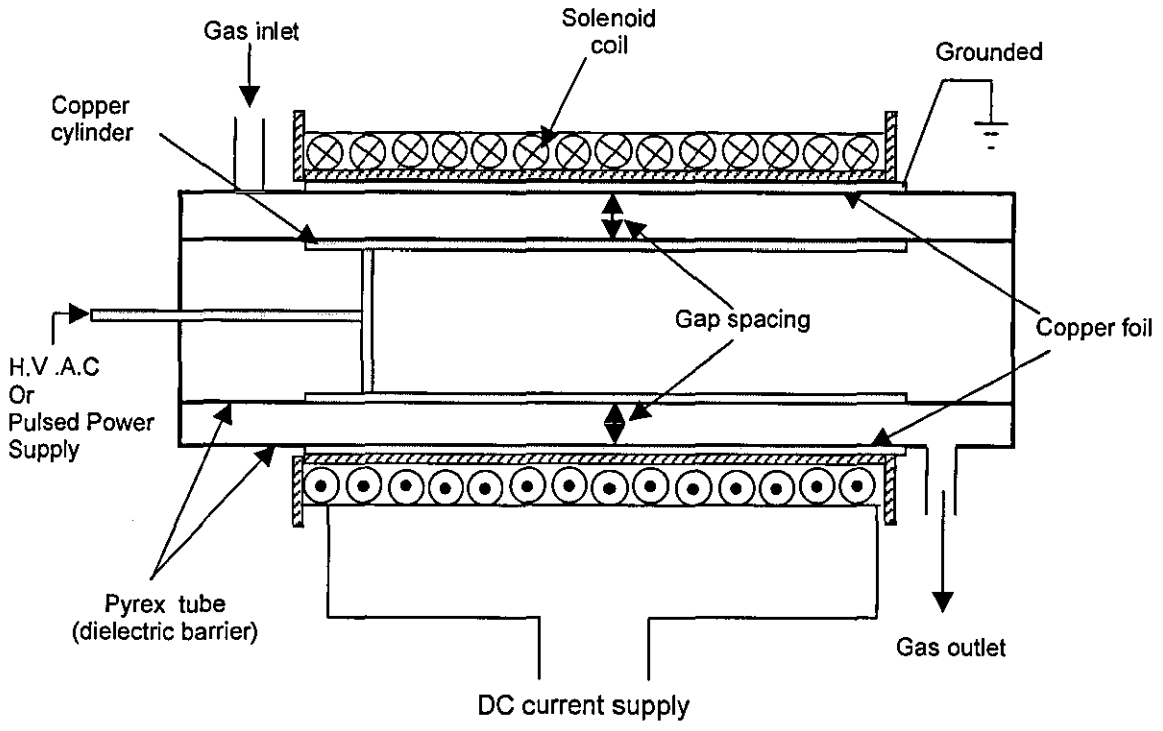

Figure 6.1 : Schematic diagram of discharge reactor.

Fig. 6.1 presents a schematic diagram of a discharge reactor in a coaxial tube configuration, with and without a cross magnetic field. The copper cylinder serves as the high voltage electrode on the inner side of the discharge chamber and a copper foil wrapped around the dielectric barrier tube provides the ground electrode. A double barrier was used, with two different diameters of pyrex glass tube of relative permittivity 7.2 and thickness 2 mm forming the barrier each side of the discharge electrodes, with a gap spacing of 1.4 mm. A long solenoid of 1000 turns of copper wire was wound on a PVC former on top of the ground electrode and used to generate a nearly uniform magnetic field throughout the volume of the discharge reactor orthogonal to the electric field. A DC current between 2 A to 8 A fed to the solenoid produced magnetic flux densities from 0.0265 T to 0.1058 T. As before, the ozone reactor was fed by cylinder dry air with oxygen content (by volume) between 17 to 21%. The air flow rate was varied between 0.2 to 1 l/min and was monitored using a flow-rate meter. The pressure of the dry air was kept constant at 1 bar throughout

the investigation. Any movement of the discharge caused by the magnetic field was observed through a viewing window located on one side of the discharge chamber.

The arrangement of Fig. 4.1 was used to generate AC corona. Input voltages between 1 and 20 kV at a frequency of 50 Hz were used to supply the reactor. For the generation of PSD, the system uses the electrical circuit arrangement given in Fig. 5.2, 5.3 and 5.4, with the peak pulsed voltage varied from 13 to 17 kV.

The applied voltage was measured using a high voltage probe (Tektronix P6015A, 1000x) and the charge signal obtained with the aid of a 0.22 μF capacitor connected in series to ground. The discharge current was measured by a Rogowski coil Pearson current monitor (model 2877, 1: 1 V/A). The output signals were recorded on a digital oscilloscope (LeCroy 9344) with a bandwidth of 500 MHz and a sample rate of 1 GS/s.

6.3 Results and discussions

Visual observations indicated that the discharge was similar when magnetic fields between 0.0265 T to 0.1058 T were applied to the AC corona and PSD configurations. No apparent movement of the discharge was noticeable for either discharge technique. Further investigation on the effect of the magnetic field on the corona starting voltage, the breakdown voltage, the corona discharge current and ozone concentration were therefore carried out. To confirm the results obtained, each experiment was repeated at least three times and the magnetic flux density was measured as the current was increased from 1 to 8 A.

Figs.6.2 and 6.3 shows the I-V characteristics of AC corona and PSD with a magnetic flux density ranging between 0.0265 T and 0.1058 T. The result shows that, in neither case, does the application of the magnetic field produce any apparent effect on the I-V characteristic. The result for AC corona is in fact

in general agreement with previous findings [88], but no previous result has been reported for the PSD technique.

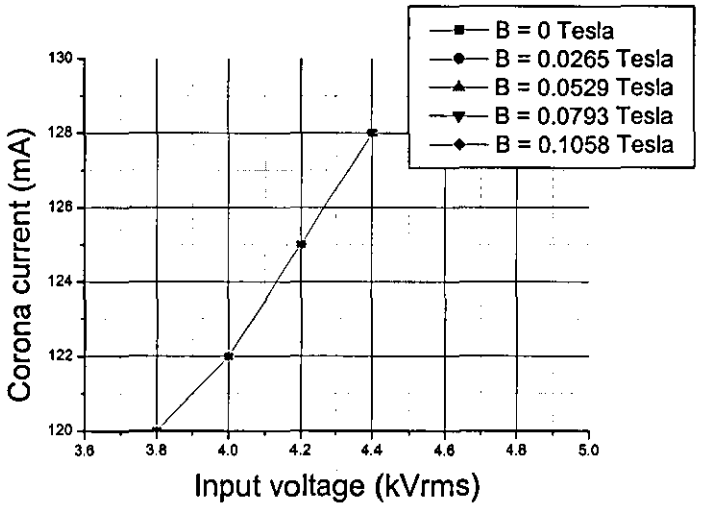

Figure 6.2: I-V characteristic of AC corona discharge with and without magnetic field. Condition: dielectric material pyrex glass (ε_r = 7.2), gap spacing 1.4 mm, air flow rate 1.0 l/min, chamber length 100 mm, pressure 1 bar.

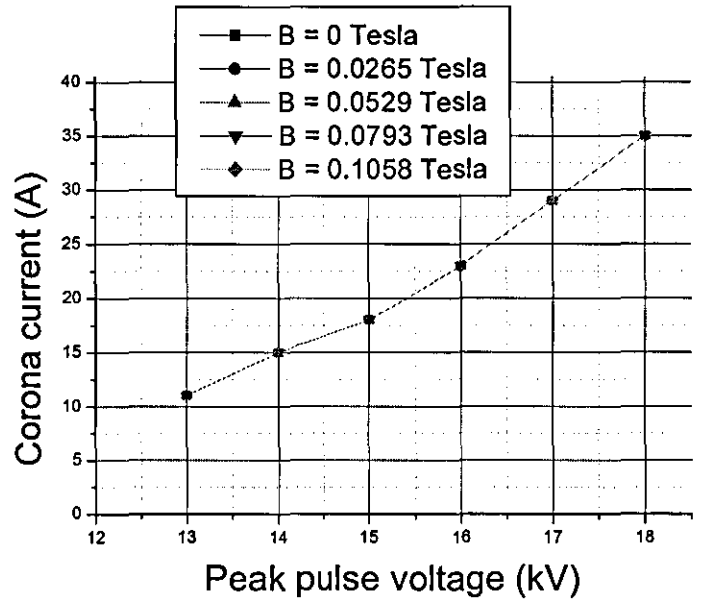

Figure 6.3: I-V characteristic of PSD with and without magnetic field. Condition: dielectric material pyrex glass (ε_r = 7.2), gap spacing 1.4 mm, air flow rate 1.0 l/min, chamber length 100 mm, pressure 1 bar.

Figs. 6.4 and 6.5 shows the effect of increasing the magnetic flux density on the ozone concentration at increasing input voltage for AC corona and PSD techniques. It can be observed that, at zero magnetic field and with a constant air flow rate of 1.0 l/min, an increased input voltage results in an increased ozone concentration in both techniques, with the maximum concentration obtained in the AC corona and the PSD being approximately 600 ppmv and 1100 ppmv. However, increasing the magnetic flux density from 0.0265 T to 0.1058 T produced no effect on the concentration in either technique, which confirmed the previously finding on AC corona [88], although the reason for this remains unclear. It may be related to the use of an alternating voltage or a pulse repetitive voltage, but no reason has yet have been obtained and further investigation is required.

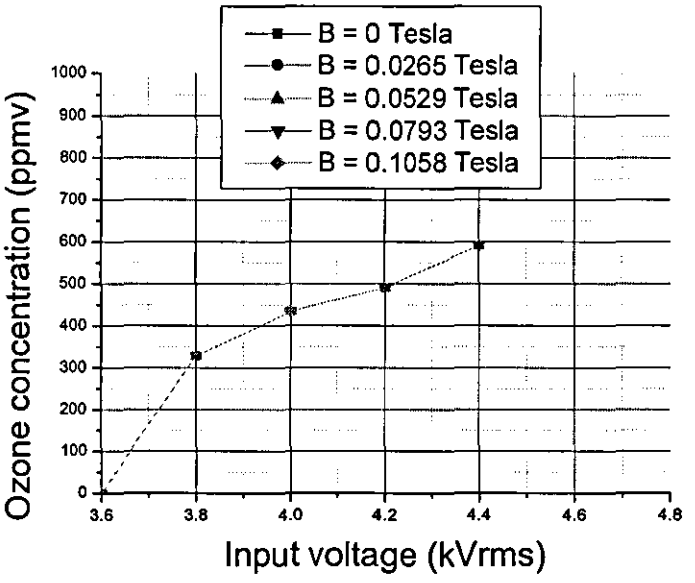

Figure 6.4: Ozone generation characteristic of AC corona discharge with and without magnetic field. Condition: dielectric material pyrex glass (ε_r = 7.2), gap spacing 1.4 mm, air flow rate 1.0 l/min, chamber length 100 mm, pressure 1 bar.

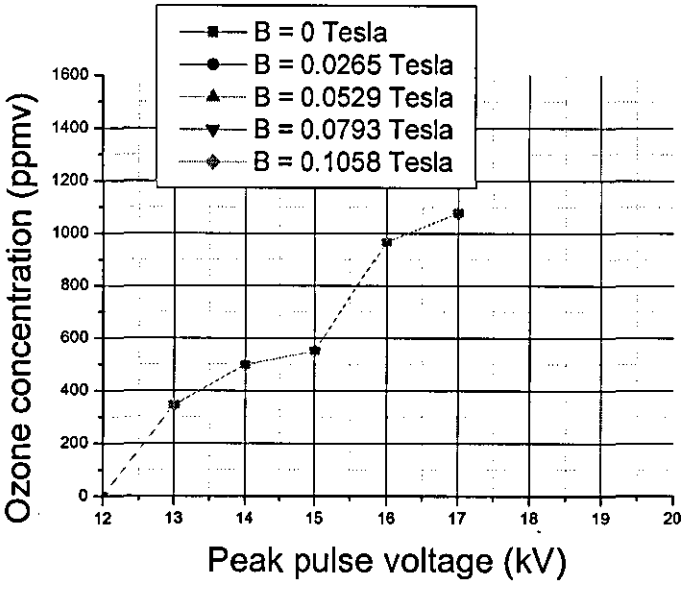

Figure 6.5: Ozone generation characteristic of Pulsed streamer discharge with and without magnetic field. Condition: dielectric material pyrex glass (ε_r = 7.2), gap spacing 1.4 mm, air flow rate 1.0 l/min, chamber length 100 mm, pressure 1 bar.

Further experiments were conducted to observe the effect of the air flow rate on the ozone concentration, when each systems was subject to a cross magnetic field. The result in Figs. 6.6 and 6.7 show that with no magnetic field, an increased air flow rate results in a decreased ozone concentration. However, no apparent effect can be observed when the magnetic field is applied, on the ozone concentration even with the change in the air flow rate.

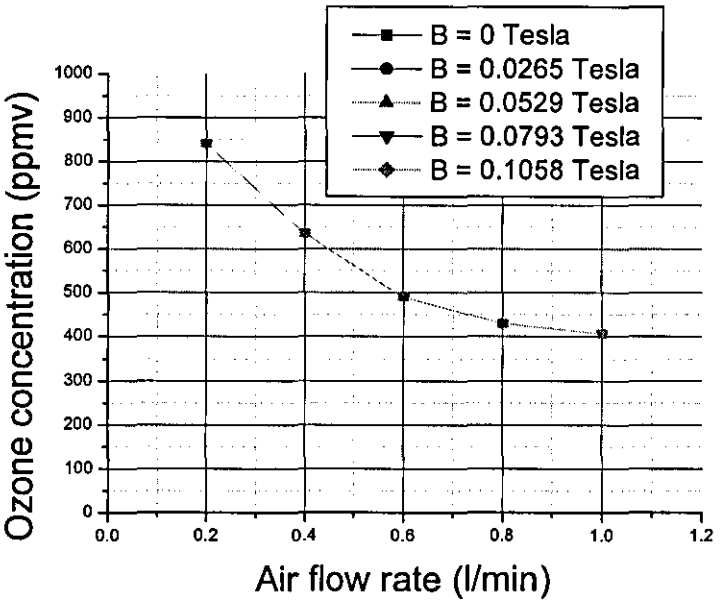

Figure 6.6: Effect of air flow rate on ozone concentration in AC corona discharge with and without magnetic field. Condition: dielectric material pyrex glass (ε_r = 7.2), gap spacing 1.4 mm, input voltage 4.2 kVrms, chamber length 100 mm, pressure 1 bar.

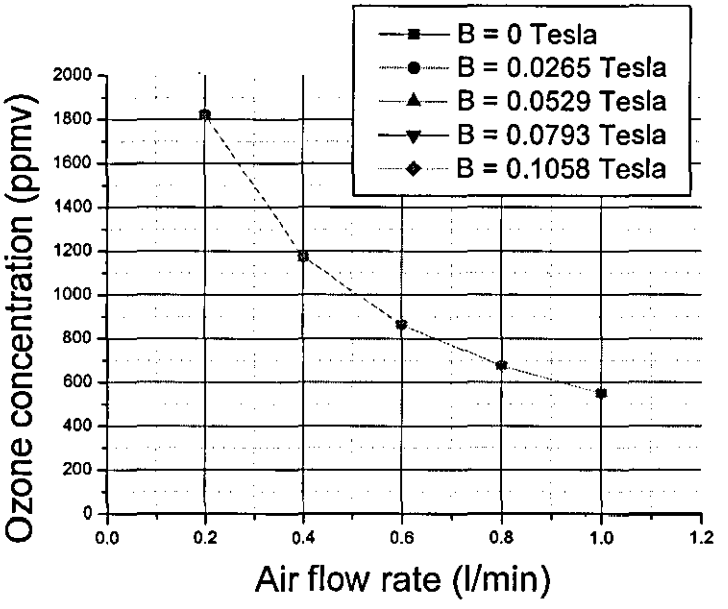

Figure 6.7: Effect of air flow rate on ozone concentration in pulsed streamer discharge with and without magnetic field. Condition: dielectric material pyrex glass (ε_r = 7.2), gap spacing 1.4 mm, peak pulsed voltage 15 kV, chamber length 100 mm, pressure 1 bar.

6.4 Conclusions

The effects of a magnetic field on the ozone generation characteristics of an AC corona and PSD have been investigated. It can be concluded that the magnetic field has no influence on the efficiency of ozone generation in either techniques. Result for investigations on AC corona confirmed the conclusions reached by previous researchers [88] and the present study on PSD revealed no influence in ozone efficiency when subject to a cross magnetic field. Although, no positive results can be reported from this study, the present finding at least provides important information for future reference.

CHAPTER 7

MODELLING THE RELATIONSHIP BETWEEN OZONE PRODUCTION BY PULSED STREAMER DISCHARGE IN OXYGEN AND THE PRINCIPAL PARAMETERS INVOLVED

7.1. Introduction

This Chapter focuses on ozone production in oxygen by means of a PSD. A mathematical model is developed for the discharge chamber, with dimensional analysis being used to identify both the electrical and the physical parameters that are of importance in its design. Predicted results obtained using the analysis are compared with practical ones.

7.2 Experimental set-up and procedure

The PSD is created by applying a series of fast-rising, high-voltage pulses to a field-enhanced geometry, employing a coaxial cylinder-to-cylinder configuration as shown typically in Fig. 7.1. The system uses the electrical circuit arrangement given in Fig. 5.2, 5.3 and 5.4 of Chapter 5. The copper cylinder serves as the high voltage electrode on the inner side of discharge chamber and a copper foil wrapped around the dielectric barrier tube provides the ground electrode, as can be seen from Fig. 7.1.

A double barrier was used, with two different diameters of pyrex glass tube of relative permittivity 7.2 and thickness 2 mm forming the barrier each side of the discharge electrodes as shown in Fig. 7.1. Introducing the dielectric barrier inhibits the formation of an arc discharge between the two electrodes, and thereby promotes the development of streamer discharges [20]. The

charge transported by a single streamer is reduced by the dielectric layer and the streamers are distributed over a wider area near the dielectric layer [20].

The gap spacing d_g, pressure p , relative permittivity ε_r and pulse duration τ, were kept constant at 1.4 mm, 1 atm, 7.2 and 120 ns respectively, whereas the applied pulse voltage V, pulse repetition frequency f and gas flow rate f_r were varied from 0 to 20 kV, 25 to 100 pps and 0.2 to 1.8 l/min respectively. The ozone reactor was fed by cylinder dry oxygen (99.99% purity) supplied by BOC.

A cooling system is unnecessary, since a PSD results in the production of streamers having a short lifetime. Therefore, less energy is transferred to both the ions and the background gas in the discharge volume, thus reducing any temperature rise. The ozone yield itself is influenced by several factors, as is discussed in the following section.

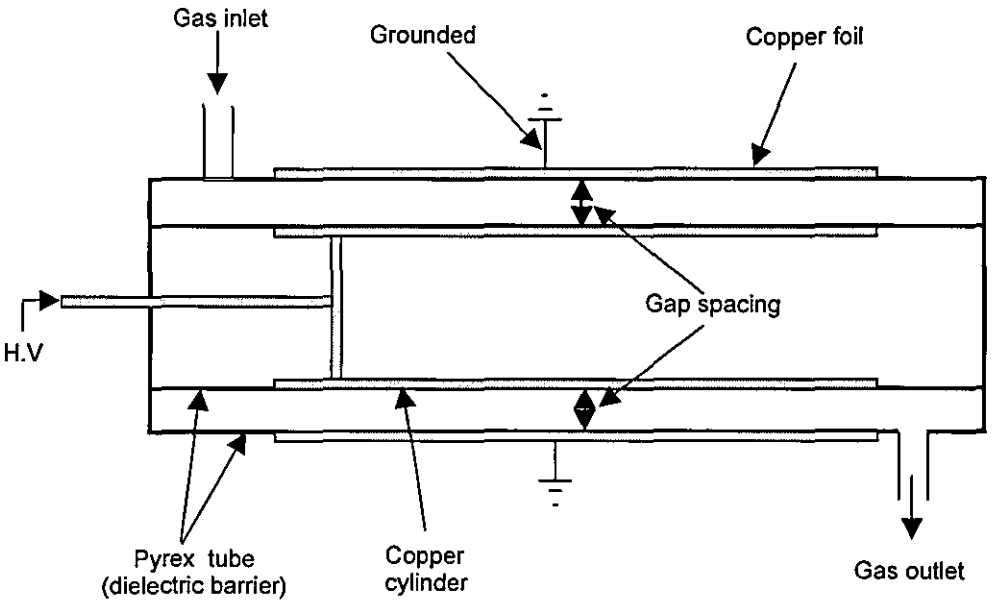

Figure 7.1: Reactor configuration for a PSD experiment

The results from the above experiment are compared with results obtained from mathematical modelling.

7.3 Theoretical Development

There are a number of parameters of a pulsed power supply and the discharge chamber that are known to have a significant influence on the ozone yield. Most prominent amongst these are the pulse repetition frequency f, the peak pulse voltage V, the pulse duration τ, the gap length d_g, the relative permittivity ε_r, the pressure p and the gas flow rate f_r.

Mathematically, the relationship between the ozone production yield (O_3) and the above parameters can be written in the form

$$(O_3) = (O_3)(f_r, \varepsilon_r, f, V, , d_g, p, \tau) \qquad (7.1)$$

When all the parameters in equation (7.1) are expressed in terms of the four fundamental dimensions; length L, mass M, time T and current A, the corresponding dimensional matrix is,

	(O_3)	f_r	V	τ	ε_r	d_g	p	f
L	-2	3	2	0	-3	1	-1	0
M	0	0	1	0	-1	0	1	0
T	2	-1	-3	1	4	0	-2	-1
A	0	0	-1	0	2	0	0	0

(7.2)

the determinant of which is non zero and the rank is four. Since the number of variables is eight, it follows immediately that the number of dimensionless variables needed to characterize the system is also four. Following Langhaar [89] enables the dimensional matrix to be rewritten in the form:

	k1	*k2*	*k3*	*k4*	*k5*	*k6*	*k7*	*k8*
	(O_3)	f_r	V	τ	ε_r	d_g	p	f
L	-2	3	2	0	-3	1	-1	0
M	0	0	1	0	-1	0	1	0
T	2	-1	-3	1	4	0	-2	-1
A	0	0	-1	0	2	0	0	0

(7.3)

where *k1, k2, k3, k4 , k5, k6, k7* and *k8* are the indices of the variables in equation (7.1). The following set of homogeneous linear algebraic equations can then be derived from consideration of the four rows of this matrix [89] :

$$-2k1 + 3k2 + 2k3 - 3k5 + k6 - k7 = 0 \quad (7.4)$$

$$k3 - k5 + k7 = 0 \quad (7.5)$$

$$2k1 - k2 - 3k3 + k4 + 4k5 - 2k7 - k8 = 0 \quad (7.6)$$

$$-k3 + 2k5 = 0 \quad (7.7)$$

which may be solved for *k5, k6, k7* and *k8* in terms of *k1, k2, k3* and *k4*. If four dimensionless variables written as $\pi 1$, $\pi 2$, $\pi 3$ *and* $\pi 4$ are now introduced, these may be determined from the matrix :

	k1	*k2*	*k3*	*k4*	*k5*	*k6*	*k7*	*k8*
	(O_3)	f_r	V	τ	ε_r	d_g	p	f
$\pi 1$	1	0	0	0	0	2	0	2
$\pi 2$	0	1	0	0	0	-3	0	-1
$\pi 3$	0	0	1	0	0.5	-1	-0.5	0
$\pi 4$	0	0	0	1	0	0	0	1

(7.8)

In forming this matrix, each row is considered in turn [90]. Thus, for example, in the first row *k1* is written as unity and *k2, k3* and *k4* all as zero. Substituting these values in equations (7.4) to (7.7) gives the values shown for *k5, k6, k7* and *k8*. Similar considerations applied to each of the other three rows enable matrix (7.8) to be completed. It then follows from this matrix that the set of dimensionless products is

$$\pi 1 = (O_3) d_g^{\,2} f^2 \qquad (7.9)$$

$$\pi 2 = \frac{f_r}{d_g^{\,3} f} \qquad (7.10)$$

$$\pi 3 = \frac{\sqrt{\varepsilon_r} V}{d_g \sqrt{p}} \qquad (7.11)$$

$$\pi 4 = f\tau \qquad (7.12)$$

According to Buckingham's Theorem [89], the dimensionless parameters are related by the function

$$\pi 1 = \Psi\{\pi 2, \pi 3, \pi 4\} \tag{7.13}$$

which, by considering the monomial form [90], leads to the relationship

$$\pi 1 = Dc.\ \pi_2^{\epsilon_2}.\pi_3^{\epsilon_3}\pi_4^{\epsilon_4} \tag{7.14}$$

where Dc is a dimensional constant.

Introducing equations (7.9), (7.10), (7.11) and (7.12) into equation (7.14) gives

$$(O_3) = Dc\left(\frac{1}{d_g^{\,2} f^2}\right)\left(\frac{f_r}{d_g^{\,3} f}\right)^{\epsilon_2}\left(\frac{\sqrt{\varepsilon_r} V}{d_g\sqrt{p}}\right)^{\epsilon_3}(f\tau)^{\epsilon_4} \tag{7.15}$$

where Dc, ϵ_2, ϵ_3 and ϵ_4 are all constants yet to be determined. Available experimental evidence however enables equation (7.15) to be much simplified, since the ozone yield (O_3) has been confirmed experimentally as proportional to both the gas flow rate f_r and the input voltage V [2,20,66] and as inversely proportional to the pulse duration τ [2]. Hence ϵ_2 and ϵ_3 are both 1, whereas ϵ_4 is –1. Under these constraints equation (7.15) reduces to

$$(O_3) = Dc.\left(\frac{f_r\sqrt{\varepsilon_r} V}{d_g^{\,6} f^4 \tau\sqrt{p}}\right) \tag{7.16}$$

The dimensional constant Dc is determined through variation of the independent parameters. In the present modelling, only three independent parameters (variables) are varied in accordance with the experimental study. In the modelling, any variation in an independent variable will change the value of the dimensional constant. Therefore, a common dimensional constant that applies for all parameters has to be determined. Following this procedure (explained in appendix 4) changes the equation given in (7.16) to the new equation given below.

$$(O_3) = Dc.(\frac{f_r^{0.24.}\sqrt{\varepsilon_r}V}{d_g^{6} f^{0.15}\tau\sqrt{p}}) \qquad (7.17)$$

Equation (7.17) has been developed without considering the ozone destruction factor (*DF*) that accounts for the increased destruction of ozone occuring as more ozone is generated. This phenomena arises since, at higher voltages, the electron have sufficient energy not only to dissociates oxygen molecules into oxygen atoms to generate ozone but also to dissociate the generated ozone molecules into oxygen atom and molecules. As a consequence of this, the production of ozone decreases as the voltage is increased, rather than increasing [20]. To account for this effect, the dimensionless equation (7.18) can be formulated from available experimental data, provided that the peak of the pulsed voltage is less than the electrical breakdown value, *Vbreakdown* (see Appendix 4).

$$DF = [\,-(V/V_o - 1.6135)(V/V_o - 0.6135)] \qquad (7.18)$$

where V_o is the corona inception voltage. Combining equation (7.17) and (7.18), gives the final equation for the ozone yield as

$$(O_3) = Dc(\frac{f_r^{0.24}\sqrt{\varepsilon_r}V}{d_g^{6} f^{0.15}\tau\sqrt{p}})\,[\,-(V/V_o - 1.6135)(V/V_o - 0.6135)] \qquad (7.19)$$

showing that in addition to the dependencies noted earlier, the ozone yield (O_3) is directly related to the square root of the relative permittivity ε_r and is inversely proportional to the sixth power of the gap spacing *dg* and the square root of the gas pressure *p*.

7.4 Comparison with experimental evidence

The validity of the above analysis was verified by comparing results obtained using equation (7.19) with experimental data. In particular, the effect on the

ozone yield of changing the peak value of the voltage pulse considered for a number of different repetition frequencies and different gas flow rates. The pressure, pulse duration, dielectric constant and gap spacing were all kept constant. *Dc* was obtained (as described in Appendix 4) and the value of the corona inception voltage was readily deduced from corresponding experimental results.

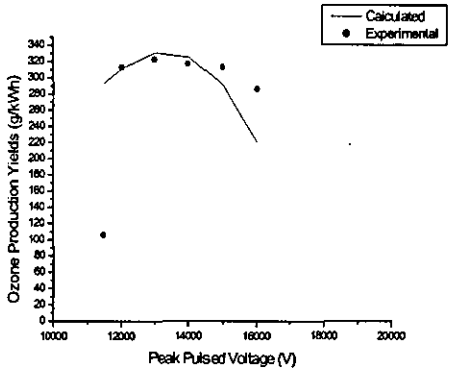

(a)

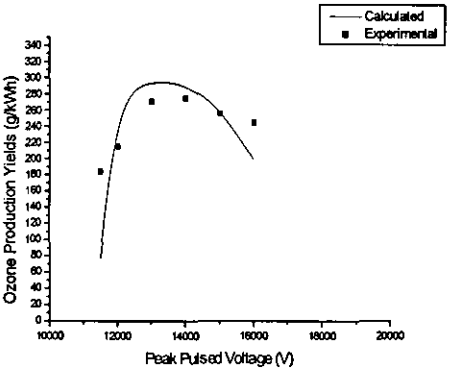

(b)

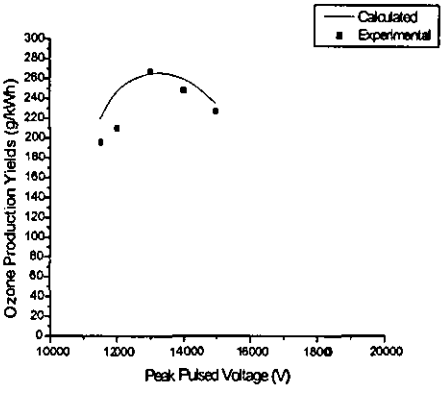

(c)

Figure 7.2 : Ozone yields versus peak pulsed voltage at repetition frequencies of (a) 25 pps; (b) 50 pps; (c) 100 pps;

Conditions: f_r = 0.01667 l/sec, ε_r = 7.2, d_g = 1.4 mm, τ = 120 ns, p = 1.05 x 10^5 Pa. and V_o = 11.5 kV. Dc = 4.86 x 10^{-23} .

The comparisons made between theoretical and experimental results in Fig. 7.2 can be seen to show generally good agreement. They confirm that although at any given repetition frequency the ozone yield initially increases as the voltage is raised, it subsequently decreases after reaching a maximum at about 13 kV due to the increasing significant of the ozone destruction factor.

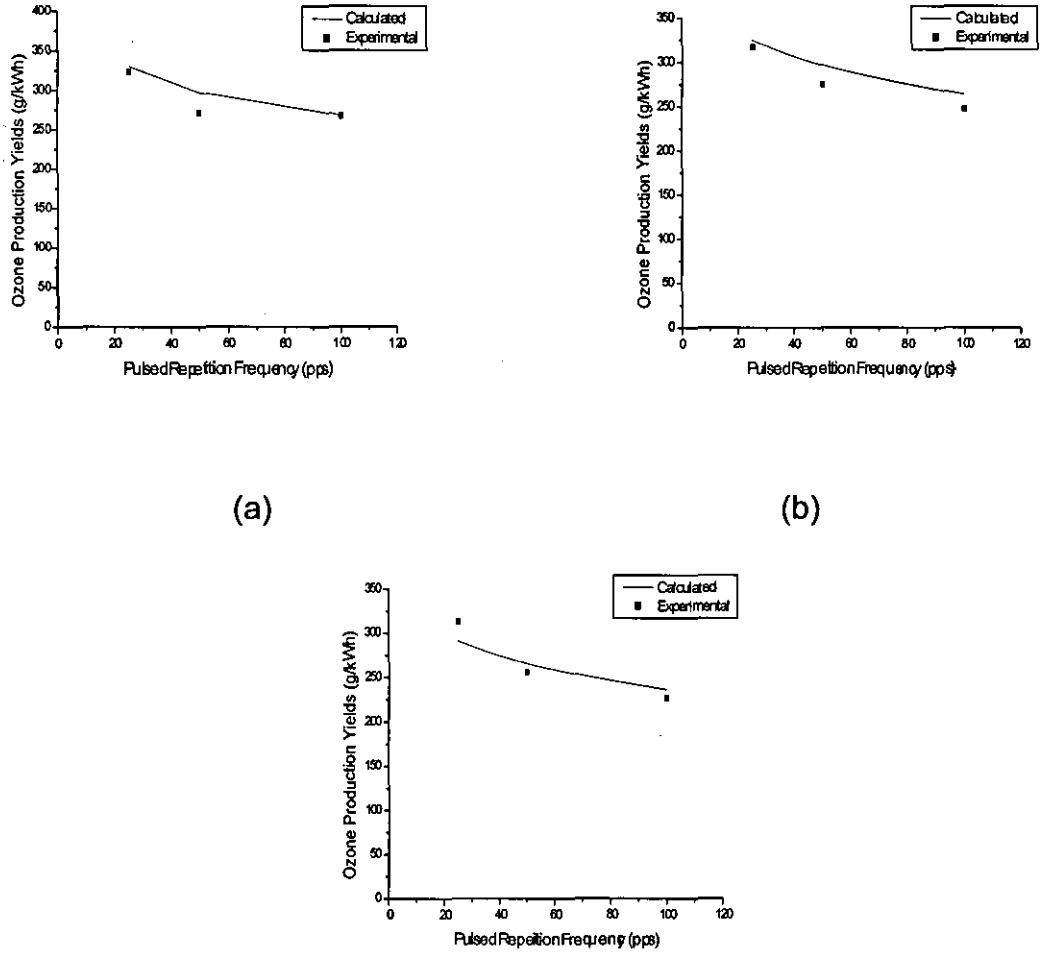

Figure 7.3: Ozone yield versus pulse repetition frequency at peak pulsed voltage of (a) 13 kV (b) 14 kV (c) 15 kV . $Dc = 4.86 \times 10^{-23}$.

The results in Fig. 7.2 are re-presented in different form in Fig. 8.3, in order to compare theoretical and experimental results for the ozone yield against the pulse repetition frequency at a fixed peak voltage. Good agreement is again evident, with the results confirming that with an increase in the pulse repetition frequency the ozone yield is slightly decreased. It can also be seen that the ozone yield is higher at a lower pulse repetition frequency (i.e at 25 pulse per second (pps)). Increasing the pulse repetition frequency above this value leads to a decrease in the ozone yield. This is because, as the pulse repetition frequency is increased, the ozone concentration will also increase, which in turn will slightly decrease the ozone yield [20,66]. This effect is clearly related to the increased ozone density, causing more ozone to decomposed back to oxygen atoms and molecules.

The results in Fig. 7.3 also show that one requirement for an increased amount of ozone is the application of either a higher pulsed voltage with a lower pulse frequency or a lower pulsed voltages at a higher pulse frequency [20].

Figure 7.4 present a comparison between theoretical and experimental results showing the effect of the peak pulsed voltage on the ozone yield at different gas flow rates. It can be seen that the results are again in generally good agreement. They also confirm that although at any given gas flow rate the ozone yield initially increases as the voltage is raised, it subsequently decreases after reaching a maximum at about 13 kV, due to the increasing significant of the ozone destruction factor.

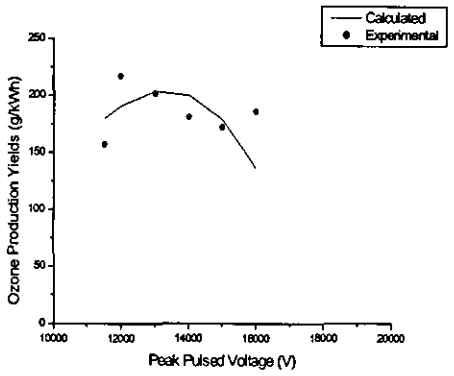

(b)

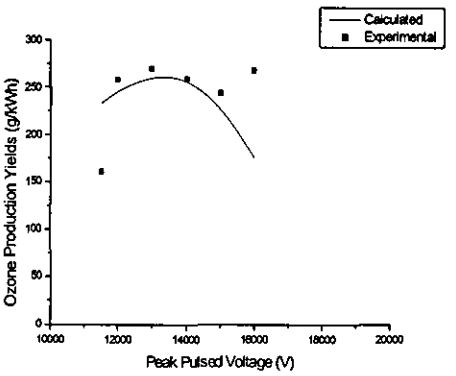

(b)

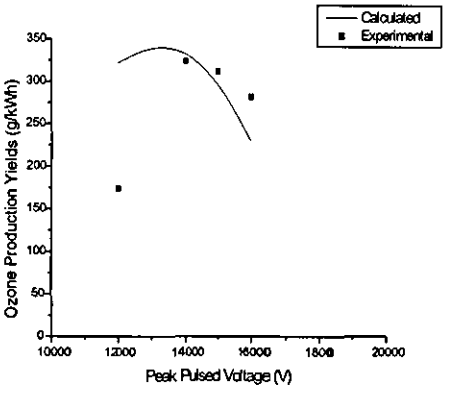

(c)

Figure 7.4 : Ozone yields versus peak pulsed voltage at gas flow rate of (a) 0.2 l/min (b) 0.6 l/min (c) 1.8 l/min.

Conditions:f = 50 pps, ε_r = 7.2, d_g = 1.4 mm, τ = 120 ns, p = 1.05 x 10^5 Pa. and V_o = 11.5 kV. Dc = 4.86 x 10^{-23} .

In order to compare theoretical and experimental results for the ozone yield against the gas flow rate at a fixed peak voltage, the result in Fig.7.4 are re-presented in different form in Fig. 7.5. Good agreement is again evident, with the results confirming that an increase in ozone yield is observed with an increase in gas flow rate. The efficiency increases because, for higher flow

rates, the ozone concentration is lower. Raising the flow rate at constant power input decreases the ozone concentration but increases the ozone and energy yields. However, the efficiency curves tend to saturate at a level, which appears to be independent of voltage.

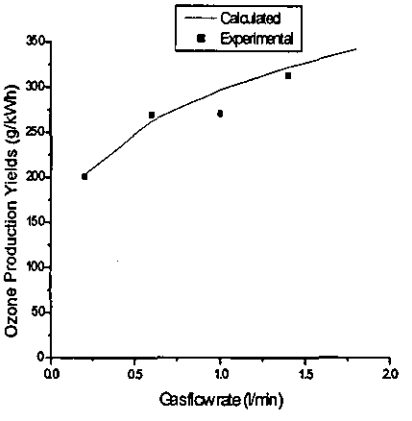

(a)

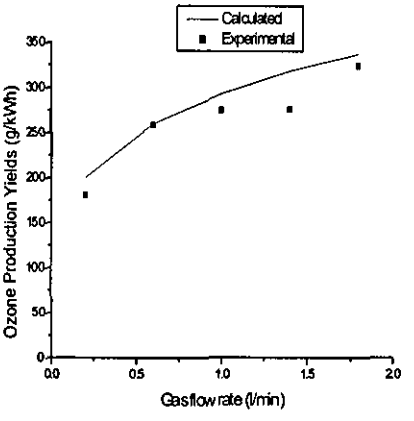

(b)

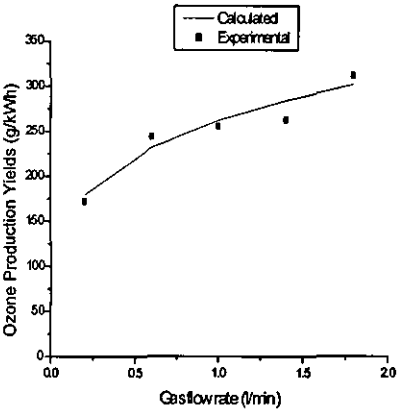

(c)

Figure 7.5: Ozone yield versus gas flow rate at peak pulsed voltage of (a) 13 kV (b) 14 kV (c) 15 kV . $Dc = 4.86 \times 10^{-23}$.

7.5 Conclusion

The above analysis is believed to be the first application of dimensional analysis to the study of ozone yield, and it has been shown to provide results that are in good agreement with experimental results. It can be used both to calculate the yield expected from the use of PSD with dielectric barrier configuration in oxygen and to investigate the significance of the various parameters that are involved. Positive and negative voltages are known to lead to different corona inception voltages [91], and inserting the appropriate voltage into equation (7.19) will enable the effects of polarity on the ozone yield to be investigated.

CHAPTER 8

CONCLUSION AND FUTURE WORK

8.1 Conclusions

The increasing demand for environmental friendly disinfectant and oxidizer compounds provides a strong incentive for an investigation directed toward increasing the efficiency of ozone generation, to promote further its use in industry. The present investigation has considered ozone generation using electrical discharges, and provides a comparative study between atmospheric pressure glow discharge and pulsed streamer discharge, with the aim of assessing their feasibility and effectiveness.

As part of the present investigation, a study was conducted to improve the stability of the glow discharge in air at atmospheric pressure. One of the novelties of the present work is the use of perforated aluminium instead of the well established fine steel wire mesh for the generation of APGD. A stability comparison of the two materials showed that the perforated aluminium has a better stability than does fine steel wire mesh. Furthermore, the glow discharge produced in this configuration has been used for ozone generation and has been confirmed to be effective for ozone production.

Ozone generation by both APGD and PSD has been demonstrated experimentally in the same discharge configuration, using a double barrier arrangement in which the facing surfaces of the two electrodes are covered with both a dielectric material and perforated aluminium. The use of two different input

voltages are central to the investigation that considers i) pulses of very short duration (less than 1μs), and of magnitudes in the order of a few tens of kilovolts and a pulse repetition frequency of 50 Hz in a PSD arrangement and ii) an A.C supply with a magnitude of a few tens of kilovolts and an applied frequency of 50 Hz in an APGD arrangement. In a comparative study carried out to investigate the efficiency of the both systems and the resulting ozone generation, PSD is found to generate a higher ozone concentration but a lower ozone yield. On the other hand, the APGD generates a lower ozone concentration but a higher ozone yield. The different performance of the APGD and PSD techniques was related to the difference in the discharge profile in the discharge gap, thus influencing the rate of increase of ozone concentration and the input energy to the discharge.

The role played by important parameters such as input voltage, gap spacing, chamber length, air flow rate and gas residence time has been investigated in both APGD and PSD techniques. The effect of input voltage on ozone concentration and yield has been observed, in the belief that the electric field at the high voltage electrode will be strengthened with the increase in input voltage. The process of ozone generation is based on the ionisation of the gas under treatment, in which the ionisation is taking place by means of electronic collisions. The rate of ionisation depends on the amount and energy of the electron distribution and ultimately is a function of the intensity and profile of the applied field. It has been shown that the ozone concentration increases with increasing input voltage even up to the maximum input voltage in both techniques. Ozone yield instead increases at increasing voltage up to a certain level of maximum and then decreases.

The effect of the gap spacing for different input voltages, air flow rates and gas residence times has been studied. At a lower input voltage and a constant air flow rate, the small gap spacing generates a higher ozone concentration in both techniques. At a higher voltage, a limitation of the small gap spacing is its low saturation level, and a lower maximum input voltage in both techniques results to

a lower maximum ozone concentration. In general, the larger gap spacing seems to promise higher concentration and yield. With proper control of the air flow rate and thus the gas residence time, as well as the optimum input voltage, it is expected that the ozone yield can also be improved.

The effect of chamber length provides important information on the optimum length to achieve an optimum yield in both experimental condition The optimum chamber length is found to depend on the gas residence time and hence the air flow rate, which controls the ozone concentration.

The effects of air flow rate and gas residence time were also investigated. It was found that both of these played an important role in controlling the ozone concentration, as well as the ozone yield, since the yield is related to its dependence on the concentration.

A study of ozone generation using both high voltage A.C corona discharge and PSD in a configuration with and without the use of a magnetic field was also conducted. Although no apparent effect was observed, the results obtained can be used as a reference for future research.

A mathematical model was developed which focused on ozone production in oxygen by means of a PSD, with dimensional analysis being used to identify both the electrical and the physical parameters that are of importance. Predicted results obtained using the analysis were compared with practical results, and were shown to be in good agreement.

Finally suggestions for future work are given, aimed at making ozone generation by those techniques even more competitive.

8.2 Recommendations for future work

The results presented in this thesis provide important guidelines for the future researchers working on APGD and PSD techniques, and particularly on how to optimize the efficiency of both techniques. The investigation has however uncovered several points which are in need of further investigation. These

1. Improvement of the stability of the APGD. The APGD stability should be further investigated so that a high concentration of ozone and an efficient ozone reactor can be obtained. The work presented has shown that perforated aluminium provides more stable APGD than does the commonly used material (a fine steel wire mesh). However, the stability considerations in this study are limited to a certain gap spacing and input voltage that limit the maximum concentration. It could be expected that the stability can be further improved if particular attention is given to the influence of the shape (cone or vee shape) and the diameter (in milli or micro meter) of the hole, the electrode thickness (thicker or thinner) and the electrode materials (aluminium, copper, etc). The study should include the improvement of the stability of the APGD at greater gap spacings and higher input voltages.

2. Scale-up of the size of the ozone reactor. From the results presented it can be noted that the efficiency of the ozone generation depends on the concentration and input energy to the discharge. To increase both parameters inevitably requires the size of the reactor to be increased. This could provide important information on the potential of both the APGD and PSD techniques for higher ozone concentration, and particular attention should be given to the use of the reactor in a co-axial configuration. With this configuration the size of the reactor can be optimized and the space used can be minimized even at increasing gap spacing compared to plane-to-plane configuration and therefore

more efficient configuration can be obtained. Since the stability of the APGD relies on the gap spacing, not much room for the gap spacing to be used for increasing the size of the reactor unless an improvement on the stability at bigger gap spacing is achieved. However, research can be focused on the improvement of the APGD stability in an individual reactor as proposed in (1) for obtaining a higher concentration. The size of APGD can be increased by combining several individual reactor in one bigger chamber. In the case of the PSD technique, with no limitation on the gap spacing, the reactor size can be increased either by increasing the gap spacing or the length of the chamber.

3. Determination of the optimum gap spacing and the chamber length. The results in this study indicate that the use of an increased gap spacing and a longer chamber length produced a higher maximum ozone concentration than does a smaller and a shorter one. No sign of saturation is observed, even at a maximum input voltage, especially in PSD technique. Since a greater gap spacing can be employed with a PSD technique, particular attention should be paid to the optimum gap spacing, the chamber length and the gas residence time on ozone concentration. An increased gap spacing and chamber length result in an increase gas residence time. Under the conditions at which the experiments were performed, a gap spacing of 3.0 mm and a chamber length of 160 produced a higher ozone yield at an optimum gas residence time of 2.3 s. In future research this result can be used as a guideline to obtain an optimum efficiency by increasing the gap spacing and chamber length.

4. Investigation on the effect of sheath breakdown. The investigation of the APGD technique presented in this thesis does not take into account the effect of sheath breakdown. It is suggested therefore that

in future research this effect should be included. Particular attention should be given to the influence of the sheath breakdown on the ozone yield.

APPENDICES

Appendix 1a

Reactions for ozone formation and decomposition considered in the analysis characteristics of oxygen-fed ozone generation are shown below [10].

Reactions by electron impact

$$e + O_2 \xrightarrow{k_1=\sigma(B)v_{de}} e + O(^1D) + O(^3P)$$
$$e + O_2 \xrightarrow{k_2=\sigma(C)v_{de}} e + O(^1P) + O(^3P)$$
$$e + O_2 \xrightarrow{k_3=\sigma_{de}v_{de}} e + O + O^-$$
$$e + O_2 \xrightarrow{k_4=\sigma(b)v_{de}} e + O_2(b)$$
$$e + O_2 \xrightarrow{k_5=\sigma(a)v_{de}} e + O_2(a)$$
$$e + O_3 \xrightarrow{k_6=\sigma(O_3)v_{de}} e + O + O_2.$$

Reactions between oxygen species

$$O(^1D) + O_2 \xrightarrow{k_7} O_2(b) + O$$
$$O(^1D) + O_2 \xrightarrow{k_8} O_2(a) + O$$
$$O(^1D) + O_3 \xrightarrow{k_9} O_2 + O_2$$
$$O(^1D) + O_3 \xrightarrow{k_{10}} O + O + O_2$$
$$O + O_2 + O_2 \xrightarrow{k_{11}} O_3^* + O_2$$
$$O + O_2 + O \xrightarrow{k_{12}} O_3^* + O$$
$$O + O_2 + O_3 \xrightarrow{k_{13}} O_3^* + O_3$$
$$O + O + O_2 \xrightarrow{k_{14}} O_2 + O_2$$
$$O + O + O \xrightarrow{k_{15}} O_2 + O$$
$$O + O_3 \xrightarrow{k_{16}} O_2 + O_2$$
$$O + O_3 \xrightarrow{k_{17}} O_2 + O_2(b)$$

$$O + O_3^* \xrightarrow{k_{18}} O_2 + O_2$$

$$O_3^* + O \xrightarrow{k_{19}} O_3 + O$$

$$O_3^* + O_2 \xrightarrow{k_{20}} O_3 + O_2$$

$$O_3^* + O_3 \xrightarrow{k_{21}} O_3 + O_3$$

$$O_2(b) + O_3 \xrightarrow{k_{22}} O + O_2 + O_2$$

$$O_2(b) + O_3 \xrightarrow{k_{23}} O_3^* + O_2(a)$$

$$O_2(b) + O \xrightarrow{k_{24}} O_2 + O$$

$$O_2(b) + O_2 \xrightarrow{k_{25}} O_2 + O_2$$

$$O_2(b) + O_3 \xrightarrow{k_{26}} O_2 + O_3$$

$$O_2(a) + O_3 \xrightarrow{k_{27}} O + O_2 + O_2$$

$$O_2(a) + O_3^* \xrightarrow{k_{28}} O + O_2 + O_2$$

$$O_2(a) + O \xrightarrow{k_{29}} O_2 + O$$

$$O_2(a) + O_2 \xrightarrow{k_{30}} O_2 + O_2$$

$$O_2(a) + O_3 \xrightarrow{k_{31}} O_2 + O_3$$

$$O_2(a) + O_2(a) \xrightarrow{k_{32}} O_2(b) + O_2$$

$$O_3 + O \xrightarrow{k_{33}} O_2 + O + O$$

$$O_3 + O_2 \xrightarrow{k_{34}} O_2 + O + O_2$$

$$O_3 + O_3 \xrightarrow{k_{35}} O_2 + O + O_3$$

$$O + O_3 \xrightarrow{k_{36}} O_2(a) + O_2$$

$$O(^1D) \xrightarrow{k_{37}} O + h\nu$$

$$O_2(b) \xrightarrow{k_{38}} O_2 + h\nu$$

$$O_2(a) \xrightarrow{k_{39}} O_2 + h\nu.$$

Appendix 1b

The reactions of ozone formation and decomposition considered in the analysis of ozone generation from air are shown below [9].

Reactions by electron impact

$$e + O_2 \xrightarrow{ke1} O(^1D) + O + e \qquad \text{(Re1)}$$

$$e + O_2 \xrightarrow{ke2} O + O + e \qquad \text{(Re2)}$$

$$e + O_2 \xrightarrow{ke3} O + O^- \qquad \text{(Re3)}$$

$$e + O_2 \xrightarrow{ke4} O_2(b) + e \qquad \text{(Re4)}$$

$$e + O_2 \xrightarrow{ke5} O_2(a) + e \qquad \text{(Re5)}$$

$$e + O_3 \xrightarrow{ke6} O(^1D) + O_2(a) + e \qquad \text{(Re6)}$$

$$e + N_2 \xrightarrow{ke8} N + N + e \qquad \text{(Re7)}$$

$$e + N_2 \xrightarrow{ke9} N_2(C) + e \qquad \text{(Re8)}$$

$$[N_2(C) + M \rightarrow N_2(B) + M]$$

$$e + N_2 \xrightarrow{ke10} N_2(a) + e \qquad \text{(Re9)}$$

$$[N_2(a) + M \rightarrow N_2(B) + M]$$

$$e + N_2 \xrightarrow{ke11} N_2(B) + e \qquad \text{(Re10)}$$

$$e + N_2 \xrightarrow{ke12} N_2(A) + e \qquad \text{(Re11)}$$

Reaction between neutral particles

$$O(^1D) + O_2 \xrightarrow{k1} O_2(b) + O \qquad \text{(Rn1)}$$

$$O(^1D) + O_2 \xrightarrow{k2} O_2(a) + O \qquad \text{(Rn2)}$$

$$O(^1D) + O_3 \xrightarrow{k3} O_2 + O_2 \qquad \text{(Rn3)}$$

$$O(^1D) + O_3 \xrightarrow{k4} O + O + O_2 \qquad \text{(Rn4)}$$

$$O + O_2 + O_2 \xrightarrow{k5(O_2)} O_3^* + O_2 \qquad (Rn5a)$$

$$O + O_2 + O \xrightarrow{k5(O)} O_3^* + O \qquad (Rn5b)$$

$$O + O_2 + O_3 \xrightarrow{k5(O_3)} O_3^* + O_3 \qquad (Rn5c)$$

$$O + O_2 + N_2 \xrightarrow{k5(N_2)} O_3^* + N_2 \qquad (Rn5d)$$

$$O + O + O_2 \xrightarrow{k6(O_2)} O_2 + O_2 \qquad (Rn6a)$$

$$O + O + O \xrightarrow{k6(O)} O_2 + O \qquad (Rn6b)$$

$$O + O + N_2 \xrightarrow{k6(N_2)} O_2 + N_2 \qquad (Rn6c)$$

$$O + O_3 \xrightarrow{k7} O_2 + O_2 \qquad (Rn7)$$

$$O + O_3 \xrightarrow{k8} O_2 + O_2(b) \qquad (Rn8)$$

$$O + O_3 \xrightarrow{k9} O_2 + O_2(a) \qquad (Rn9)$$

$$O + O_3^* \xrightarrow{k10} O_2 + O_2 \qquad (Rn10)$$

$$O_3^* + O \xrightarrow{k11(O)} O_3 + O \qquad (Rn11a)$$

$$O_3^* + O_2 \xrightarrow{k11(O_2)} O_3 + O_2 \qquad (Rn11b)$$

$$O_3^* + O_3 \xrightarrow{k11(O_3)} O_3 + O_3 \qquad (Rn11c)$$

$$O_2(b) + O_3 \xrightarrow{k12} O + O_2 + O_2 \qquad (Rn12)$$

$$O_2(b) + O_3 \xrightarrow{k13} O_3^* + O_2(b) \qquad (Rn13)$$

$$O_2(b) + O \xrightarrow{k14(O)} O_2 + O \qquad (Rn14a)$$

$$O_2(b) + O_2 \xrightarrow{k14(O_2)} O_2 + O_2 \qquad (Rn14b)$$

$$O_2(b) + O_3 \xrightarrow{k14(O_3)} O_2 + O_3 \qquad (Rn14c)$$

$$O_2(a) + O_3 \xrightarrow{k15} O + O_2 + O_2 \qquad (Rn15)$$

$$O_2(a) + O_3^* \xrightarrow{k16} O + O_2 + O_2 \qquad \text{(Rn16)}$$

$$O_2(a) + O \xrightarrow{k17(O)} O_2 + O \qquad \text{(Rn17}a\text{)}$$

$$O_2(a) + O_2 \xrightarrow{k17(O_2)} O_2 + O_2 \qquad \text{(Rn17}b\text{)}$$

$$O_2(a) + O_3 \xrightarrow{k17(O_3)} O_2 + O_3 \qquad \text{(Rn17}c\text{)}$$

$$O_2(a) + O_2(a) \xrightarrow{k18} O_2(b) + O_2 \qquad \text{(Rn18)}$$

$$O_3 + O \xrightarrow{k19(O)} O_2 + O + O \qquad \text{(Rn19}a\text{)}$$

$$O_3 + O_2 \xrightarrow{k19(O_2)} O_2 + O + O_2 \qquad \text{(Rn19}b\text{)}$$

$$O_3 + O_3 \xrightarrow{k19(O_3)} O_2 + O + O_3 \qquad \text{(Rn19}c\text{)}$$

$$O_3 + N_2 \xrightarrow{k19(N_2)} O_2 + O + N_2 \qquad \text{(Rn19}d\text{)}$$

$$O(^1D) \xrightarrow{k20} O + h\nu \qquad \text{(Rn20)}$$

$$O_2(b) \xrightarrow{k21} O_2 + h\nu \qquad \text{(Rn21)}$$

$$O_2(a) \xrightarrow{k22} O_2 + h\nu \qquad \text{(Rn22)}$$

$$O_3 + O_3 \xrightarrow{k23} O_2 + O_2 + O_2 \qquad \text{(Rn23)}$$

$$N + O_3 \xrightarrow{k24} NO + O_2 \qquad \text{(Rn24)}$$

$$NO + O_3 \xrightarrow{k25} NO_2 + O_2 \qquad \text{(Rn25)}$$

$$NO_2 + O_3 \xrightarrow{k26} NO_3 + O_2 \qquad \text{(Rn26)}$$

$$N + O_2 \xrightarrow{k27} O + NO \qquad \text{(Rn27)}$$

$$N_2(B) + O_2 \xrightarrow{k28} N_2 + O(^1D) + O \rightarrow N_2 + O + O \qquad \text{(Rn28)}$$

$$N_2(B) + N_2 \xrightarrow{k29} N_2 + N_2(A) \qquad \text{(Rn29)}$$

$$N_2(A) + O_2 \xrightarrow{k30} N_2 + O + O \qquad \text{(Rn30)}$$

$$N_2(A) + O_2 \xrightarrow{k31} N_2O + O \qquad \text{(Rn31)}$$

$$N_2(A) + O_2 \xrightarrow{k32} N_2 + O_2 \qquad \text{(Rn32)}$$

$$N_2(A) + N_2 \xrightarrow{k33} N_2 + N_2 \qquad \text{(Rn33)}$$

$$O + NO_2 \xrightarrow{k34} NO + O_2 \qquad \text{(Rn34)}$$

$$O + N_2O_3 \xrightarrow{k35} NO_2 + NO_2 + O_2 \qquad \text{(Rn35)}$$

$$NO + NO_3 \xrightarrow{k36} NO_2 + NO_2 \qquad \text{(Rn36)}$$

$$NO_2 + NO_3 + N_2 \xrightarrow{k37} N_2O_3 + N_2 \qquad \text{(Rn37)}$$

$$N_2O_3 + N_2 \xrightarrow{k38} NO_2 + NO_3 + N_2 \qquad \text{(Rn38)}$$

$$N + NO \xrightarrow{k39} N_2 + O \qquad \text{(Rn39)}$$

$$N + NO_2 \xrightarrow{k40} N_2 + O + O \qquad \text{(Rn40)}$$

$$O_2(a) + N \xrightarrow{k40} NO + O \qquad \text{(Rn41)}$$

$$O(^1D) + N_2O \xrightarrow{k42} N_2 + O_2 \qquad \text{(Rn42)}$$

$$O(^1D) + N_2O \xrightarrow{k43} NO + NO \qquad \text{(Rn43)}$$

$$N + NO_2 \xrightarrow{k44} N_2O + O \qquad \text{(Rn44)}$$

Appendix 2

Breakdown condition: Paschen's Law

The breakdown condition for gases can be obtained using Townsend's theory, including the fact that the influence of the space charge can be neglected in the early stage of the breakdown. The breakdown condition is represented by [46,49,50]:

$$\gamma [\exp(\alpha d)-1] = 1 \qquad (2.1)$$

or

$$\alpha d = \ln (1 + \gamma^{-1}) \qquad (2.2)$$

where α is the first Townsend coefficient, which depends on the gas type and gas pressure p, as well as on the electric field in the inter-electrode space E, γ is the secondary Townsend coefficient, which depend on the cathode material; d is the distance between the electrode. From Townsend's semi-empirical relation [49]

$$\alpha/p = A \exp [-B/(E/p)] \qquad (2.3)$$

therefore

$$\alpha = Ap \exp (-Bp/E) \qquad (2.4)$$

where the constant A and B are specific to a given gas.

Combining (2.2) and (2.4) we obtain

$$Apd \exp(-Bp/E) = \ln(1 + \gamma^{-1}) \qquad (2.5)$$

If the electrodes are plane-parallel $E = V_b/d$, and includes this into (2.5) gives

$$Apd \exp(-Bpd/Vb) = \ln(1 + \gamma^{-1})$$

$$\exp(-Bpd/ V_b) = \ln (1 + \gamma^{-1})/Apd$$

$$-Bpd/ V_b = \ln (\ln (1 + \gamma^{-1})) - \ln (Apd))$$

and therefore that the breakdown voltage is given by

$$V_b = \frac{Bpd}{\ln (Apd) - \ln (\ln (1 + \gamma^{-1}))} \qquad (2.6)$$

Appendix 3a

Power measurement

The equivalent circuit for the discharge configuration used in this present investigation is shown in Fig. 3.1, in which, for the double barrier arrangement, the dielectric capacitance C_d and the gap capacitance C_g are given by

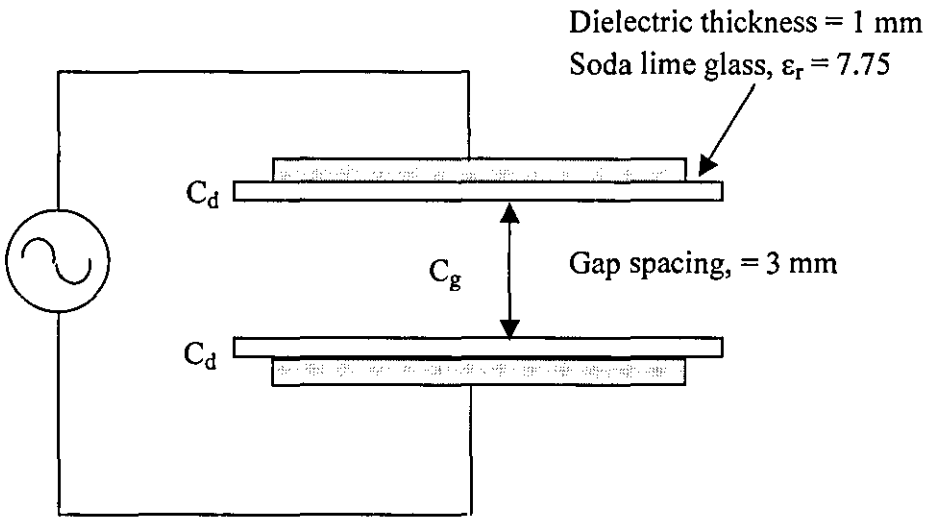

Fig. 3.1 The discharge configuration

$$C_d = \frac{\varepsilon_o \varepsilon_r A}{2d_d} \qquad (3.1)$$

$$C_g = \frac{\varepsilon_o A}{d_g} \qquad (3.2)$$

where A is the electrode area, d_d and d_g are the dielectric thickness and gap distance respectively, ε_o is the absolute dielectric constant of air and ε_r is the relative dielectric constant of the dielectric.

In the experimental rig; the gap spacing = 3 mm , dielectric thickness = 1 mm, absolute permittivity of air, $\varepsilon_o = 8.85 \times 10^{-12}$, dielectric permittivity, $\varepsilon_r = 7.75$, discharge area, $A = 2.56 \times 10^{-3}$ mm^2. The dielectric capacitance and the gap capacitance are therefore

$$Cd = \frac{(8.85\times10^{-12})(7.75)(2.56\times10^{-3})}{2(1\times10^{-3})} = 87.79 \text{ pF}$$

$$Cg = \frac{(8.85\times10^{-12})(2.56\times10^{-3})}{(3\times10^{-3})} = 7.552 \text{ pF}$$

The power in the discharge for glow discharge experiment P can be calculated from [64]:

$$P = 4fCd(1/1+\beta)Vmin\,[\,Vp - Vmin] \qquad (3.3)$$

where

f = supply frequency

Vmin = minimum voltage at which the ignition occur measured from lissajous figure..

Vp = input peak voltage measured from lissajous figure

Cd = dielectric capacitance

Cg = gap capacitance.

$\beta = Cg/Cd = (7.552 \times 10^{-12})/(87.89 \times 10^{-12}) = 0.086$

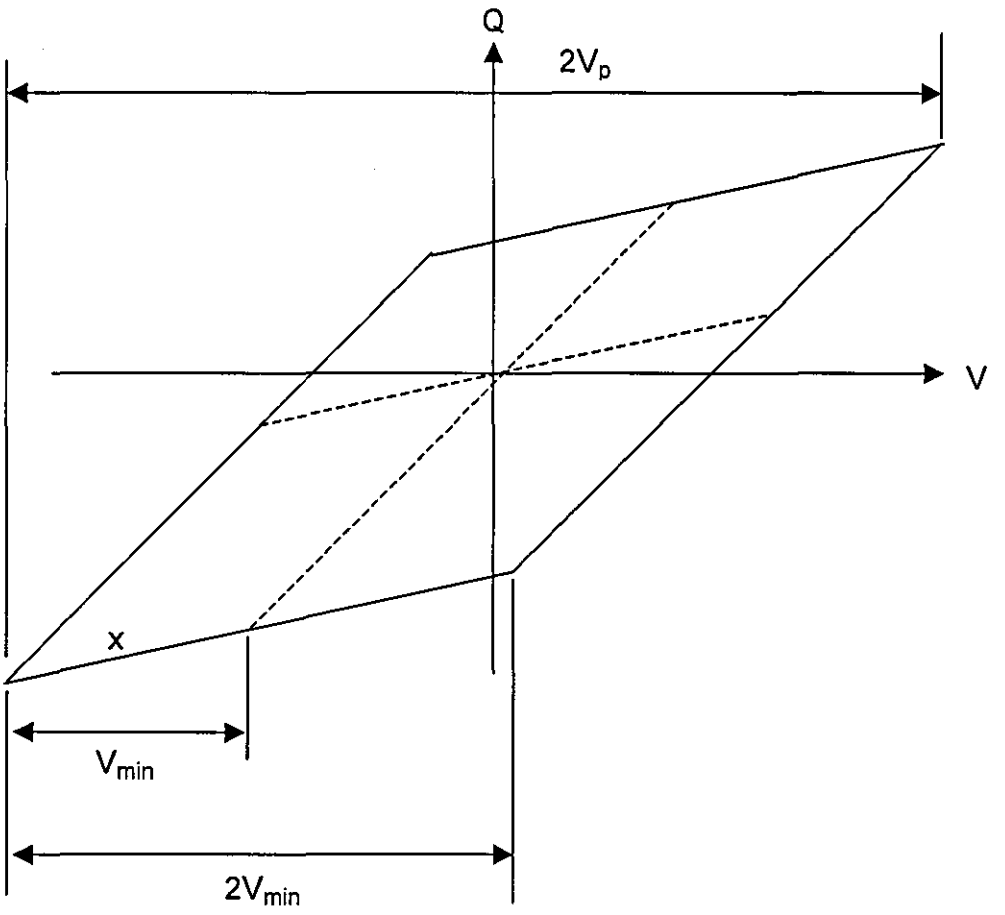

Figure 3.2: Idealized voltage-charge Lissajous figure [65]

In this present study, the Lissajous figure for the APGD obtained at 3.8 kV input voltage is used as an example for the calculation of the discharge power as follow

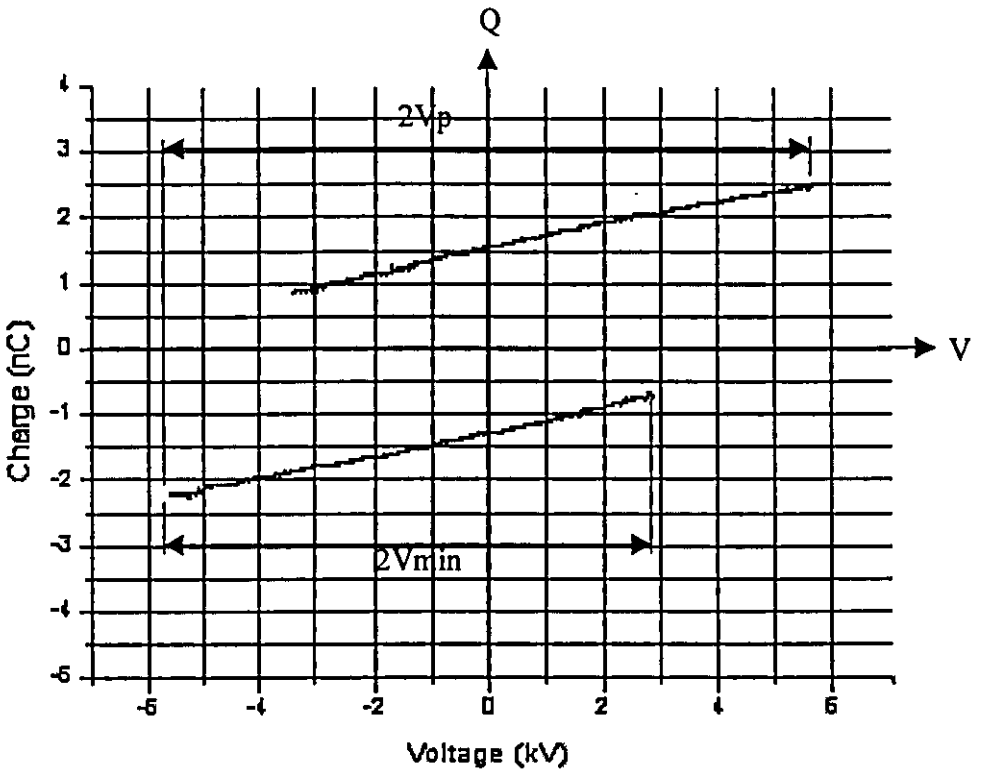

Figure 3.3: Voltage-charge Lissajous figure for present experiment

With proper scaling, the following measurements were obtained

Scale: 1 mm = 202.9 V

i) 2Vmin = 47 mm

Vmin = 47/2 x 202.9

= 4763 V = 4.763 kV

ii) 2Vp = 60 mm

Vp = 60/2 x 202.9

= 6087 V = 6.087 kV,

so that the discharge power is

$$P = 4(50)(87.89 \times 10^{-12})(1/1+0.086)(4.768 \times 10^{3})[(6.087 \times 10^{3}) - (4.768 \times 10^{3})$$

$$= 101.67 \approx 0.102\ W$$

Atmospheric Pressure Glow Discharge		**Pulse Streamer Discharge**	
Input voltage (kVrms)	Discharge power (W)	Input voltage (kV)	Discharge power (W)
3.8	0.102	13	0.183
4	0.127	14	0.433
4.2	0.149	15	0.508
4.4	0.217	16	0.78
4.6	0.266	17	0.96
4.8	0.319	18	1.174

Table 3.1: Measured discharge power for APGD and PSD techniques

Appendix 3b

Calculation of ozone yield in APGD

Before the ozone yield can be calculated, the air flow rate in liter per minute (l/min) has to be changed to gram per hour (g/h) using the following relationships:

1. 1 mol = 22.4 litre and
2. 1 mol = 28.9 grams (molecular weight of air)

Hence

22.4 litre = 28.9 grams (molecular weight of air)
22.4 liter/min = 28.9 grams /min

If the air flow rate is 0.2 l/min, the air flow rate in g/h is

$$f_r = (28.9 / 22.4)(0.2) \text{ gram/min}$$
$$= 1.293(0.2) \text{ g/min}$$
$$= 15.52 \text{ g/h}$$

For the ozone concentration $C(O_3)$ = 490 ppmv, where 1 ppmv = 1.504×10^{-4} % by weight. Therefore the ozone concentration in percent by weight is

$$C(O_3) = 490 \times 1.504 \times 10^{-4}$$
$$= 0.074 \text{ \% by weight}$$

The ozone generation rate in g/h is given by

Ozone generation rate $= C(O_3) \times f_r$ (3.4)

$= ((0.074/100) \times 15.52)$ g/h

$= 11.48$ mg/h

To calculate the ozone yield in g/kWh, the ozone generation rate in g/h has to divide by the discharge power *P*. The ozone yield is calculated from

$$\eta = \left[\frac{C(O_3) f_r}{P} \right] \quad (3.5)$$

For a discharge power of 101.67 mW = 101.67×10^{-6} kW (appendix 3a), the ozone yield is

$(\eta) = 0.01148$ g/h / 101.67×10^{-6} kW

$= 112.96$ g/kWh.

Appendix 4

Derivation of Ozone Destruction Factor

The first step in deriving equation (4.1) for the ozone destruction factor (DF) is to input the necessary experimental data into the equation

$$(O_3) = Dc.(\frac{f_r\sqrt{\varepsilon_r}V}{d_g{}^6 f^4 \tau\sqrt{p}}) \text{ [DF]} \qquad (4.1)$$

If the constant factor $(\frac{f_r\sqrt{\varepsilon_r}V}{d_g{}^6 f^4 \tau\sqrt{p}})$ in this equation is replaced by K, then

$$(O_3) = DcK \text{ [DF]} \qquad (4.2)$$

Dividing the measured ozone yield (O_3) by the constant term *K* gives a numerical values for *Dc.* Any variation in any of the terms in K will also change the value of *Dc.* For example, the variation of the air flow rate f_r, from 3.33×10^{-3}, 1.0×10^{-2}, 1.67×10^{-2}, 2.33×10^{-2} and 3.0×10^{-2} l/sec changes the values of Dc to 2.35×10^{-22}, 1.03×10^{-22}, 6.70×10^{-23}, 4.95×10^{-23} and 4.70×10^{-23} respectively. In order to obtain a single constant *Dc* for the variation of this parameter, a plot of *Dc* against the variable of air flow rate f_r using Excell software (see Fig. 4.1) gives a single equation as follows;

$$Dc = 3.02x10^{-24} f_r{}^{-0.76} \qquad (4.3)$$

In this present study, the only three parameters that have been varied are pulse repetition frequency, air flow rate and applied pulse voltage. The process is continued for each of the above parameters until a single constant *Dc* is obtained. Following this procedure changes equation (4.1) to the new equation.

$$(O_3) = Dc.(\frac{f_r^{0.24}.\sqrt{\varepsilon}V}{d_g^{\,6} f^{0.15} P_d \sqrt{p}}) \text{ [DF]} \qquad (4.4)$$

where

$$Dc = 4.86 \times 10^{-23}$$

This value of *Dc* used for figures (7.2), (7.3), (7.4) and (7.5) in Chapter 7, and holding it constant while the peak pulsed voltage is increased, enables DF to be calculated throughout the experiment and up to the gap breakdown voltage. Plotting the values so obtained against the ratio V/V_o using regression techniques and on factorising, it becomes equation (4.5) given below and which is valid only for *V* below the gap breakdown voltage, when $V/Vo<1.6135$.

$$DF = -(V/V_o - 1.6135)(V/V_o - 0.6135)] \qquad (4.5)$$

This takes into account the relationship of the input voltage *V* and the corona inception voltage V_o to the ozone generation and destruction rate.

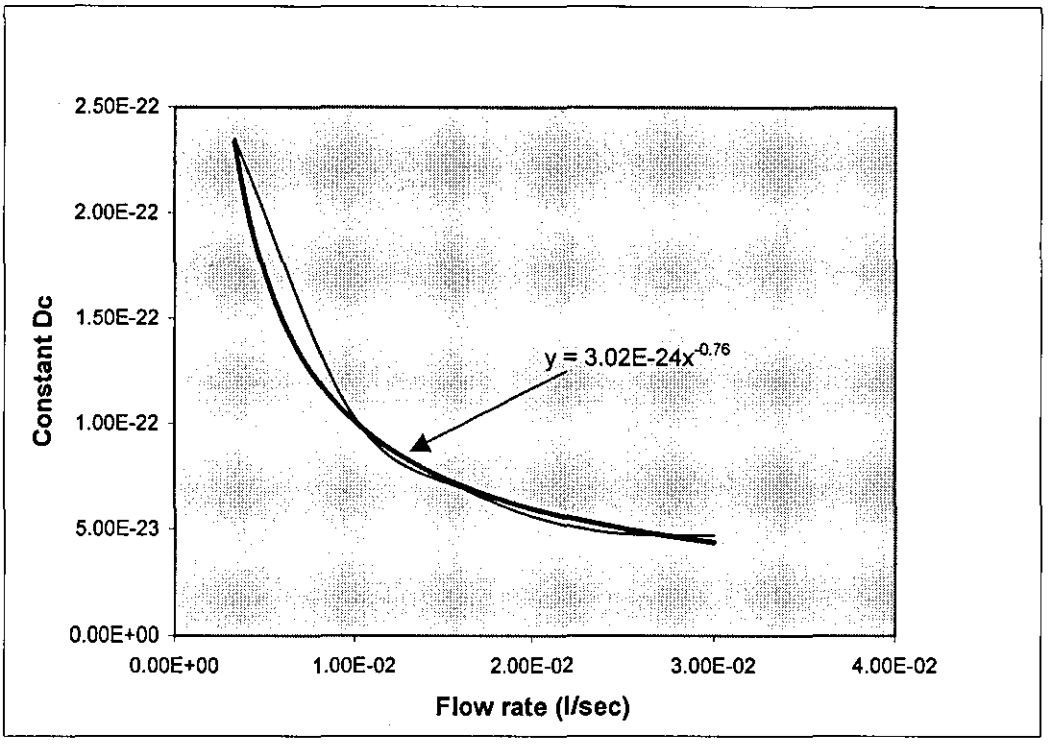

Figure 4.1: Plot of constant *Dc* against flow rate *fr*

REFERENCES

REFERENCES

1. Potivejkul S, Kinnares V, and Rattanavichien P, 1998, "Design of ozone generator using solar energy." Proc. of IEEE Asia-Pacific Conference on Circuit and Systems (APCCAS), pp. 217-220.

2. Chalmers I D, Zanella L, and Macgregor S J, 1995, "Ozone synthesis In oxygen in a dielectric barrier free configuration.", 10th IEEE Int. Pulsed Power Conference, Albuquerque, pp. 1249-1254.

3. Eliasson B, Hirth M and Kogelschatz U, 1987, "Ozone synthesis from oxygen in dielectric barrier discharges" J. Phys. D: Appl. Phys., Vol 20, No.11, pp. 1421-1437.

4. Samaranayake W J M, Miyahara Y, Namihira T, Katsuki S, Hackam R and Akiyama H, 2000, "Pulsed streamer discharge characteristics of ozone production in dry air". IEEE Trans. on Dielectrics and Electrical Insulation, Vol. 7 No. 2, pp. 254-260.

5. Eliasson B and Kogelschatz U, 1991, "Modeling and applications of silent discharge plasmas." IEEE Trans. on Plasma Science, Vol. 19, No.2, pp 309-323.

6. Nomoto Y, Ohkubo T, Kanazawa S and Adachi T, 1995 "Improvement of ozone yield by a silent-hybrid discharge ozonizer", IEEE Transactions on Industry Applications, Vol.31, No.6, pp. 1458-1462.

7. Samaranayake W J M, Miyahara Y, Namihira T, Katsuki S, Hackam R and Akiyama H, 1999, "Ozone production by pulsed power in dry air". Digest of

Technical Papers-IEEE International Pulsed Power Conference, Vol.2, pp. 1326-1329

8. Kogelschatz U, Eliasson B and Egli W, 1997, "Dielectric barrier discharges: Principles and application", J.de Physique IV, Vol.7, No.4, pp. C4-47 – C4-63.

9. Kitayama J and Kuzumoto M, 1999, "Analysis of ozone generation from air in silent discharge", J.Phys. D: Appl.Phys., Vol 32, pp. 3032-3040.

10. Kitayama J and Kuzumoto M, 1997, "Theoretical and experimental study on ozone generation characteristics of an oxygen-fed ozone generator in silent discharge", J.Phys. D: Appl.Phys. , Vol 30, pp. 2453-2461.

11. Kogelschatz U, Elliasson B and Egli W, 1999, "From ozone generators to flat television screens: History and future potential of dielectric-barrier discharges", Pure Appl. Chem., Vol. 71, No.10, pp. 1819-1828.

12. Goldman M. and Sigmond R S, 1982, "Corona and Insulation", IEEE Trans. on Electrical Insulation, Vol. EI-17, No.2, pp. 90-105.

13. Held B, 1995, "Corona and their applications", 11th. Int. Conf. of Gas Discharges and Their Applications, Tokyo, Vol.2, pp. 514-526.

14. Haacke M. and Pietsch G.J., 2000, "Some features of dielectric barrier discharge", Proc. 13th Int. Conf. Gas Discharges & Their Applications, Glasgow, pp.267-270

15. Pietsch G, 1996, "Investigation and properties of the discharge in dielectric barrier reactors", J.Adv. Oxid. Technol., Vol.1 No.1, pp. 61-66,.

16. Pietsch G.J. and Haacke M., 1999 "Parameters influencing the yield of surface discharge ozone generators", Proc. 14th Ozone World Congress, Michigan, Vol.1, pp. 311-323.

17. Chalmers I D, Zanella L, and MacGregor S J, 1994, "Ozone generation by pulsed corona discharge in a wire cylinder arrangement.", IEE Colloquium (Digest), No.229, pp. 6/1-6/4.

18. Chalmers I D, Zanella L and MacGregor S J, 1996, "Ozone generation using pulsed corona in a wire/cylinder arrangement." London: IEE Colloquium (Digest), No. 059, pp. 7/1-7/5.

19. Samaranayake W J M, Miyahara Y, Namihira T, Katsuki S, Hackam R and Akiyama H, 1999, "Ozone production using cylindrical reactors with and without solid dielectric layers in dry air". IEEE Conference on Electrical Insulation and Dielectric Phenomena (CEIDP), Annual Report, Vol.1, pp. 379-382.

20. Samaranayake W J M, Namihira T, Katsuki S, Miyahara Y, Sakugawa T, Hackam R and Akiyama H, 2001, "Pulsed power production of ozone using nonthermal gas discharges", IEEE Electrical Insulation Magazine, Vol.17, No.4, pp.17-25.

21. Simek M and Clupek M, 2002, "Efficiency of ozone production by pulsed positive corona discharge in synthetic air", J.Phys. D: Appl.Phys., Vol. 35, pp. 1171-1175.

22. Harry J E and Yahya A A, 1999, "Factors affecting the glow-to-arc transition at the cathode of an electric discharge at atmospheric pressure", Int. J. Electronics, Vol.86, No.6, pp. 755-762.

23. Harry J E and Yuan Q, 2000, "Distinguishing discharge modes using their spectral lines", Int. J. Electronics, Vol.87, No.9, pp. 1105-1112.

24. Kanazawa S, Kogoma M, Moriwaki T and Okazaki S, 1988, "Stable glow plasma at atmospheric pressure", J.Phys. D: Appl.Phys., Vol 21, pp. 838-840.

25. Kogoma M and Okazaki S, 1994, "Raising of ozone formation efficiency in a homogeneous glow discharge plasma at atmospheric pressure", J.Phys. D : Appl.Phys., Vol 27, pp. 1985-1987.

26. Okazaki S, Kogoma M, Uehara M and Kimura Y., 1993, "Appearance of stable glow discharge in air, argon, oxygen and nitrogen at atmospheric pressure using a 50 Hz source", J.Phys. D: Appl.Phys., Vol 26, pp. 889-892.

27. Tepper J and Lindmayer M, 2000 "Investigations on two different kinds of homogeneous barrier discharges at atmospheric pressure", Proc. of Int. Symp. On High Pressure, Low Temperature Plasma Chemistry, Hakone VII, Greifwald, Germany, pp. 38-43.

28. Trunec D, Brablec A and Buchta J, 2000 "Efficiency of ozone production in atmospheric pressure glow and silent discharges", Proc. of Int. Symp. On High Pressure, Low Temperature Plasma Chemistry, Hakone VII, Greifwald, Germany, pp. 313-317.

29. Yokoyama T, Kogoma M, Moriwaki T and Okazaki S, 1990, "The mechanism of the stabilisation of glow plasma at atmospheric pressure", J.Phys. D : Appl.Phys., Vol. 23, pp. 1125-1128.

30. Evan F L, 1972, "Ozone in water and wastewater treatment", Ann Arbor Science Publishers Inc., First Edition.

31. Cotton F A and Wilkinson G, "Advanced inorganic chemistry", 5th Edition, John Wiley & Sons.

32. Ballantine B, Morris T and Turner P ed., 1995 "General and applied toxicology", abridged edition, The MacMillan Press Ltd.

33. Lopez A., Fontan J and Minga A, 1993 "Analysis of atmospheric ozone measurements over a pine forest", Atmospheric Environment, Vol. 27A, No.4, pp. 555-563.

34. Chalmers I D, 1993 "A generalised approach to ozone generator design", Private Communication.

35. Chalmers I D, Baird R C and Kelly T, 1998, "Control of an ozone generator- theory and practice" Meas. Sci. Technol. Vol 9, pp. 983-988.

36. Dorsey J A and Davidson J H, 1994 " Ozone production in electrostatic air cleaners with contaminated electrodes", IEEE Transaction on Industry Applications, Vol 30, No. 2, pp. 370-376

37. Boonseng C, Kinnares V and Apriratikul P, 2000 "Harmonic analysis of corona discharge ozone generator using brush electrode configuration", IEEE Power Engineering Society Winter Meeting, Vol.1, pp. 403-408.

38. Kuzumoto M, Kitayama J and Tabata Y, 1997, "Effect of electron impact on ozone decomposition", Proceedings of 13th. Ozone World Congress, Kyoto, Japan, Vol. 2, C2-1-5, pp. 815-820.

39. Yagi S, Tanaka M and Tabata N, 1979, "Generation of NOx in ozonizers", IEE of Japan 99, pp. 41-48.

40. Eliasson B and Kogelschatz U, 1987, "Nitrogen oxide formation in ozonizers", Proc.8th Int. Symp. On Plasma Chemistry, Tokyo, pp. 736-741.

41. van Veldhuizen E.M., 1999, "Electrical discharges for environmental purposes: Fundamentals and application", Nova Science Publisher, Inc. New York.

42. Kirk R E and Othmer D F ed.,!996, "Encyclopedia of chemical technology", Wiley Interscience, 4th. Edition, Vol. 17.

43. "Ozone information", Hankin Atlas Ozone Systems Limited, http://www.hankinozone.com/ozone.html.

44. Howatson A.M, 1965, "An Introduction to gas discharges" Pergamon Press Ltd, First Edition, pp.67-128.

45. Meek J M and Craggs J D, 1978, "Electrical breakdown of gases", John Wiley & Sons, New York.

46. Raizer Y P, 1997, "Gas discharge physics" Berlin: Springer.

47. Schutze A, Jeong J Y, Babayan S E, Park J, Selwyn G S and Hicks R F, 1998, "The atmospheric-pressure plasma jet: a review and comparison to other plasma sources" IEEE Trans. on Plasma Science, Vol.26, No.6, pp. 1685-1693

48. Von Engel A, 1983, "Electric plasmas: their nature and uses", Taylor and Francis Ltd., London and New York.

49. Von Engel A, 1965, "Ionized gases", Clarendon Press, Oxford.

50. Eliasson B and Kogelschatz U, 1991, "Non-equilibrium volume plasma chemical processing." IEEE Transactions on Plasma Science, Vol. 19, No.6, pp. 1063-1077.

51. Penetrante B M, Bardsley J N and Hsiao M C, 1997, "Kinetic analysis of non-thermal plasmas used for pollution control", Jpn. J. Appl. Phys. Vol 36, part 1, No.7B, pp. 5007-5017.

52. Yehia A, Mizuno A and Takashima K, 2000, "On the characteristics of the corona discharge in a wire-duct reactor", J.Phys. D: Appl. Phys. Vol. 33, pp. 2807-2814.

53. Chang J S, Lawless P A and Yamamoto T, 1991, "Corona discharge processes", IEEE Trans. on Plasma Science, Vol.19, No.6, pp. 1152-1166.

54. Pietsch G J and Haacke M, 2000 "Parameter Influencing the yield of surface discharge ozone generator", Proc. 13th Int. Conf. Gas Discharges and their Applications, Glasgow, Vol.1, pp. 267-270.

55. Bogaerts A, 1999, "The glow discharge: an exciting plasma" Invited Lecture, J. Anal. At. Spectrom., Vol.14, pp.1375-1384.

56. Park J, Henins I, Hermann H. W, Selwyn G. S, Jeong J. Y, Hicks R. F, Shim D, and Chang C. S, 2000, "An atmospheric pressure plasma source", Appl. Phys. Lett. Vol.76, No. 3, pp.288-290.

57. Tien C L, "Annual review of heat transfer", Vol.10, Begell House Inc., New York, pp.66-76.

58. Massines F., Rabehi A., Decomps P., Gadri R.B., Ségur P., Mayoux C., 1998, "Experimental and theoretical study of a glow discharge at atmospheric pressure controlled by dielectric barrier", J. Appl. Phys, Vol. 83, pp 2950-2957.

59. Takaki K, Taguchi D, Fujiwara T, 2001, "Voltage–current characteristics of high-current glow discharges" Appl. Phys. Lett. Vol. 78, No 18, pp. 2646-2648.

60. Tepper J, Li P and Lindmayer M, 2002 "Effect of interface between dielectric barrier and electrode on homogeneous barrier discharges at atmospheric pressure", XIV International Conference on Gas Discharges and their Application, Liverpool, pp. 1-4.

61. Kamase Y, Shimizu M, Nagahama T and Mizuno A, 1993, "Erosion of spark gap of square-wave high-voltage source for ozone generation". IEEE Transaction on Industry Application, Vol., 29, No. 4, pp. 793-797.

62. Lawless P A, Yamamoto T, Poteat S, Boss C, Nunez C M, Ramsey G H and Engels R, 1993, "Characteristics of a fast rise time power supply for a pulsed plasma reactor". Conference Record - IAS Annual Meeting (IEEE Industry Applications Society), Vol.3, pp. 1875-1881

63. Grothaus M G, Hutcherson R K and Korzekwa R A, 1994, "Non-thermal plasma discharge for hazardous gas abatement", IEEE International Conference on Plasma Science, pp. 128-129.

64. Kogelschatz U, 1988, "Advanced ozone generation", Symposium on Process Technologies for Water Treatment, S. Stucki, Ed. New York and London, pp. 87-120.

65. Chalmers I.D and Zanella L, 1996, "Wire/cylinder device with space charge distortion: ozone production", IEE Colloquium (Digest), No. 008 , pp. 8/1-8/3.

66. Samaranayake W.J.M, Miyahara Y, Namihira T, Katsuki S, Hackam R and Akiyama H, 2000, "Ozone production using pulsed dielectric barrier discharge in oxygen," IEEE Trans. on Dielectrics and Electrical Insulation, Vol.7, No.6, pp 849-854.

67. Yagi S and Tanaka M, 1979 "Mechanism of Ozone Generation in Air-fed Ozonisers," J. Phys. D: Appl. Phys. Vol.12, pp. 1509-1520.

68. Niessen W, Wolf O, Schruft R and Neiger M, 1998, "The influence of ethene on the conversion of Nox in a dielectric barrier discharge", J.Phys.D: Appl. Phys. Vol. 31, pp. 542-550.

69. Garamoon A.A., Elakshar F.F, Nossair A.M and Kotp E.F, 2002, "Experimental study of ozone synthesis", Plasma Sources Sci. Technol. Vol. 11, pp. 254-259.

70. Falkenstein Z and Coogan J.J, 1997, "Microdischarge behaviour in the silent discharge of nitrogen-oxygen and water-air mixtures" J. Phys. D: Appl. Phys. Vol. 30, pp. 817-825.

71. Miller B B, Haverkemp R G, Free K W, Dawson G J and Kitchenman O R G, 1997, "The effects of frequency, power, pressure and gas flow on a novel ozone generator", Proc. of 13th. Ozone World Congress, C-2-3-6, pp. 915-920.

72. Hegeler F and Akiyama H, 1997, "Ozone generation by positive and negative wire-to-plate streamer discharge", Japan J. Appl. Phys., Vol. 36, pp. 5335-5339.

73. Masuda S, Sato M and Seki T, 1986, "High-efficiency ozonizer using traveling wave pulse voltage", IEEE Trans. On Plasma Sci., Vol. IA-22, No. 5, pp. 886-891.

74. Salam M A, Mizuno A and Shimizu K, 1997, "Ozone generation as influenced by gas flow in corona reactors", J.Phys. D: Appl.Phys. Vol. 30, pp. 864-870.

75. Masuda S, Akutsu K, Kuroda M, Awatsu Y and Shibuya Y, 1988, "A ceramic based ozonizer using high-frequency discharge", IEEE Trans. Ind. Appl., Vol. 24, No.2, pp 223-231.

76. Satoh S, Katsuki N, Hakiai K, Ihara S, Ishimine M and Yamabe C, 1997, "An effect of superposition of positive streamer and surface discharge on ozone generation", Proc. of 13th. Ozone World Congress, Kyoto, Japan Vol.2, C2-2-5, pp. 865-869.

77. Buntat Z, Harry J.E and Smith I.R, 2002, "Atmospheric pressure glow discharge and pulsed streamer discharge for ozone generation" European Pulsed Power Symposium, Saint Louis, France, pp. 38/1-38/5.

78. Massines F, Rabehi A, Decomps Ph, Gadri R B, Segur P, and Mayoux C, 1998, "Experimental and theoretical study of a Glow Discharge at Atmospheric Pressure Controlled by Dielectric Barrier", Journal of Applied Physics, Vol. 83, No. 6, pp. 2950-2957.

79. Spence P and Roth J. R, 1994, "Electrical and plasma characteristics of a one atmosphere glow discharge plasma reactor," Paper 1P-25, Proc. 21st IEEE International Conference on Plasma Science, Santa Fe, NM, June 6-8, ISBN 7803-2006-9, pp. 97.

80. Montie T.C, Kelly-Wintenberg. K, Roth.J.R, 2000, "An Overview of research using a one Atmosphere Uniform Glow Discharge Plasma (OAUGDP) for sterilization of surfaces and materials", IEEE Trans. Plasma Science, Vol.28, No.1, pp. 41-50.

81. Sawada Y, Ogawa S, and Kogoma M, 1995, "Synthesis of Plasma-Polymerized Tetraethoxysilane and Hexamethyldisiloxane Films Prepared by Atmospheric Pressure Glow Discharge ", J. Phys. D., Appl. Phys., Vol. 28, pp. 1661-1669.

82. Somerville I C, MacGregor S J and Farish O, 1990, " An efficient stacked-Blumlein h.v pulse generator," Meas. Sci. Technol. Vol.1, pp. 865-868.

83. British Standard BS 1741-12:1993/ISO 10313:1993 "Methods for measurement of air pollution – Part 12: Determination of the mass concentration of ozone in ambient air: chemiluminescence method".

84. Shi J J, Deng X T, Hall R, Punnett and Kong M G, 2003, "Three modes in a radio frequency atmospheric pressure glow discharge", Journal of Applied Physics, Vol. 94, No. 10, pp 6303-6310.

85. Jana D C and Pradhan S S, 2001, "The influence of a transverse magnetic field on a subnormal glow discharge in air" Pramana- J. Phys., Vol. 56, No. 1, pp. 107-115.

86. Lieberman M A and Lichtenberg A J, 1994 "Principles of plasma discharges and materials processing" John Wiley & sons, Inc., New York.

87. Moon J.D, Lee G.T and Chung S.H, 1999 "SO_2 and CO gas removal and discharge characteristics of a non-thermal plasma reactor in a crossed DC magnetic field" IEEE Trans. On Industry Application, Vol. 35, No. 5, pp . 1198-1204.

88. Moon J.D, Lee G.T and Lee D.H, 1996, "A magnetic field effect on ozone generation characteristics of wire-to-cylinder airgap discharge", IEJ-ESA Proceeding of 1996 Joint Symposium on Electrostatics, Tokyo, Japan, pp. 118-125.

89. H L Langhaar, 1951, " Dimensional Analysis and Theory of Models", New York: Wiley.

90. T Szirtes, 1997, "Applied Dimensional Analysis and Modeling", McGraw-Hill, New York.

91. Yehia A, Abdel-Salam M and Mizuno A, 2000, " On assessment of ozone generation in dc coronas", J Phys D: Appl Phys, vol 33, pp. 831-835.

PRESENTED PAPERS

CONFERENCES

1. Z.Buntat, J.E.Harry and I.R.Smith, "Atmospheric pressure glow discharge and pulsed streamer discharge for ozone generation" European Pulsed Power Symposium, St. Louis, France, October 2002.

2. Z.Buntat, J.E.Harry and I.R.Smith, "Atmospheric pressure glow discharge for ozone generation" 16th. Int. Symposium on Plasma Chemistry, Taormina, Italy, 22-27, June 2003.

3. Z.Buntat, J.E.Harry and I.R.Smith, " Modelling the relationship between ozone production by pulsed streamer discharge in oxygen and the principal parameters involved", IEE Pulsed Power Symposium, Loughborough, 23rd. September 2003.

JOURNAL

1. Z.Buntat, J.E.Harry and I.R.Smith, "Application of dimensional analysis to ozone production by pulsed streamer discharge in oxygen", J. Phys. D: Appl. Phys. Vol. 36, pp. 1553-1557, published June 2003.